The Production of Polymeric Fibres Using Nozzle-Pressurised Gyration

Yanqi Dai

A dissertation submitted for the degree of

Doctor of Philosophy

of

University College London

Department of Mechanical Engineering

University College London

June 2025

Declaration

I, Yanqi Dai, declare that this thesis and the work presented in it are my own and have been generated by me as the result of my original research.

I confirm that:

1. Results derived from others' published work are cited, as well as figures are reproduced with permission from the original publishers.

2. All the main sources of help for this thesis have been acknowledged.

3. Parts of this work have been published as:

[1] **Y. Dai**, J. Ahmed, A. Delbusso, and M. Edirisinghe, "Nozzle-pressurized gyration: a novel fiber manufacturing process," Macromolecular Materials and Engineering, vol. 307, no. 9, pp.2200268, Sep. 2022.

[2] **Y. Dai**, J. Ahmed, and M. Edirisinghe, "Pressurized gyration: fundamentals, advancements, and future," Macromolecular Materials and Engineering, vol. 308, no. 7, pp. 2300033, Jul. 2023.

[3] **Y. Dai**, D. Sun, S. Sundaram, A. Delbusso, D. O'Rourke, M. Dorris, and M. Edirisinghe, "Facile synthesis: from *Laminaria hyperborea* to cellulose films and fibers," Cellulose, vol. 31, no. 1, pp. 205-216, Jan. 2024.

[4] **Y. Dai**, M. Gultekinoglu, C. Bayram, H.B. De Silva, M. Edirisinghe, "Antibacterial properties of natural cinnamon-alginate fibrous patches produced by modified nozzle-pressurized spinning," MedComm, vol. 5, no. 9, pp. e731, Sep. 2024.

[5] **Y. Dai**, D. Sun, D. O'Rourke, S. Velusamy, S. Sundaram, M. Edirisinghe, "Harnessing cow manure waste for nanocellulose extraction and sustainable small-structure manufacturing," Journal of Cleaner Production, vol. 509, pp. 45530, Jun. 2025.

Figures, tables and texts in these five parts are adapted with permission from Wiley-VCH GmbH, Springer Nature, SAGE, and Elsevier. The five publications listed above are all open-access.

Some parts of the writing process, such as rewording and improving clarity, were supported using ChatGPT (OpenAI). All content was reviewed and edited by the author to ensure accuracy and originality.

I Abstract

Materials are the basis for the survival of human beings, as well as the symbol of the development process of human civilisation. Polymeric fibres have been widely used in filtration, energy storage, healthcare, and the environment due to their physical and chemical properties, especially the unique surface effects. The manufacturing of fibrous materials at the micro-scale has emerged as a prominent focus in materials science. Electrospinning is currently one of the most widely adopted fibre production technologies in both academic and industrial fields. Centrifugal spinning, phase separation, template synthesis, and self-assembly are also common methods for fibre formation. Given the rapid growth in market demand and the pressing quest for sustainable production, the development of scalable fibre manufacturing technologies has become increasingly urgent.

Pressurised gyration (pressurised spinning or pressure spinning) is a more recent fibre production method. It combines the features of centrifugal spinning and solution blowing for efficient production of fibres through a facile one-pot process. The process involves a perforated cylindrical vessel that spins at high speed, where polymer jets are ejected from orifices due to the combined effects of rotational force and externally applied gas pressure. Originally developed as a scalable alternative to electrospinning, pressurised gyration has been used with a wide range of polymers and allows for high-throughput fibre production. The method has been adapted for various applications, including tissue engineering scaffolds, air/water filters, and drug delivery systems. In this study, a modified nozzle-based pressurised gyration system is developed to improve fibre morphology and spin biopolymer fibres from natural sources. This new spinning

system is proven to produce polymeric fibres with greater uniformity and alignment, compared with conventional nozzle-free pressurised gyration. The efficacy of this enhancement is validated across different synthetic polymers (polycaprolactone (PCL), polyvinylpyrrolidone (PVP), and poly(ethylene oxide) (PEO)). The improved fibre alignment effectively enhances their mechanical strength along the fibre length compared to electrospun fibres, which typically exhibit anisotropic properties. In addition, nozzle-pressurised gyration further reduced the fibre diameter. PCL fibres and PVP fibres with diameters of approximately 1 micron and PEO nanofibres with a diameter of 172 nm are produced by nozzle-pressurised gyration. This new method achieves a remarkable fibre production rate that is 20 ~ 40 times higher than that of electrospinning.

To expand the application scenarios of nozzle-pressurised gyration, this equipment was further modified by incorporating a $CaCl_2$ coagulation bath to produce alginate fibres, addressing the current challenges associated with the processing of biopolymers. It leverages the precise control and impressive efficiency of nozzle-pressurised gyration, combined with the adaptability of wet-spinning alginate-based materials. This makes it a highly promising and cost-effective technology for scaling up alginate fibre production with simplicity and ease. By meticulously adjusting the solution concentration and the processing parameters, a comprehensive protocol for producing alginate fibres using this innovative method is established. The resulting alginate fibres combine the inherent biological properties of biopolymers and surface characteristics of fine fibres to maximise their potential in biomedical applications, showing 94 ± 2.8% cell viability. Combined with *Cinnamomum verum* extracts, these alginate-based

fibres show significant antibacterial efficiency. The decrease in bacterial adhesion and biofilm formation is detected log 1 ~ log 5 for gram-negative *Escherichia coli* and gram-positive *Staphylococcus aureus* bacteria species.

The modified nozzle-pressurised gyration device is also being used to spin natural cellulose, sourced from *Laminaria hyperborea* seaweed and recycled dairy farm waste, into micro-scale fibrous materials. This process explores extended sources of raw materials for nozzle-pressurised gyration, achieving the conversion of low-grade plants into value-added products while also promoting the upcycling and reuse of waste materials. This work aligns with the principles of a circular economy by fostering sustainability and resource efficiency.

II Impact Statement

This research introduces nozzle-pressurised gyration, an advanced and scalable fibre production method designed to meet growing industrial demands for fine fibres. This new method effectively mitigates the common limitation associated with gyro-spun fibres, particularly in achieving consistent and uniform morphology, making the technology more suitable for practical production and clinical applications. By enabling the efficient and uniform fabrication of fibres from both synthetic and natural polymers, the technology holds strong potential for future applications in healthcare, including wound dressings, tissue scaffolds, and drug delivery systems, ultimately contributing to improved human wellbeing.

From an economic perspective, nozzle-pressurised gyration offers a low-cost, high-throughput alternative to conventional spinning techniques, such as electrospinning and wet spinning, with simpler equipment, faster production rates, and lower energy consumption. Its industrial scalability makes it highly suitable for commercial adoption in diverse sectors, including filtration, energy storage, smart textiles, and biomedical devices.

The technology also supports environmental sustainability by facilitating the use of renewable, biodegradable biopolymers, such as alginate and cellulose, without the need for toxic additives. This reduces the environmental and public health impacts associated with synthetic polymer wastes and processing chemicals. Furthermore, by enabling the use of upcycled and natural resources, the method aligns with the principles of a circular economy, offering a more responsible path for future material innovation.

Overall, the impact of this research extends across industry, health, economics, and environmental sustainability, positioning nozzle-pressurised gyration as a next-generation fibre production technology with wide-ranging future benefits.

III Publications & Conferences

III. 1 Publications

1. **Y. Dai**, J. Ahmed, A. Delbusso, and M. Edirisinghe, “Nozzle-pressurized gyration: a novel fiber manufacturing process,” *Macromol. Mater. Eng.*, vol. 307, no. 9, pp. 2200268, Sep. 2022.

2. **Y. Dai**, J. Ahmed, and M. Edirisinghe, “Pressurized gyration: fundamentals, advancements, and future,” *Macromol. Mater. Eng.*, vol. 308, no. 7, pp. 2300033, Jul. 2023.

3. **Y. Dai**, D. Sun, S. Sundaram, A. Delbusso, D. O’Rourke, M. Dorris, and M. Edirisinghe, “Facile synthesis: from Laminaria hyperborea to cellulose films and fibers,” *Cellulose*, vol. 31, no. 1, pp. 205-216, Jan. 2024.

4. **Y. Dai**, M. Gultekinoglu, C. Bayram, H.B. De Silva, M. Edirisinghe, “Antibacterial properties of natural cinnamon-alginate fibrous patches produced by modified nozzle-pressurized spinning,” *MedComm*, vol. 5, no. 9, pp. e731, Sep. 2024.

5. **Y. Dai**, and M. Edirisinghe, “How can pressurized gyration revolutionize drug delivery?” *Expert. Opin. Drug. Deliv.*, Oct. 2024.

6. N. Qosim[#], **Y. Dai**[#], G.R. Williams, M. Edirisinghe, “Structure, properties, forming, and applications of alginate fibers: A review,” *Int. Mater. Rev.*, vol. 69, no. 5-6, pp. 309-333, Sep. 2024. ([#] Contributed equally.)

7. R. Huang, **Y. Dai**, J. Ahmed, and M. Edirisinghe, “Facile one-step synthesis of PVDF bead-on-string fibers by pressurized gyration for reusable face masks,” *Polymers*, vol. 14, no. 21, pp. 4498, Oct. 2022.

8. M. Ghamaria, D. Sun, **Y. Dai**, C. H. See, H. Yu, M. Edirisinghe, S. Sundaram, “Valorization of diverse waste-derived nanocellulose for multifaceted applications: A review,” *Int. J. Biol. Macromol.*, Oct. 2024.

9. **Y. Dai**, D. Sun, D. O’Rourke, S. Velusamy, S. Sundaram, M. Edirisinghe, “Harnessing cow manure waste for nanocellulose extraction and sustainable small-structure manufacturing,” *J. Clean. Prod.*, vol. 509, pp. 45530, Jun. 2025.

III. 2 Conferences

Y. Dai, M. Edirisinghe, "Nozzle-Pressurised Gyration: A Novel Fibre Manufacturing Process," Department of Mechanical Engineering PhD Students Conference, University College London, London, UK. 9th June 2022. Oral and poster presentation.

Y. Dai, M. Edirisinghe, "Sustainable Fibrous Patches: Harnessing Polysaccharides from Seaweed for Wound Care," Department of Mechanical Engineering PhD Students Conference, University College London, London, UK. 6th June 2023. Oral and poster presentation.

Y. Dai, M. Edirisinghe, "The Dawn of the Next Generation of Biomaterials: Scalable and Sustainable Fibrous Product Manufacture Using Inverted Pressure Spinning," MS&T24: Materials Science&Technology, Pittsburgh, Pennsylvania, USA. 7th October 2024. Oral presentation.

IV Acknowledgements

This PhD journey has been one of the most rewarding and challenging experiences of my life, and it would not have been possible without the guidance, support, and love of many individuals.

First and foremost, I would like to express my sincere gratitude to my supervisors, Professor Mohan Edirisinghe and Dr Francis Brako, for their unwavering guidance, thoughtful advice, and continual support throughout this entire process. Their expertise and mentorship have been invaluable, which helped me navigate through challenges and inspired me to continue pursuing excellence in my research.

I would like to express my appreciation to the following collaborative supervisors: Professor Senthilarasu Sundaram at Teesside University and Dr Dongyang Sun at Edinburgh Napier University for their support with the cellulose derivation work, and Dr Merve Gultekinoglu at Hacettepe University for her support with the biological analysis. I am grateful for their academic collaboration and valuable contributions to my research.

I am also immensely grateful to my incredible colleagues and the dedicated staff at UCL MechEng. Their camaraderie, assistance, and friendship have made this journey not only productive but also enjoyable. The countless conversations, shared experiences, and support have been a source of strength, and I am truly thankful for each of them.

My greatest thanks go to my family, Mr Zhangcheng Dai, Ms Huiqiong Zhu and Mr Yifan Dai, and my significant one, Dr Xuze Guan. To my family, their

unconditional love, patience, and belief in me have been the foundation of everything I have accomplished. They have stood by me every step of the way, even from afar, and their support has been my constant source of motivation and courage. To my boyfriend, his love, encouragement, and understanding have carried me through the toughest moments. His hard work, dedication, and success have inspired me to strive for my best.

Lastly, I want to thank myself for the persistence, dedication, and strength I've shown throughout this journey. I am proud of the person I've become through this experience, and I honour the effort I have put in to reach this point. I remain confident that the road ahead is full of promise and possibilities.

To all of you, and myself, thank you for believing in me and for making this achievement possible. This achievement is every bit your achievement as it is mine.

V Table of Contents

VI List of Figures

VII List of Tables

VIII Abbreviations

Alg	Alginate
AMIMCl	1-Allyl-3-Methylimidazolium Chloride
BC	Bacterial Cellulose
BMIMCl	1-Butyl-3-Methylimidazolium Chloride
CA	Cinnamaldehyde
CEO	Cinnamon Essential Oil
CNFs	Carbon Nanofibres
CNTs	Carbon Nanotubes
CUR	Curcumin
DMEM	Dulbecco's Modified Eagle's Medium
ECM	Extracellular Matrix
E. coli	*Escherichia coli*
EE	Encapsulation Efficiency
EIDs	Emerging Infectious Diseases
EMIM OAc	1-Ethyl-3-Methylimidazolium Acetate
FBS	Fetal Bovine Serum
FETs	Field-Effect Transistors

FTIR	Fourier Transform Infrared Spectroscopy
GC	Ground Cinnamon
GC-MS	Gas Chromatography-Mass Spectrometry
HEPA	High-Efficiency Particulate Air
MCE	Mixed Cellulose Ester
MP-AES	Microwave Plasma Atomic Emission Spectroscopy
MSCs	Mesenchymal Stem Cells
NMMO	N-Methylmorpholine N-Oxide
OI	Orientation Index
PCIG	Pressure-Coupled Infusion Gyration
PG	Pressurised Gyration
PMG	Pressurised Melt Gyration
QS	Quorum Sensing
S. aureus	*Staphylococcus aureus*
SEM	Scanning Electron Microscopy
Na-Alg	Sodium Alginate
UTS	Ultimate Tensile Strength
WHO	World Health Organization

XRD	X-Ray Diffraction
w/v%	Weight/Volume Percentage
wt%	Mass Fraction

1 Introduction

1.1 Research Background

The global outbreak of SARS-CoV-2 has heightened public awareness and concern about personal healthcare and the need for effective measures to prevent the spread of viruses. Face masks, generally using fibrous materials as filter media, are recommended by the World Health Organization (WHO) as the simplest and a highly effective tool of personal protection [1, 2]. Aleksandra et al. [3] further underscored the critical role of this non-pharmaceutical measure in containing the rapid spread of the pandemic in their study. Fibrous materials with very fine diameters (micro- or nano-scale) exhibit superior filtration performance due to their high specific surface area, tunable porosity, and unique surface effects. Given that the SARS-CoV-2 viruses and other coronaviruses have a very small particle diameter (100 ± 10 nm), treatments leveraging nano-materials have garnered significant attention, driving a growing demand for fine fibres [4]. In addition to personal protective equipment, fibrous membranes play an essential role in air and water filtration systems. High-efficiency particulate air (HEPA) filters, typically composed of fine fibres, remove contaminants such as dust, bacteria, and viruses via microscopic sieves. According to the U.S. Department of Energy, compliant HEPA filters achieve up to 99.97% filtration efficiency for aerosols as small as 0.3 μm in diameter [5].

The application of fibres is by no means limited to filtration. There is increasing interest in the versatility and the ability to be engineered with specific properties of polymeric fibres, especially biopolymer fibres that are inherently biocompatible

and biodegradable. These fibres are encouraging candidates in biomedical fields, such as drug delivery carriers, tissue engineering scaffolds, wound dressings, and biosensors for diagnosis and therapy [6-9]. The additional attention on bio-based polymer fibres aligns with global efforts to promote circular economies and sustainable practices. Beyond healthcare, fibrous materials find applications in energy and environmental fields. Particularly, conductive polymeric fibres show remarkable potential in green energy (fuel cells, solar cells), optical devices, and transistors due to their unique electrical and optical properties [10, 11]. Ultra-lightweight polymer fibre composites are also increasingly used in aerospace and automotive sectors for their high specific strength and stiffness compared to traditional inorganic materials [12]. Additionally, their outstanding thermal and acoustic insulation properties have garnered increasing interest in the construction industry [13].

In view of the surging interest and demand for fibrous materials, research on advancing fibre manufacturing and processing methods is both critical and urgent. Electrospinning is currently the most versatile method for continuous fibre manufacturing [14]. However, the difficulty of scale-up is the most prominent impediment to the further development of this technology. Pressurised gyration (PG) has emerged as a promising alternative, offering scalability alongside competitive efficiency in fibre production [15]. Despite the many successes that have been achieved since its proposal in 2013, PG is not ideally perfect. While PG offers notable advantages in fibre production efficiency, this comes at the cost of reduced control over fibre fineness. Fibres produced by electrospinning are typically much thinner (down to 200 nm in diameter), compared to the several micrometres commonly achieved through PG, and can exhibit greater uniformity

in diameter. This is likely attributed to the significantly lower infusion rate used in electrospinning, which allows for more precise control over fibre formation. Addressing these challenges, this research focuses on advancing PG-based fibre manufacturing techniques to improve the quality and quantity of gyrospun fibres. By refining the PG process, this work aims to bridge the gap between scalability and precision, meeting the growing demand for high-performance fine fibres in diverse applications, while supporting sustainable development principles.

1.2 Aims and Objectives

The focus of this research is to develop advanced fibre manufacturing processes based on the PG technique. The aim is to refine fibre morphology and to expand the diversity of spinning materials to a more natural aspect through innovative methods. The polymeric fibres produced will be used in specific biomedical applications, especially as wound-healing patches and drug delivery carriers.

1.2.1 Novel Design of Pressurised Gyration

Through the novel design of the spinning vessel to improve fibre uniformity and production consistency of the PG technique. The new PG setup will be used to enhance fibre morphology and structure. The effects of processing parameters will be discovered by extensive experiments. The outcomes will be validated on different materials. The morphological characteristics, mechanical properties and drug release behaviours of the obtained fibres will be compared with fibres prepared using the prevailing spinning method—electrospinning, to demonstrate the remarkable enhancement of the new design.

1.2.2 Fabrication of Biopolymer Fibres using Advanced Pressurised Gyration

The new spinning apparatus will be upgraded by integrating a coagulation bath to facilitate the wet spinning of alginate (Alg) fibres. The spinnability of Na-Alg/H_2O solutions and processing parameters will be discovered by extensive experiments. The primary aim is to produce Alg fibres with a well-defined fibrous morphology and a consistently narrow diameter distribution, ensuring high-quality outcomes in the spinning process.

1.2.3 Assess the Efficacy of the Cinnamon-Alginate Fibres as Natural Antimicrobial Patches.

Considering the outstanding biocompatibility of Alg, Alg fibres incorporated with a natural antioxidant-rich spice—*Cinnamomum verum*, will be manufactured using the upgraded PG setup. These cinnamon-Alg fibres will undergo thorough evaluation for cell viability and antibacterial properties to indicate their potential as innovative and effective alternatives to conventional antimicrobial biomaterials.

1.2.4 Manufacture of Cellulose Fibres from Recycled Waste Materials

Cellulose derived from natural sources (*Laminaria hyperborea* seaweed and recycled dairy farm waste) will be used as the feedstock for the upgraded PG process, to investigate their spinnability. Besides their morphology, the produced cellulose products will be characterised by Fourier transform infrared spectroscopy (FTIR) and X-ray diffraction (XRD) to indicate their chemical compositions and crystallisation form. A more sustainable and environmentally friendly fibrous biomaterial is highly sought after.

1.3 Thesis Outline

This dissertation details the way in which the research proceeded and is ordered in the following chapters:

Chapter 1 provides a brief introduction of the background information relevant to the themes explored in this work, outlines the research aims and objectives, and offers an overview of the thesis structure.

Chapter 2 presents an in-depth review of the existing knowledge in this interdisciplinary field. Details regarding the fundamentals of fibres, materials used for fibre production, fibre manufacturing techniques, and their application prospects in various areas. It addresses the current challenges of fibre manufacturing and explores future development trends in fibre processing.

Chapter 3 presents the design of the spinning equipment, the preparation of spinning materials, the spinning parameters, and the methods used for fibre characterisation.

Chapter 4 presents a novel design of pressurised gyration and discusses the associated parameter effects, highlighting its advantages in the manufacturing of polymeric fibres in terms of fibre morphology and performance, as well as fibre productivity, compared to the current spinning technologies.

Chapter 5 elucidates the adaptation of the advanced pressurised gyration apparatus for biopolymer fibre spinning and assesses the cell viability and antimicrobial properties of the obtained cinnamon-Alg fibres, highlighting their potential as sustainable and innovative biomaterials.

Chapter 6 explores extended raw material sources for the proposed pressurised gyration equipment from recycled waste streams and assesses their spinnability, alongside an analysis of their chemical characteristics.

Chapter 7 sums up the key outcomes and current limitations of the research and outlines potential directions for future research.

2 Literature Review

2.1 Fundamentals of Polymeric Fibres

The term *fibre* originates from the Latin word *fibra*, having the meaning of the thread-like structures in plants and animals since the 17th century, that is, natural fibres [16, 17]. Plant fibre materials such as cotton, hemp, and flax have been important textile materials for centuries, dating back to the Neolithic in ancient Egypt [18, 19]. Animal fibres are primarily composed of proteins, such as those found in silk, hair, fur, and feathers [20]. The technique of manufacturing silk cloth from silkworm filaments originated in ancient China, which had been the only silk producer for over 300 years [21]. Exquisite silk products were important trade commodities between ancient China and Persia, Egypt, bringing China a numerous income.

Although the idea of man-made fibres rather than being obtained directly from nature had been proposed in 1664, it was not until 1855 that Swiss chemist Georges Audemars made the first rayon from mulberry trees [17]. Using a needle, Audemars pulled cellulose-based long filaments from a mixed solution of mulberry bark pulp and gummy rubber [22, 23]. Rayon was then expected to become the replacement for high-priced silk due to the wide resources and low price of its raw materials. Nevertheless, the process was cumbersome and time-consuming, hindering its suitability for large-scale production. In the late 19th century, French chemist Hilaire de Chardonnet discovered a method of man-made silks from cellulose nitrate, called “Chardonnet silk” [24]. Chardonnet patented the technique and established the first artificial silk manufacturing

company in Besançon, France [25, 26]. Chardonnet was widely known as the "Father of Rayon" for revolutionising textile manufacturing by pioneering the large-scale production of artificial silk. Subsequently, viscose spinning was developed, a versatile approach for producing regenerated cellulose fibres (also known as “rayon”) via cellulose dissolution in alkaline solutions. The rayon, obtained from natural long-chain polymers, is a semi-synthetic fibre, that dominated the fibre industry for decades in the early 20th century. However, the use of highly toxic carbon disulfide in the viscose process has raised significant safety concerns [27]. Lyocell rayon was later proposed as a more eco-friendly and high-performing alternative in the late 20th century, eliminating toxic chemicals and reactions, while significantly reducing air and water emissions [28]. Despite that, the high production cost remains a significant barrier to the broader adoption and application of Lyocell.

Nylon fibres are the first synthetic fibres, synthesised entirely from petroleum. In 1935, nylon was developed by Wallace Hume Carothers and his colleagues at the DuPont Experimental Station [29]. The invention of nylon led to the era of commercial synthesis fibres. Women's stockings made of nylon were enthusiastically sought after by the market and became the vane of the trend of the times, with 800 000 sold on the first day of release [29]. In World War II, nylon replaced silk to be used in various military items such as parachutes, cords, and bulletproof vests [30, 31]. Synthetic fibres such as Orlon acrylic, Dacron polyester, Lycra spandex, Teflon fluorocarbon, and Nomex high-temperature fibres were successively launched by DuPont in the 1950s [24]. Today, synthetic fibres are widely used in textile, construction, environment, military, medicine, and other fields due to their low cost and huge quantity.

2.2 Materials for Fibre Production

The choice of materials for fibre production plays a critical role in determining the morphologies, properties, performance, and potential applications of the resulting fibres. In fibre manufacturing, both synthetic and natural polymers are used due to their ability to form continuous filaments, enabled by their viscoelastic behaviour in solution or melt form. The chemical composition, molecular weight, chain branches, solution viscosity and surface tension of these materials are essential impact factors in the fibre formation process and fibre properties.

Synthetic polymers refer to polymers that are artificially produced by chemical reactions in laboratories [32], such as polycaprolactone (PCL), polyvinylpyrrolidone (PVP), and poly(ethylene oxide) (PEO). PCL is a biodegradable polyester, composed of repeating single units of ε-caprolactone $(C_6H_{10}O_2)_n$. Owing to its superior viscoelastic properties compared to other biodegradable polymers, PCL is well-suited for manufacturing into various structures, such as films, fibres, microbubbles, etc [33]. Additionally, PCL is widely recognised as a promising biomaterial duo to its excellent mechanical strength and biocompatibility, making it a popular choice for biomedical devices and healthcare. However, its slow degradation rate has raised concerns regarding its long-term presence when used in implantable devices [34]. PVP is a hydrophilic synthetic polymer, composed of repeating N-vinylpyrrolidone units $(C_6H_9NO)_n$. It is also widely used in biomedical applications due to its excellent biocompatibility and solubility in green solvents, such as water and alcohols. Its hydrophilicity makes it particularly valuable when used as biomaterials, where it helps reduce protein adhesion and improve surface properties [35]. However, the

polymer's non-biodegradability restricts its use in long-term or implantable applications, as it cannot be naturally broken down or metabolised in the body. Moreover, its extensive use may raise environmental concerns, particularly regarding its potential accumulation in soil and aquatic ecosystems [36]. PEO is a hydrophilic synthetic polymer, composed of repeating ethylene oxide units $(CH_2CH_2O)_n$. PEO is widely recognised for its excellent water solubility, low toxicity, and high biocompatibility, and is approved by the FDA for various biomedical and pharmaceutical applications [37]. Biomaterials with PEO-based surface can restrict protein adhesion, thereby reducing complement activation system, immunogenicity and antigenicity in vivo [38]. Therefore, it becomes a promising matrix for tissue engineering applications. However, PEO is also non-biodegradable under physiological conditions, restricting its application in long-term or implantable medical devices.

Overall, synthetic polymers offer excellent solubility in common solvents and are widely used in fibre fabrication due to their consistent fibre-forming capability and reproducible results. In addition, synthetic polymers provide structural stability and can be easily functionalised, making them suitable for a wide range of applications, including filtration, energy storage, and biomedical scaffolds. However, concerns regarding their environmental impact and limited degradability present significant challenges for extensive use, particularly in contexts requiring sustainability and eco-compatibility.

Natural biopolymers are macromolecular materials synthesised by living organisms and are generally considered as a renewable resource [39]. Owing to their distinctive biocompatibility, biodegradability, and sustainability, biopolymers,

encompassing proteins, polysaccharides, lipids, and nucleic acids [40], have attracted increased interest for applications in the biomedical and pharmaceutical fields [41, 42]. Among them, water soluble Alg $(C_6H_8O_6)_n$ is of particular interest due to its unique gelling properties and water absorption capacity [43-47].

In addition to Alg, cellulose ($(C_6H_{10}O_5)n$) is also a popular option among renewable polymers, owing to its favourable mechanical and thermal properties [48]. Cellulose has conventionally been sourced from botanical constituents such as wood, plant stems, and leaves. Recent efforts have turned towards exploring alternative sources through waste recycling streams that are rich in cellulose content [49-54]. This approach not only prolongs the use cycles of materials but also effectively mitigates the environmental impact of waste disposal, integrating with the concept of circular economy. Agricultural residues, e.g. rice straw and bagasse fibres, have received much attention due to their functionalities that are very similar to hardwood cellulose [55]. In addition, the derivation of cellulose from animal waste presents a promising pathway for sustainable cellulose production, contributing to a broader objective of resource efficiency and environmental sustainability [56].

However, the poor solubility of cellulose poses a significant challenge to its secondary processing and large-scale production. Cellulose is insoluble in water and most organic solvents due to the strong inter and intra-molecular hydrogen bonds [57]. Chemical derivatisation and direct solvent systems, such as *N*-methylmorpholine *N*-oxide (NMMO) and lithium chloride/*N*, *N*-dimethylacetamide (LiCl/DMAc) [58, 59], are common strategies for cellulose dissolution. However, cumbersome processes, thermal instability, and harmful by-products are

significant drawbacks of these methods. Recently, imidazolium-based ionic liquids have attracted attention due to their excellent ability to dissolve cellulose without any pre-activation [60, 61]. Ionic liquids dissolve cellulose by forming hydrogen bonds with their hydroxyl groups and both anions and cations are involved in this process [60, 62, 63]. The advantages of ionic liquids as solvents for cellulose and other biomass are enormous, including chemical and thermal stability, non-flammability, low vapour pressure, and excellent solvency [63, 64]. In addition, ionic liquids are considered green solvents and can be recycled for reuse [65]. Various methods can be used to recover the ionic liquid, for example, liquid-liquid extraction [66], supercritical CO_2 separation [67], and membrane separation [68], depending on the ionic liquid used and their applications. 1-Butyl-3-methylimidazolium chloride (BMIMCl), 1-ethyl-3-methylimidazolium acetate (EMIM OAc), and 1-allyl-3-methylimidazolium chloride (AMIMCl), etc. have been used for cellulose dissolution [61, 69-72]. This new dissolution process offers the potential to fabricate cellulose fibres as sustainable alternatives to viscose and Lyocell in the textile industry [73].

Despite their many inherent advantages, the transformation of natural polymers into commercially value-added products still faces many challenges. The primary and secondary processing of natural polymers without altering their structure and properties is notably more challenging than that of synthetic polymers. As such, there is an urgent need to develop a straightforward, efficient, and low-cost technology for processing natural polymers.

2.3 Fibre Manufacturing Technologies

A variety of fibre-forming technologies have evolved over the long history of polymeric fibre development, with each generation of scientists building upon the innovations of their predecessors. Today, global demand for fibre materials is at an all-time high, with expectations extending beyond texture and comfort in textiles to include enhanced functionality such as strength, elasticity, durability, lightweight, flame insulation, and biocompatibility. These qualities are essential for their applications in diverse fields.

Currently, spinning—where continuous fibres are extruded through a spinneret—is the most widely used fibre-forming approach. Among the various spinning techniques, electrospinning and centrifugal spinning have gained significant attention due to their simplicity, controllability, and relative cost-effectiveness. A comprehensive analysis of these fibre technologies helps to understand their unique features, advantages, and limitations, thus determining their appropriate applications and perspectives on their future development potential.

PG, a more recent fibre-manufacturing technique, shows promise as a leading future technology in this field. By addressing the challenges of existing spinning methods, it offers exceptional spinning performance and economic efficiency, positioning it as a potential game-changer in fibre manufacturing. This thesis focuses on the research of advanced spinning technologies based on PG.

2.3.1 Electrospinning

Electrospinning has played a pivotal role in the advancement of fibre production over recent decades. The theoretical foundation of this technology dates back to

1964-1969, when Geoffrey Taylor first elucidated the dynamics of electrically charged jets [74, 75]. A slightly conductive viscous liquid, extruded through a capillary, deforms under a strong electric field due to its surface tension, resulting in a cone—known as the “Taylor cone”. This deformation intensifies as the voltage increases. Once a critical threshold voltage (Rayleigh limit) is reached, the rounded tip of the cone emits a jet of polymer fluid. The jet then travels through the air accompanied by solvent evaporation, leaving behind charged fibres that can be electrically deflected or collected on a metal plate [76].

The apparatus used in electrospinning consists of a high-voltage supplier, a needle with a small inner diameter connected to a capillary tube, an infusion syringe pump and an adjustable metal plate [77], as shown in **Figure 2-1.** The electrospinning process starts with the delivery of polymer solutions with a determined flow rate using an infusion pump [78-80]. As the electrical forces increase, a force opposite to the surface tension occurs on the surface of the electrically charged polymer liquid coming out of the needle, causing a “Taylor cone” of the ejected droplet. When the charge on the droplet accumulates to a certain critical value, this force overcomes the surface tension and forms a liquid stream. This stream is followed by forming a jet when the molecular cohesion of the polymer liquid is sufficiently high, rather than split into large droplets [81]. Thereafter, the jet undergoes violent whipping or splitting motions in the electric field due to bending instability [82, 83]. During this process, the jet greatly stretches and thins while the solvent largely evaporates, ultimately depositing on the collector as fine fibres. Electrospinning is exceptionally effective at creating ultrafine fibres, capable of generating polymeric fibres with diameters ranging from 40 nm to 2 microns [81]. Certain technical parameters affect the morphology

of electrospun fibres, involving solution parameters (molecular weight, viscosity, surface tension, conductivity, and volatility of solvent), processing parameters (voltage, flow rate, collection design and distance), and ambient parameters (relative humidity, temperature) [14, 77, 84].

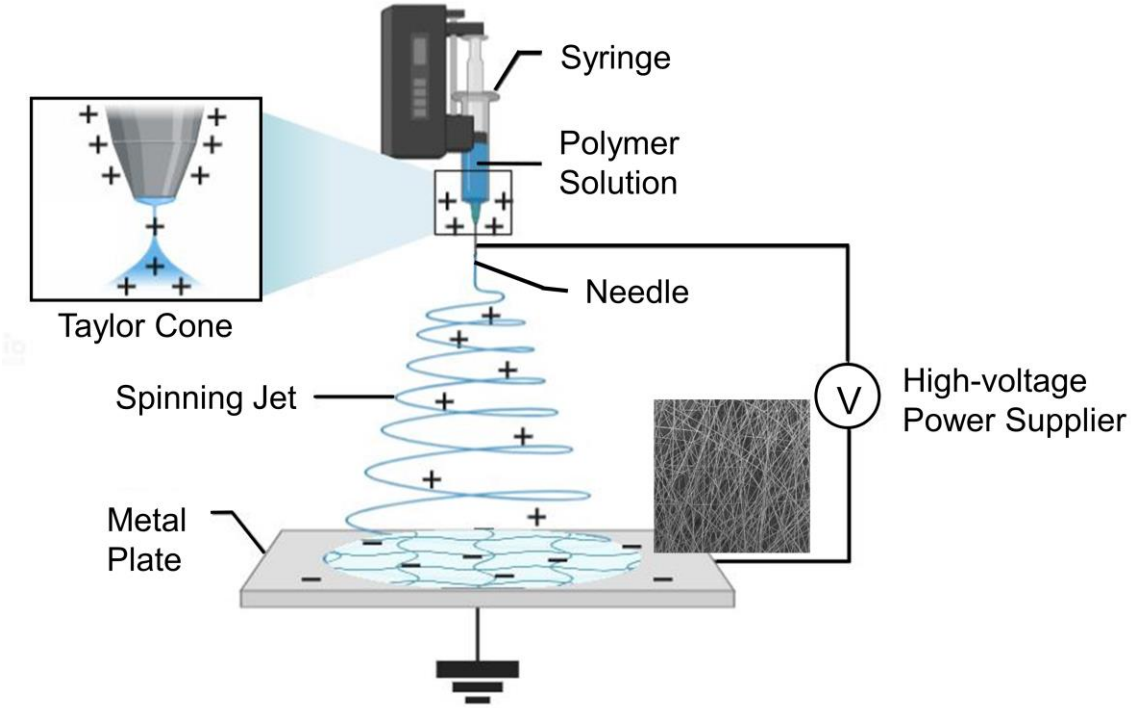

Figure 2-1 Schematic diagram of an electrospinning apparatus.

Electrospinning is no doubt a highly successful fibre fabrication technology, offering numerous advantages such as a simple experimental setup, ease of processing, the ability to produce ultrafine fibres at the nanoscale, versatile and flexible applications and controlled patterning [85]. However, this technique has certain limitations. These can be specified as low yield capacity (about 0.01 - 0.3 g/h) [25, 85], crystallisation at the needle tip for specific polymer solutions [86], and intricate structure of the fibre scaffolds. In addition, the applied voltage can adversely affect sensitive materials such as enzymes, biotins, and proteins, as

well as decrease fibre uniformity [87]. By incorporating a rotating drum collector or an auxiliary electrode, the jet motions and fibre deposition can be regulated to produce well-aligned fibres [88]. However, this significantly increases the complexity of the equipment construction. Furthermore, the dense two-dimensional structure of electrospun scaffolds poses limitations for tissue engineering applications, as they fail to replicate the inherently three-dimensional architecture of human tissues. This structural mismatch can hinder cell infiltration, nutrient diffusion, and overall tissue integration, making it less suitable for regenerating complex biological environments. Despite considerable research aimed at overcoming the current challenges of electrospinning, many of these solutions have compromised the simplicity of the equipment and the ease of the process [85, 88]. Efforts to address issues such as scalability, fibre uniformity, and material limitations often involve complex modifications or additional components [83, 89], which can detract from the straightforward nature of the original electrospinning setup.

2.3.2 Centrifugal Spinning

Centrifugal spinning was proposed as an efficient spinning strategy to eliminate the many limitations encountered in electrospinning and is known for its rapid production rate and low cost. Centrifugal spinning was initially applied for the production of glass fibres in industry, with its origins dating back to a patent by Ernst Pick in 1909 [90]. In this process, molten glass is drawn by centrifugal force generated by a rotating spinner (a bowl-shaped container with orifices in the walls), enabling the continuous formation of glass fibres [91]. This early innovation laid the groundwork for the modern use of centrifugal spinning in

various fibre production industries. It wasn't until the late 1990s that centrifugal spinning attracted significant attention as a viable method for producing polymeric fibres.

A typical centrifugal spinning setup is shown in **Figure 2-2**, which consists of a perforated spinneret connected by a high-speed motor, and a fibre collector. The activated motor can provide the spinneret with a rotational speed of up to 12 000 rpm so that the loaded spinning liquid can overcome its surface tension to be ejected from the orifices on the spinneret wall, initiating the fibre formation process [92]. Similar to electrospinning, centrifugal spinning ejects the polymer solution at high velocity, leading to rapid solvent atomisation and evaporation. Once the jet is expelled from the spinneret, it follows a centrifugal trajectory around the axis of rotation. During this process, the drawn jet is continuously stretched and thinned, resulting in the formation of fine fibres. Eventually, the dried fibres are deposited on the collector in a high alignment.

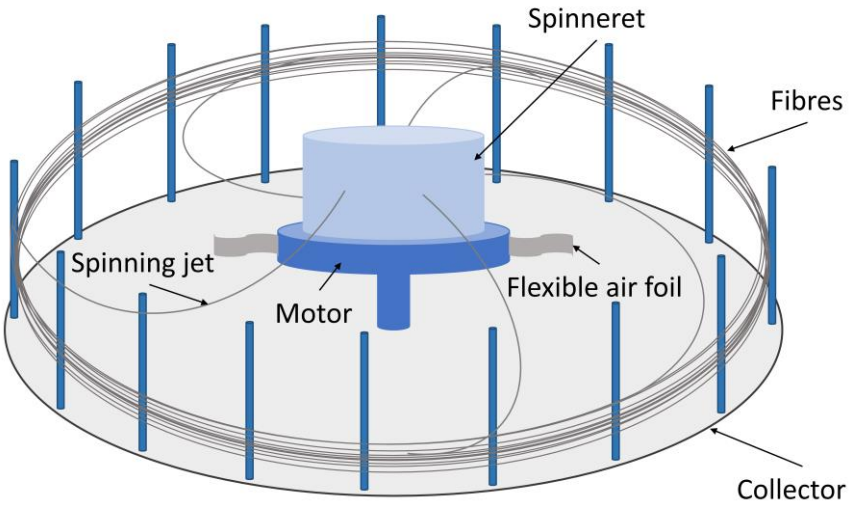

Figure 2-2 Schematic diagram of a centrifugal spinning setup.

Instead of an electric field, centrifugal force drives the fibre formation process in centrifugal spinning, minimising the energy consumption and safety concerns related to high-voltage fields in electrospinning and widening its range of material selections (conductive or non-conductive, melt or solution) [93], making the technique more versatile and accessible for various applications.

Fibres manufactured by centrifugal spinning generally feature a high fibre alignment due to the coaxial unidirectional rotation. Moreover, centrifugal spinning can be adapted with different spinnerets, either with nozzles or without nozzles (featuring small orifices), and can be configured as single-channel or multi-channel systems [84, 92]. The multi-channel spinneret enables centrifugal spinning to achieve a fibre yield several orders of magnitude higher than that of electrospinning [94]. The easy-to-replace spinneret makes this technology allows for enhanced control over the spinning process, making it versatile to accommodate different materials and production requirements. Overall, centrifugal spinning is considered an efficient and low-cost fibre manufacturing method.

2.3.3 Pressurised Gyration

PG is a scalable fibre-forming technology that combines high-pressure and gyratory spinning systems [95]. Much like in centrifugal spinning, PG primarily relies on centrifugal force to generate polymer jets for fibre formation, effectively addressing many of the limitations of current fibre-forming strategies. The introduction of the high-pressure system enhances PG's capability to produce ultrafine nanofibres, expanding its potential in advanced applications. Its highly controllable processing parameters, easy-to-replace spinning vessels, and

compatibility with a broader range of materials offer unique advantages for fibre customisation. These attributes establish PG as a highly versatile and promising technology to meet the evolving demands of modern fibrous material manufacturing.

The PG apparatus consists of three main sections: the spinning vessel, the nitrogen gas circuit, and the collector (**Figure 2-3**).

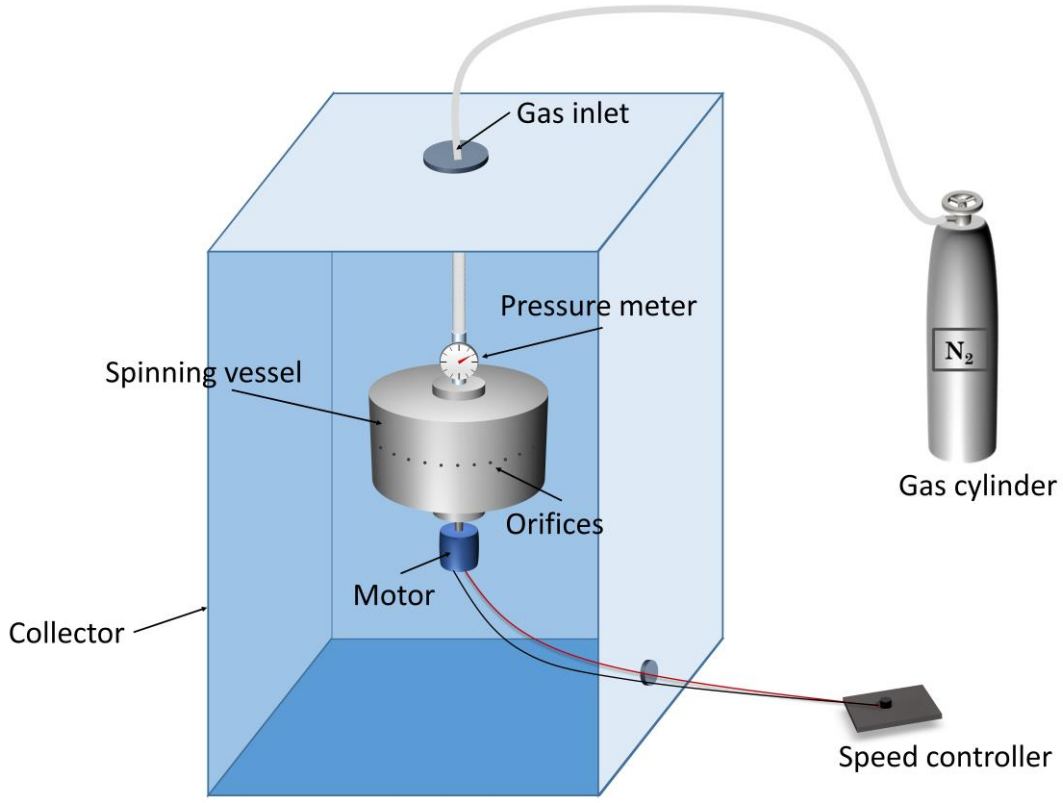

Figure 2-3 Schematic diagram of a conventional pressurised gyration setup.

In conventional laboratory PG equipment, the spinning vessel is an aluminium perforated cylindrical container (bottom diameter and side height are 60 mm and 30 mm, respectively). The number of orifices on the vessel wall is up to 24, and the diameter of each orifice is 0.5 mm. The spinning vessel is connected by bearings to an RS PRO geared DC motor, which provides a rotational speed of

up to 36 000 rpm. The electrical motor is connected to a speed control knob to adjust the rotational speed. The lid of the spinning vessel is connected to a nitrogen gas cylinder through a plastic tube, which can provide a working pressure of up to 3×10^5 Pa during spinning. The collector is placed at a certain distance (100 − 200 mm) from the spinning vessel to collect dry fibres with the desired morphology.

The fibre formation in PG can be summarised into three main stages, namely jet initiation, jet extension, and solvent evaporation [96]. Upon starting the spinning process, the polymer fluid is rapidly spread in the spinning vessel under the centrifugal force provided by the motor. The fluid profile takes on a parabolic shape [97]. After applying the nitrogen flow, the polymer fluid reaches the orifices at approximately the same time, which means that they have almost equal initial velocity and height. Subsequently, the polymer fluid starts to overflow from the orifices. The polymer droplets at the orifices form a surface tension gradient along the air-liquid interface (Marangoni effect) under the action of external forces, such as gravity, centrifugal force, and pressure differences [98]. The polymer droplet expands outward in the direction of decreasing surface tension and forms a finger shape [99]. This process is defined as jet initiation. Due to the high viscosity of the spinning fluid, the ejected fluid does not break into individual droplets but forms a continuous jet. The schematic diagram demonstrating the initial jet evolution is presented in **Figure 2-4**. During the jet extension stage, the polymer jet leaving the orifice continues to move outward and stretch under the action of inertia. At this stage, the polymer jet is subjected to centrifugal force, forming a curved jet around the circumference of the spinning vessel. The air resistance at the air-liquid interface promotes the elongation and thinning of the jet.

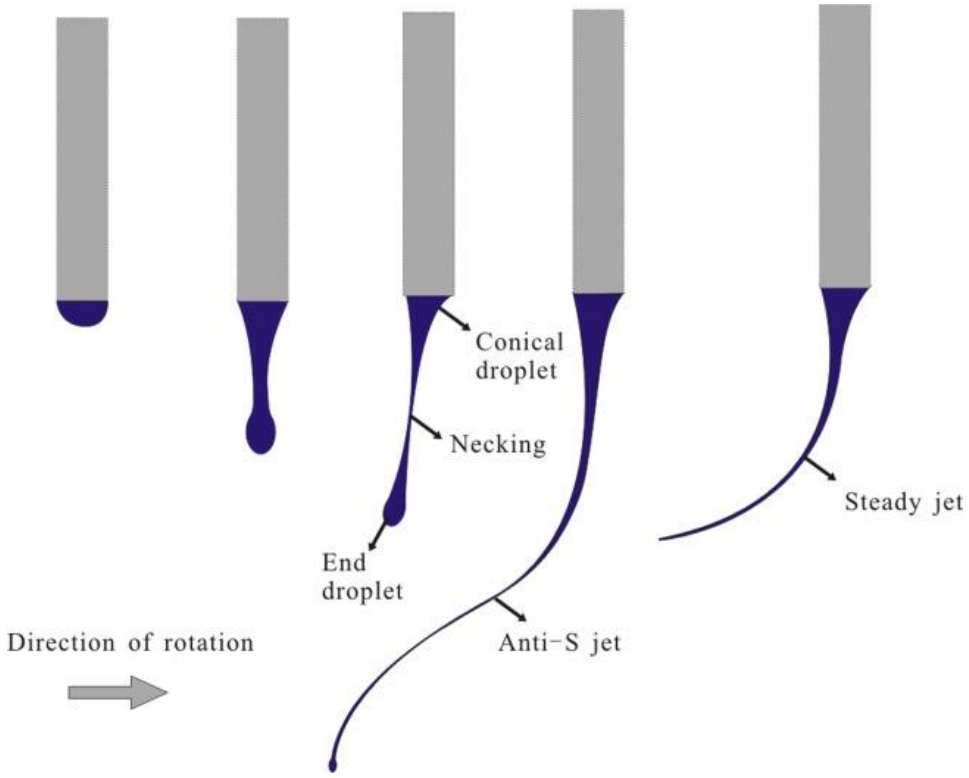

Figure 2-4 Schematic diagram of the initial jet evolution in gyratory spinning. Reproduced (Adapted) with permission from ref [99] Copyright © 2014, John Wiley and Sons.

During the jet movement, the solvent gradually evaporates, resulting in the further thinning of polymer jets. The dry fibres are eventually deposited on the collector. The fibres produced by this process generally have higher alignment than electrospun fibres that undergo whipping motions.

System Parameters

The electrical motor is one of the most significant components of the PG apparatus. Once energised, the motor drives the spinning vessel to rotate at a high speed (up to 36 000 rpm). The polymer fluid loaded in the vessel is subjected to centrifugal force (F_{centri}). According to Newton's second law:

$$F_{centri} = m\omega^2 r$$

Equation 2-1

where, *m* is the mass of the spinning fluid, *ω* and *r* are the rotational speed and the radius of the vessel, respectively. From **Equation 2-1**, it is evident that the centrifugal force acting on the spinning fluid increases with higher rotational speeds. Only when the centrifugal force is sufficient to overcome the surface tension of the spinning fluid, spinning jets can be formed and ejected from the orifices. The minimum rotational speed required to generate sufficient centrifugal force to overcome the surface tension of the polymer fluid is referred to as the critical rotational speed. Below this critical speed, the centrifugal force is insufficient to produce spinning jets. In addition, the solvent may separate from the polymer at a low rotational speed. Solution loss occurs in this scenario [15].

After the polymer fluid is ejected from the vessel, these jets are simultaneously subjected to centrifugal force and air resistance (F_{air}):

$$F_{air} = \frac{1}{2}\pi C\rho A\omega^2 D^2$$

Equation 2-2

where, *C* is the numerical drag coefficient, *ρ* is the air density, *A* is the cross-sectional area of the spinning jet, *ω* is the rotational speed of the jet, and *D* is the diameter of the jet path [92]. As indicated by **Equation 2-1** and **Equation 2-2**, both the centrifugal force and air resistance acting on the spinning jets increase with the rotational speed of the spinning vessel. This enhancement promotes jet stretching, facilitating the formation of finer, elongated fibres. Conversely, at low

rotational speeds, PG usually produces thicker and shorter fibres or droplets due to insufficient stretching.

The most prominent feature of PG is the integration of a high-pressure system within the gyratory spinning process. Working pressure plays a critical role in influencing fibre diameter. Compared to conventional pressure-free centrifugal spinning, the incorporation of gas pressure in PG significantly increases the acceleration of the spinning flow. As a result, the spinning flow ejected from the orifices has a larger initial velocity. Increased pressure also reduces the time required for spinning jet formation. Moreover, the elevated gas pressure enhances jet stretching, enabling the production of finer fibres. This effect arises because the higher pressure boosts the kinetic energy of the spinning jets, facilitating additional elongation during the stretching phase. According to the microscopic jet flow model reported by Gañán-Calvo et al., the liquid jet diameter (d_j) :

$$d_j \cong \left(\frac{8\rho}{\pi^2 \Delta p}\right)^{1/4} Q^{1/2}$$

Equation 2-3

where, ρ is the density of the liquid, Δp is the pressure difference and Q is the flow rate [100]. **Equation 2-3** suggests the inversely proportional relationship between jet diameter and pressure difference, which is consistent with experimental results [95].

The working pressure also affects fibre morphology and alignment. The higher working pressure results in greater kinetic energy of the spinning jets but also

introduces greater kinematic instability, which can result in the formation of beads and reduced fibre alignment [101]. As the solvent evaporates from the spinning jets, the enthalpy of vaporisation causes a local temperature drop [102]. This temperature reduction can lead to condensation of water vapour on the fibre surface. Upon evaporation of these water droplets, their imprints remain, creating a porous fibre surface. Higher working pressures accelerate solvent evaporation, intensifying the formation of surface pores and contributing to the unique morphology of the fibres [15].

The spinning vessel is also an important component of a PG setup. During the spinning process, the loaded spinning fluid slips on the vessel wall and extrudes from the liquid channels while overcoming its surface tension. Therefore, the materials, dimensions, and geometry of the vessel have a great impact on fibre morphology. In the reported studies, the PG vessel is typically constructed from materials such as metal (aluminium or steel) or plastic, consisting of a perforated reservoir and an adapted lid [95, 97]. Different friction factors exist between the spinning fluid and the vessel made of different materials, which affect the flow behaviour of the spinning fluid and the formation of spinning jets. Additionally, the choice of vessel material significantly impacts performance due to differences in density and other properties. Low-density metals with relatively high melting points, such as aluminium, are often preferred for their lightweight and durability. Vessels made of steel, on the other hand, offer superior corrosion resistance, making them ideal for use in chemically aggressive environments. Optically transparent plastic vessels offer a distinct advantage by allowing real-time observation of fluid behaviour within the vessel, which is invaluable for experimental investigations and process optimisation.

Fibre morphology is also affected by the vessel dimension. From **Equation 2-1** and **Equation 2-2**, the centrifugal force and air resistance of the spinning fluid increase with the increase of the vessel radius. Therefore, at a constant rotational speed, increasing the radius of the spinning vessel facilitates the formation and stretching of the jets, thereby reducing fibre diameter.

In a typical PG setup, multiple orifices (up to 24) with a diameter of 0.5 mm are evenly distributed on the perimeter of the vessel wall at equal intervals, resulting in the formation of various spinning jets at the same time [15, 95, 103, 104]. Thus, PG is considered a very promising scalable fibre manufacturing technology. In addition, vessels featuring multi-layer reservoirs have been used for the preparation of core-sheath fibres [105, 106]. The inner and outer reservoirs are loaded with different polymer solutions, enabling the formation of the core and the sheath structures of dual-layer fibres, respectively.

Fibre morphology is also significantly influenced by the type of collection method used. In addition to the typical plate collectors (**Figure 2-3**), surrounding collection meshes and collection rods (**Figure 2-5**) are also used in PG. Compared to the relatively air-closed environment of plate collectors, the collection meshes and collection rods are more favourable for solvent evaporation due to improved air convection. This setup also facilitates better fibre alignment during collection. Furthermore, the collection distance plays a crucial role, as it directly impacts fibre formation and overall morphology. When the collection distance is too short, the jets undergo insufficient stretching, resulting in thicker and shorter fibres. Additionally, a very short distance may hinder solvent evaporation, leading to bead formation or the deposition of wet jets on the collector [107]. Conversely,

increasing the collection distance facilitates jet elongation to reduce fibre diameter. However, an excessively long collection distance will cause jet rupture, reducing fibre yield and compromising the collection process. Balancing the collection distance is therefore crucial for achieving optimal fibre morphology and yield. The optimal collection distance of the PG system varies with solution properties, solvent volatility, flexibility and ductility of the polymer, ambient temperature, relative humidity, etc.

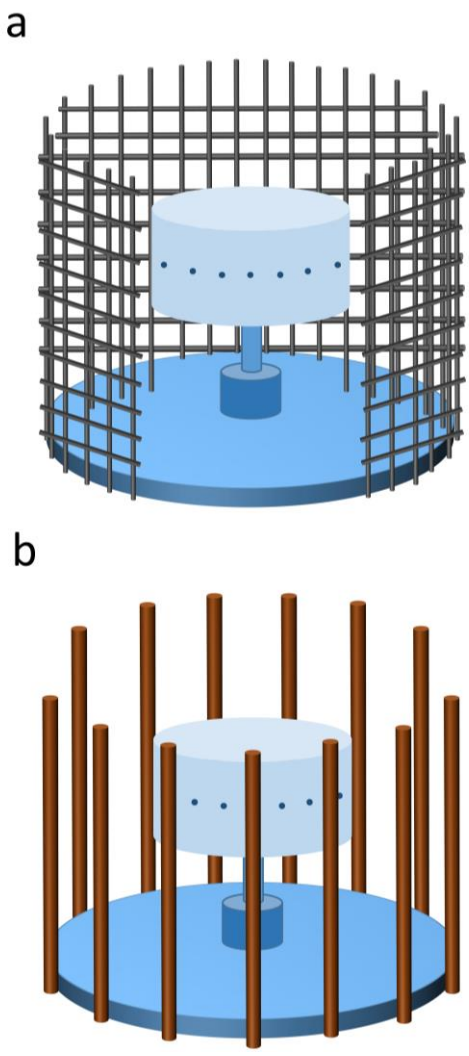

Figure 2-5 Different collector designs in pressurised gyration: (a) mesh-like collector and (b) rod collector.

Spinning Fluid Properties

The spinnability of spinning fluid (polymer solution/polymer melt) and the fibre morphology in PG are significantly affected by the inherent properties of the spinning liquid, such as molecular configuration, molecular weight, polymerisation, crystallinity, concentration, viscosity, surface tension and solvent volatility. Among them, the influence of surface tension and viscosity plays a dominant role in PG, while other liquid properties affect the spinning process by changing these two main properties.

Not all polymer liquids form fibres through the PG process. The ability of the spinning fluid to be stretched into fine jets is referred to as its spinnability, which is dependent on its viscoelasticity [108]. In general, the viscosity of a polymer solution increases with the increase of its concentration. For successful jet formation, the solution concentration must reach a critical threshold, which is determined by the polymer's molecular weight and solubility. At this critical concentration, the viscoelastic properties of the solution provide sufficient molecular entanglement to support the formation of stable spinning jets. Polymer solutions with concentrations below the critical threshold only form droplets rather than jets due to insufficient viscoelasticity. The increase in solution viscosity imposes greater resistance to centrifugal force and dynamic fluid blowing, as well as inhibits solvent evaporation [95]. Thus, for spinnable polymer solutions, the fibre diameter tends to increase with the increase of the solution concentration. However, when viscosity becomes excessively high, the centrifugal force is unable to overcome the surface tension of the solution. Spinning jets cannot be formed in this scenario. The bead formation is also affected by the solution

concentration. With the increase in concentration, the product of PG under identical working parameters gradually transitioned from beads to bead-on-string fibres, and finally to bead-free smooth fibres [109]. For polymer melts, the viscosity is typically controlled by adjusting the polymer molecular weight and processing temperature. **Table 2-1** summarises the effects of various parameters on the properties of the produced fibres.

Table 2-1 The effects of system parameters and spinning fluid properties on fibre morphology in pressurised gyration.

		Fibre Diameter	Bead	Others
System Parameters	**Rotational Speed** ↑	↓	↓	Fibre length ↑ Bead size ↓ Uniformity ↓
	Working Pressure ↑	↓	↑	Fibre length ↑ Bead size ↑ Uniformity ↓ Yield ↑
	Collection Distance ↑	↓		Fibre length ↑ Uniformity ↓
	Infusion Flow Rate (PCIG) ↑	↑	↑	Yield ↑
	Melting Temperature (PMG) ↑	↓		Surface roughness ↑
Spinning Fluid Properties	**Molecular Weight** ↑	↑	↓	Bead size ↑ Fibre length ↓
	Concentration ↑	↑	↓	Bead size ↑ Fibre length ↓
	Solvent Volatility ↑	↓		Pore size ↑

Others	**Temperature** ↑	Solvent evaporation ↑
	Humidity ↑	Pores ↑

*↑ and ↓ denote increase and decrease respectively. PCIG and PMG denote pressure-coupled infusion gyration and pressurised melt gyration respectively. It should be noted that these are the most common overall outcomes. Exceptions may exist for some polymer systems used.

Sister Technologies

Although PG has achieved a production efficiency that far surpasses that of electrospinning, there are still limitations [95]. The typical PG device cannot support the continuous spinning process. To advance the industrialisation of this technique, Hong et al. introduced a syringe pump into the device to automate the feedstock loading process, named pressure-coupled infusion gyration (PCIG) (**Figure 2-6**) [110].

Polymer solutions can be continuously fed into the spinning vessel at a controlled infusion flow rate, enabling precise regulation of fibre diameter, diameter distribution, and morphology. In addition, the increasing infusion flow rate effectively increases the fibre yield, highlighting its potential for industrial uses. Compared to conventional PG, PCIG produced fibres with smaller diameters under the same solution properties and system parameters. The interaction effects of key parameters, including solution concentration, working pressure, rotational speed and infusion flow rate, on fibre diameter in PCIG have been thoroughly studied. Hong and coworkers [111, 112] developed effective and reliable mathematical models to describe these interactions, demonstrating high consistency with experimental observations.

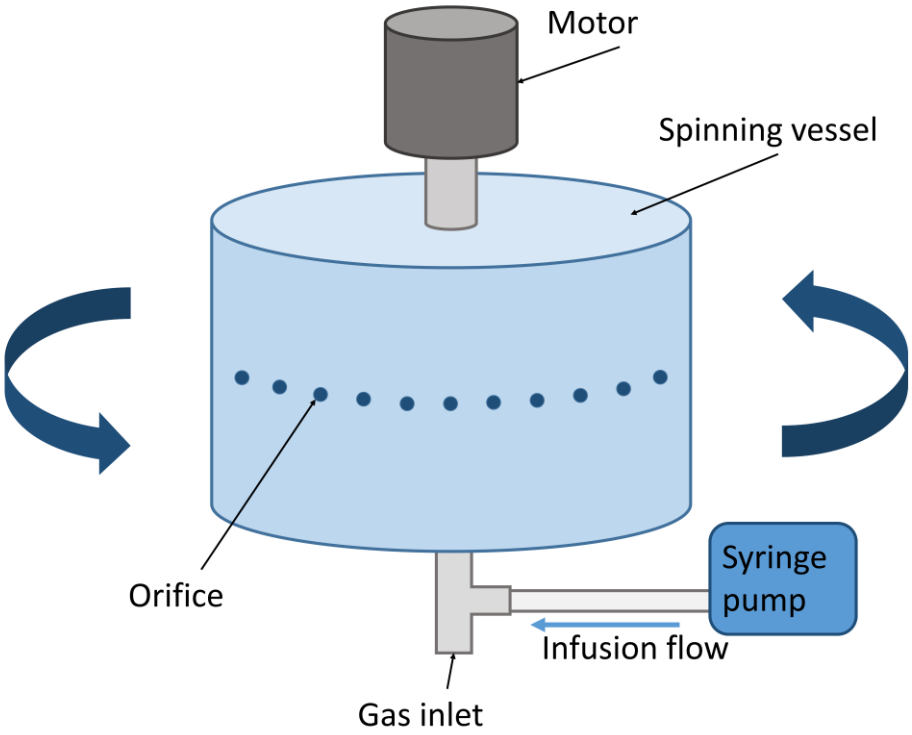

Figure 2-6 Schematic diagram of pressure-coupled infusion gyration.

Furthermore, to address the potential toxicity and environmental concerns associated with chemical solvents, as well as to facilitate the spinning of polymers with limited solubility, Xu et al. [113] introduced pressurised melt gyration (PMG), a method that combines the features of melt spinning and conventional PG (**Figure 2-7**)

In the PMG setup, a heating gun is used to elevate the temperature of the spinning vessel, reaching up to 600 °C, resulting in a molten polymer. The system is equipped with an *in-situ* thermocouple to monitor and control the temperature. The increased temperature reduces the viscosity of the molten polymer, which in turn promotes the formation of finer fibres. Using this innovative approach, Xu [113] successfully fabricated Ag nanoparticle-loaded PCL scaffolds,

demonstrating exceptional antibacterial properties and cell viability, all without the use of chemical solvents.

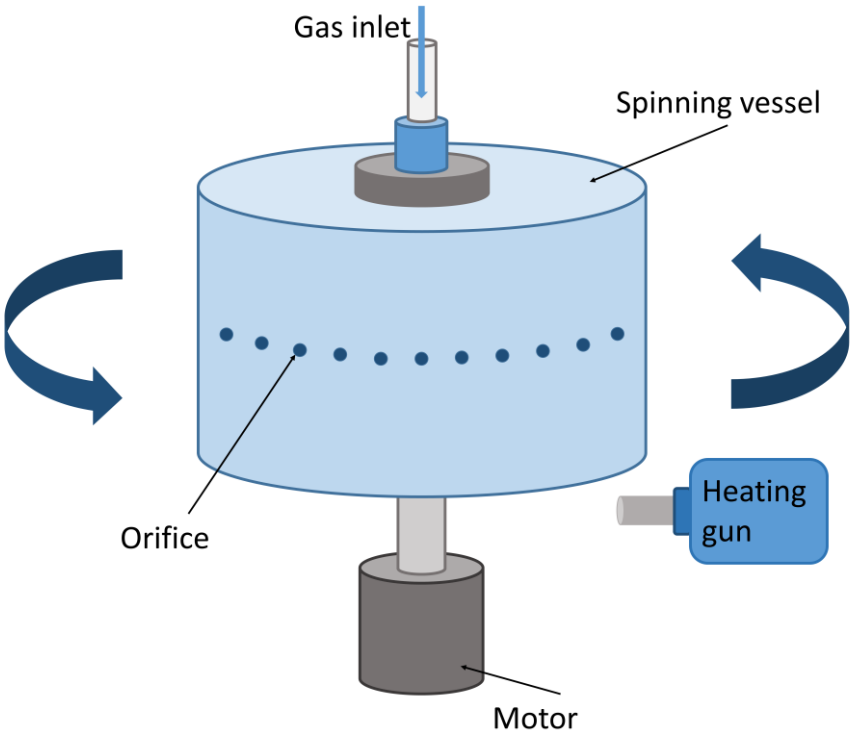

Figure 2-7 Schematic diagram of pressurised melt gyration.

Biphasic fibres can be produced through the multi-layer design of the spinning vessel in core-sheath PG [105, 106]. As shown in **Figure 2-8**a, the spinning vessel of core-sheath PG features a dual-layered reservoir, with the inner and outer reservoirs used to load different polymer solutions to form the core and sheath structures of the fibres, respectively.

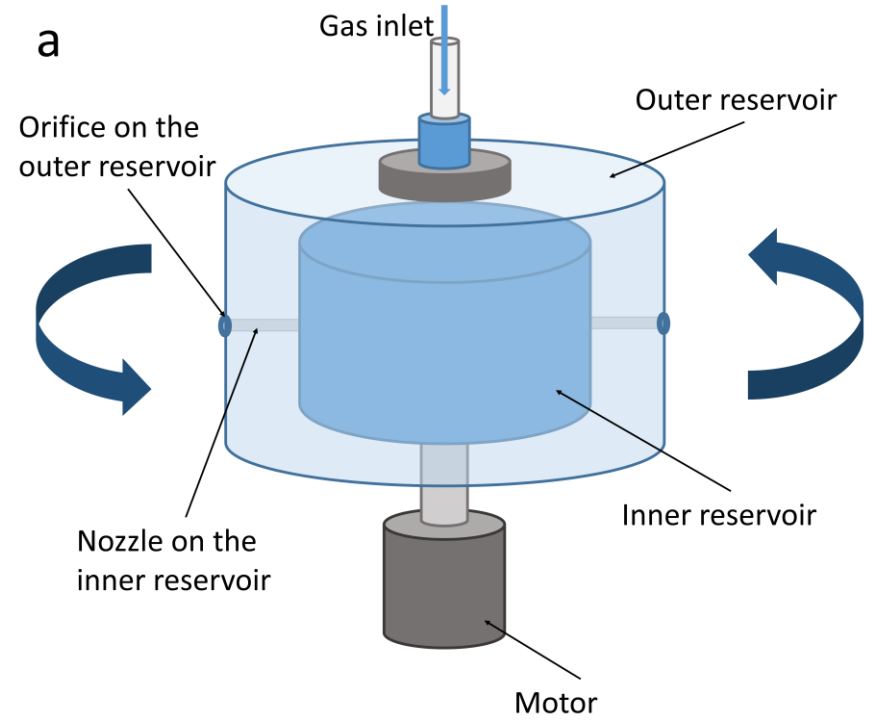

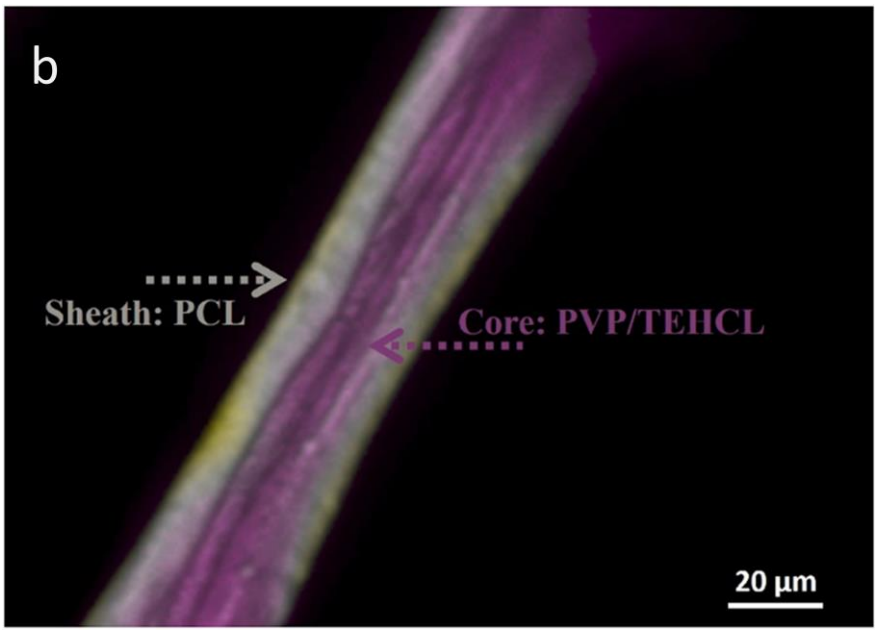

Figure 2-8 (a) Schematic diagram of core-sheath pressurised gyration and (b) confocal microscopy image of PVP-PCL core-sheath fibres. Reproduced (Adapted) with permission from ref [114] Copyright © 2022, Elsevier.

To achieve a uniformly encapsulated core-sheath structure, the essential condition is the flow synchronisation of the inner and outer polymer solutions.

Therefore, prior to the spinning process, the flow rate and production rate of the spinning solution loaded in the outer reservoir are required to be tested. Then the flow of the inner solution will be manipulated to match a synchronous flow. In core-sheath PG, the liquid volume ratio of core-solution and sheath-solution is an important factor. A portable core-sheath PG device designed by Alenezi et al. [115] has been developed to achieve continuous large-scale production of core-sheath nanofibres in a facile step.

In core-sheath fibres, the core solid and the sheath layer are formed from different polymers (**Figure 2-8**b), providing different physical and chemical properties [116]. The outer sheath of the fibre can serve as a protective barrier, effectively delaying the release of the therapeutic agents loaded in the core layer over an extended period. Alternatively, the active substance can be incorporated directly into the sheath layer, facilitating enhanced contact with the target site for immediate therapeutic action. In this case, a more robust and durable material can be used for the core layer, providing enhanced structural support. By varying the fibre design, the sheath-core configuration can be optimally tailored to maximise the desired effect, offering flexibility in therapeutic strategies. Core-sheath polymer fibres produced by core-sheath PG are fascinating candidates for biomedical materials that are used in tissue engineering scaffolds, drug release, and wound healing bandages [114, 117].

Fibres Produced by Pressurised Gyration

Thus far, there has been a wide variety of polymeric fibres produced by PG and its sister technologies. The applications of these fibrous products span a wide range of areas, especially in filtration and healthcare. Compared with

electrospinning, PG averts the influence of high voltage on sensitive materials, as well as has wider options in materials and solvents due to its controllable environmental conditions. In addition to common synthetic polymer fibres (such as PEO, PCL, PVP, poly(methyl methacrylate) (PMMA), polyacrylonitrile (PAN), polylactic acid (PLA), etc.) [95, 101, 103, 118-121], there are also biopolymer fibres synthesised using PG, including silk fibroin, polyhydroxyalkanoates (PHA), starch, etc [122-125]. These fibres have broad prospects in biomedical applications due to their inherent biocompatibility and environmental friendliness. Moreover, ceramic fibres, such as polymethyl-silsesquioxane (MK resin), polymethylphenyl-silsesquioxane (H44 resin), have been successfully fabricated by PG [126]. The products of PG are diverse in terms of their structure. Besides uniform solid fibres, PG has been used to produce beaded fibres, multi-layer fibres, and microbubbles [105, 109, 127, 128]. Microbubbles are a promising material in diagnosis, therapeutic applications, targeted drug delivery, etc [129-132]. Such many successful cases undoubtedly validate the practicability and extensibility of PG technology in the preparation of micro/nano-materials. **Table 2-2** summarises the polymers processed using PG and its sister technologies.

Table 2-2 Polymer materials processed by pressurised gyration, detailed information of final products and their potential applications.

Polymer	Molecular Weight	Solvent	Concentration	Agent	Product Type	Average Fibre Diameter	Application	Technique	Ref.
Polycaprolactone (PCL)	$M_w = 8\times10^4$ g/mol	acetone	5-30% (w/v)		beads, beaded fibres, fibres	bead: 145-658 µm fibre: 3-28 µm	drug delivery	PG	[109]
		chloroform	15% (w/v)	nano-clay (2-5 wt%)	microfibre scaffolds	1.1-3.9 µm	bone tissue regeneration	PG, Nozzle-PG	[101, 133]
			10-12 wt%	tetracycline hydrochloride (2 wt%)	porous fibres	1.7-5 µm	drug release, wound dressing	PG	[114, 134]
	$M_n \approx 8\times10^4$	chloroform	15% (w/v)	cinnamon powder (250-500 mg/mL)	fibre meshes	1.7-6 µm	antimicrobial fibres, wound healing bandages	PG	[135, 136]
			molten liquid (95-200°C)	Ag nanoparticle (0.01% (v/v))	microfibre scaffolds	14-38 µm	antibacterial fibres, muscular tissue engineering	PMG	[113]
Polyethylene oxide (PEO)	$M_w = 2\times10^5$ g/mol	water	5-21 wt%	DsRed-AuBP2-engineered protein, Au nanoparticle	nanofibres	50-1085 nm	aligned nanofibres	PG, PCIG, Nozzle-PG, Infusion Gyration	[95, 97, 101, 112, 123, 137]

Continued

		N,N-dimethyl-formamide (DMF)	30% (w/v)		nanofibres	≈ 290 nm		PG	[138]
		chloroform	20% (w/v)	hydroxyapatite (HA, 10 wt%)	nanofibre scaffolds	≈ 800 nm	targeted therapy	PG	[139]
Poly(methyl methacrylate) (PMMA)	M_w = 1.2×10^5 g/mol	chloroform, acetone, DMF, ethyl acetate, and dichloromethane (DCM)	20 wt%	graphene nanoplalete (0-8 wt%), graphene oxide nanosheet (0-8 wt%), tungsten oxide nanoparticle (0-8 wt%), W-Ag-Cu nanoparticle (0-0.5 wt%)	smooth/porous microfibres	1-20 µm	antimicrobial fibres	PG	[118, 140-144]
Polyvinyl-pyrrolidone (PVP)	M_w = 2.8×10^4-1.5×10^6 g/mol	phosphate buffered saline (PBS), ethanol	10-30% (w/v)		nanofibres	462-971 nm	pharmaceutical sciences, binders, drug delivery	PG	[103, 145]
	M_w = 1×10^5 -1.5×10^5 g/mol	ethanol	15% (w/v)	Ibuprofen (10-50% (w/v))	microfibres	1.2-5.4 µm	oral administration, drug delivery	PG	[145]
	M_w = 1.3×10^6 g/mol	ethanol	10-15% (w/v)	amphotericin B (5 wt%), itraconazole (2.5 wt%)	uniform and aligned fibres	1.3-3.5 µm	drug delivery	PG, Nozzle-PG, Core-sheath PG	[101, 114, 144]
		a mixture of ethanol and methanol (4:1, v/v)	10-20% (w/v)	pioglitazone hydrochloride (12 mg/mL)	nanofibres	0.6-3.2 µm	biodegradable drug release system	PG	[146]

Continued

			4-15% (w/v)		nanofibres	200-520 nm		PG	[138, 147]
Poly-acrylonitrile (PAN)	M_w = 1.5×10^5 g/mol	DMF	8-10 wt%	graphene nanoplatelets (0-8 wt%), graphene oxide (3-10 wt%)	carbon fibres	0.7-20 μm	conductive fibre, energy storage devices	PG	[119, 148]
			10 wt%	carbon nanotubes (0-0.5 wt%)	carbon nanofibres	400-800 nm	energy storage device, supercapacitors	PG	[120]
Poly(vinyl alcohol) (PVA)	M_w = 1.46×10^5-1.86×10^5 g/mol	water	10% (w/v)	lysozyme (4% (w/v)), gold nanoparticle	microbubbles	10-250 μm	antibacterial fibres, biosensors, intracellular probes, ultrasound contrast agents, drug delivery	PG	[127, 128]
Polylactic acid (PLA)	M_w = 1.1×10^5 g/mol	chloroform	8-15% (w/v)	progesterone (10 wt%)	drug-loaded fibrous patches	6.8-26 μm	sustained drug release system	PG	[121, 134]
Polyvinyl-idene fluoride (PVDF)	M_w = 2.75×10^5 g/mol	a mixture of DMF and acetone	15-25% (w/v)		beaded fibres	1.6-26 μm	face masks	PG	[144, 149]
Polyethylene (tere-phthalate) (PET)	$M_w = 1\times10^5$ g/mol	trifluoro acetic acid, trichloroacidic trichloro acetic acid	20 wt%		nanofibres	290-714 nm		PG	[150]
Nylon 6,6	$M_w = 3\times10^4$ g/mol	formic acid	5-20 wt%	Ag nanoparticle (1-4 wt%)	nanofibres	50-500 nm	antibacterial fibres	PG	[151]

Continued

Thermo-plastic polyurethane (TPU)		DMF	15-25 wt%	graphene nanoplatelet (5 wt%)	microfibres	1-13 μm	fuel cells, electronic packaging	PG	[152]
Poly-acrylamide (PAM)		(hydrogel)		montmorillonite (0.89 wt%), chitosan (0.16 wt%)	nanocomposite hydrogels in rod/ball shapes	≈ 5.5 μm		PG	[153]
Poly(N-isopropylacrylamide) (PNIPAm)	$M_w = 3\times10^5$ g/mol	a mixture of chloroform and ethanol (2:1, v/v)	20% (w/v)		pore-free fibres	≈ 6.3 μm		PG	[144]
Cyclodextrin		water	180-220% (w/v)		pore-free fibres	5.5-6.5 μm		PG	[154]
Polyhydroxyalkanoates (PHAs)	$M_w > 4\times10^5$ g/mol	chloroform	7.4 wt%	HA nanopowder (10 wt%)	aligned porous fibres	2.5-9.1 μm	hard (bone) and soft (nerve and cardiovascular) tissue engineering	PG	[124]
Silk fibroin (SF)		1,1,1,3,3,3-hexafluoro-2-propanol (HFIP)	8-12% (w/v)		pore-free fibres	0.8-30 μm	tissue engineering, filtration	PG	[122, 123]
PCL/PVA	$M_w = 8\times10^4$ /5×10^4 g/mol	chloroform/ water	10 wt%/ 10wt%	HA nanoparticle (1-10 wt%)	core-sheath fibres	3-4 μm	bone tissue engineering	Core-sheath PG	[117]
PCL/bacterial cellulose (BC)	M_w(PCL) = 8×10^4 g/mol	chloroform	12 wt% ($w_{PCL/BC}$ = 9:1-1:9)		composite fibres	5-9 μm		PG	[134]
PEO/PMMA	$M_w = 2\times10^5$/ 1.2×10^5 g/mol	water/ chloroform	15 wt%/ 15wt%	Ag-Cu-W nanoparticle	core-sheath fibres	core: 6-9 μm sheath: 21-32 μm	filtration, tissue engineering	Core-sheath PG	[105]

Continued

PEO/PVP	$M_w = 2\times10^5$ /1. 5×10^6 g/mol	water/ water	15 wt%/ 15wt%		core-sheath nanofibres	331-998 nm		Core-sheath PG	[106]
PEO/PCL	$M_w = 6\times10^5$ /8×10^4 g/mol	water/ a mixture of chloroform and methanol (3:1, v/v)	10 wt%/ 20 wt%		core-sheath nanofibres	≈ 740 nm		Core-sheath PG	[115]
PEO/PLA	$M_w = 6\times10^5$ /1.1×10^5 g/mol	water/ a mixture of chloroform and methanol (3:1, v/v)	10 wt%/ 20 wt%		core-sheath nanofibres	≈ 529 nm		Core-sheath PG	[115]
PEO/sodium carboxy-methyl-cellulose (CMC)	$M_w = 2\times10^5$ /2.5×10^5 g/mol	water/ a mixture of ethanol and water	12.5-15 wt%/ 0-2.5 wt%	Progesterone (0-5 wt%)	composite nanofibres	161-550 nm	drug delivery	PG	[155-157]
PEO/sodium alginate	$M_w = 2\times10^5$ g/mol /medium viscosity	water	11 wt%/ 1 wt%		composite nanofibres	≈ 170 nm	drug delivery	PG	[157]
PEO/poly-acrylic acid (PAA)	$M_w = 2\times10^5$ /4.5×10^5 g/mol	water	11 wt%/ 1 wt%		composite nanofibres	≈ 215 nm	drug delivery	PG	[157]
PEO/starch	$M_w = 2\times10^5$ /1×10^5 g/mol	a mixture of water and dimethyl sulfoxide (DMSO) (1:1, w/w)	7.5-13.5 wt%/ 1.5-7.5 wt%		composite nanofibres	163-285 nm		PG	[125]
PMMA/PAN	$M_w = 1.2\times10^5$ /1.5×10^5 g/mol	DMF	10 wt%/ 10 wt%		nanofibres	≈ 580 nm		PG	[138]

Continued

PMMA/BC	M_w(PMMA) = 1.2×10^5 g/mol	DMF:THF (1:1, w/w)	20-50 wt%/ 5-10 wt%	Cu-Ag-Zn, CuO, Cu-Ag-WC nanoparticle (0.05-1 wt%)	composite fibres	2-36 μm	wound dressing	PG	[158, 159]
PMMA/ poly(l-lactide) (PLLA)	M_w = 1.2×10^5 g/mol/ Mn = 2 500	chloroform	10 wt%/ 10 wt%	a mixture of HA and protein	composite fibres	≈ 17 μm	shape memory fibres	PG	[160]
PVP/PCL	M_w = 1.3×10^6 /8×10^4 g/mol	a mixture of chloroform and methanol (4:1 ,v/v)	12% (w/v) ($w_{PVP/PCL}$ = 6/4, 7/3, 8/2)	glibenclamide (4 mg/mL), pioglitazone (12 mg/mL)	composite nanofibres	677-900 nm	biodegradable drug release system, wound healing	PG	[146, 161]
		ethanol/ chloroform	10 wt%/ 10 wt%	tetracycline hydrochloride (2 wt%)	core-sheath fibres	4.1-5 μm	sustained drug release system, wound healing	Core-sheath PG	[114]
PAN/cellulose acetate (CA)	M_w = 1.5×10^5 /3×10^4 g/mol	a mixture of acetone and DMF (2:1)	10 wt%	vanillin (Kosher)	porous composite fibres	0.5-2 μm	drug release system	PG	[147]
PVA/PCL	M_w = 8.9×10^4-9.8×10^4 /8×10^4 g/mol	water/ a mixture of chloroform and methanol (3:1, v/v)	20 wt%/ 20 wt%		core-sheath nanofibres	≈ 743 nm		Core-sheath PG	[115]
PVA/PLA	M_w = 8.9×10^4-9.8×10^4 /1.1×10^5 g/mol	water/ a mixture of chloroform and methanol (3:1, v/v)	20 wt%/ 20 wt%		core-sheath nanofibres	≈ 542 nm		Core-sheath PG	[115]

Continued

PLA/PCL	M_w = 1.1×10^5 /8×10^4 g/mol	chloroform	12 wt% ($w_{PLA/PCL}$ = 9:1-1:9)		composite fibres	5-19 µm		PG	[134]
		water/ a mixture of chloroform and methanol (3:1, v/v)	20 wt%/ 20 wt%		core-sheath nanofibres	≈ 875 nm		Core-sheath PG	[115]
PLA/BC	M_w(PLA) = 1.1×10^5 g/mol	chloroform	12 wt% ($w_{PLA/BC}$ = 9:1-1:9)		composite fibres	6-19 µm		PG	[134]
PLA/PCL/BC	M_w = 1.1×10^5 /8×10^4 g/mol	chloroform	12 wt% ($w_{PLA/PCL/BC}$ = 7:3:3		composite fibres	≈ 10.7 µm		PG	[134]
Poly(glycerol sebacate) (PGS)/PVA	M_w(PVA) = 3×10^4-7×10^4 g/mol	HFIP	10-15% (w/v) ($w_{PGS/PVA}$ = 55:45)		composite fibres	≈ 16 µm	tissue engineering	PG	[104]
SF/PEO	30% de-gumed/ M_w = 2×10^5 g/mol	water	40-45 wt%/ 1.5-3 wt%		composite nanofibres	0.7-2.1 µm	tissue engineering	PG	[123]
Polymethyl-silsesqui-oxane/PVP	M_w = 9 100 /1.3×10^6 g/mol	a mixture of chloroform and DMF (5:3, w/w)	25 wt%/ 25 wt%		ceramic fibres	10-50 µm		PG	[126]
Polymethyl-phenyl-silsesqui-oxane/PVP	M_w = 2 100 /1.3×10^6 g/mol	a mixture of chloroform and DMF (5:3, w/w)	20.7 wt%/ 20.7 wt%	graphene (3%)	ceramic fibres	1-8 µm		PG	[126]
Phenolic resin/PVP		DMF	10-25 wt%/ 10 wt%	graphene nanoplatelet (5 wt%)	composite fibres	2-8.5 µm	fuel cells, electronic packaging	PG	[152]

2.3.4 Wet Spinning

Although the aforementioned spinning technologies have been widely used to produce a variety of polymeric fibres with notable success, they still face significant challenges when applied to biopolymers. One major issue is the solubility of biopolymers. Many biopolymers, such as Alg, chitosan, gelatin, and cellulose, are insoluble in common volatile organic solvents and can only be dissolved in water or complex solvent systems [162-165]. These solvents have limited volatility, making it difficult to achieve efficient polymer/solvent separation in electrospinning and other spinning technologies. In contrast, wet spinning offers a more suitable and effective approach for processing biopolymers, while preserving the properties of the biopolymers [166].

Wet spinning involves extruding a polymer solution directly into a coagulation bath through a spinneret/needle, forming continuous filaments [167]. Within the coagulation bath, the solvent is removed, resulting in the solidification of the polymer. The coagulant typically consists of a nonsolvent or a nonsolvent/solvent mixture that is incompatible with the polymer being processed [168]. After extrusion, the filaments undergo a series of mechanical stretching, washing, and drying steps to produce long, continuous fibres, which are then collected, as shown in **Figure 2-9**.

Rather than relying on solvent evaporation, wet spinning forms fibres through the diffusion and exchange of the solvent and the nonsolvent phases in the coagulation bath [168, 169]. In certain cases, the coagulation process is accompanied by chemical transformations, such as ion exchange reactions

between the polymer molecules and the coagulant [170], which can contribute to the structural integrity and functionality of the resulting fibres.

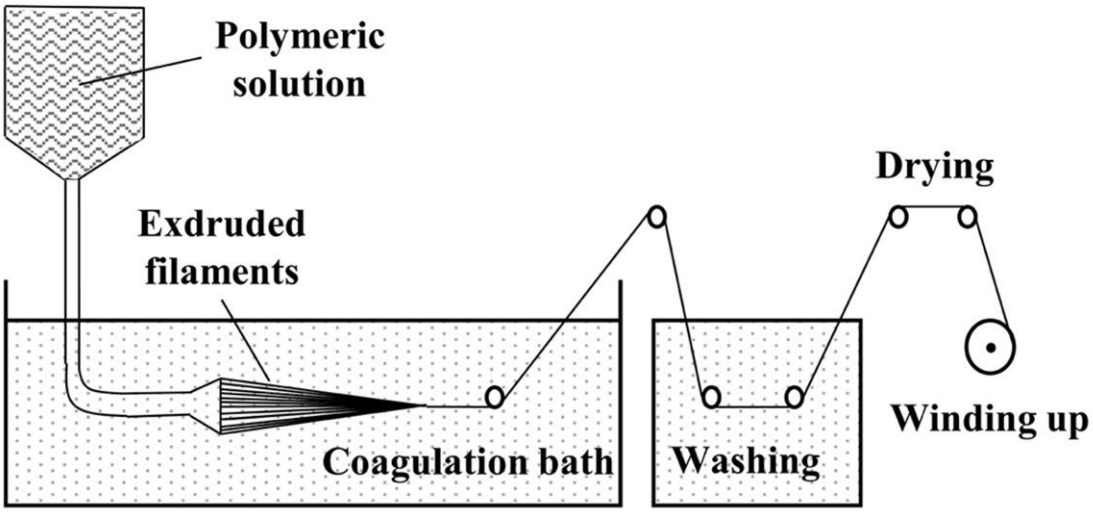

Figure 2-9 Schematic diagram of a wet spinning setup. Reproduced (Adapted) with permission from ref [166] Copyright © 2017, John Wiley and Sons.

As a result, the surface morphology, size, and properties of fibres produced through wet spinning are profoundly influenced by the conditions of the coagulation process. Critical factors such as coagulant composition, ion concentration, temperature, and coagulation time can be adjusted to control fibre morphology. Besides coagulation conditions, polymer viscoelasticity, extrusion rate, mechanical stretching, and drying conditions significantly impact fibre characteristics, including cross-sectional shape, diameter uniformity, porosity, surface roughness, and mechanical properties [171-174]. By carefully optimising these parameters, the desired fibre attributes can be achieved.

2.4 Applications of Polymeric Fibres

In terms of fibre morphology and properties, gyrospun fibres are highly similar to electrospun fibres, indicating that these fibrous products can be theoretically used in the same application areas. Although in this thesis I highlighted the biomedical applications such as tissue engineering, drug delivery, wound healing, targeted therapy, etc., fibres produced using PG have encouraging prospects in filtration, energy storage, catalysis, biosensors, electronics, and optical components [120, 149, 175-178].

2.4.1 Biomedical Applications

Tissue Engineering

Polymeric fibres play significant roles in tissue engineering as scaffolds supporting cell seeding and tissue growth, as well as carriers of bioactive factors [179-181]. Polymer fibrous scaffolds serve as a temporary extracellular matrix (ECM) in tissue engineering. The desired 3D structures of these polymer scaffolds provide specific mechanical and biological properties to modulate cellular behaviour [182]. The aligned orientation of fibres induces the polarisation and migration of cells along the fibre direction, accelerating wound closure [183, 184]. Seeding cells on gyrospun scaffolds, which typically have a highly aligned orientation, promotes cellular activities. This is due to the regular or defined architecture of most of the ECMs in the human body [185]. In addition, the surface topography of gyrospun fibres is determined by the solvent types and the environmental conditions, which is tunable to form the desired pore size and porosity for cell infiltration [186, 187]. Gyrospun fibrous scaffolds have been

reported to be promising material candidates for tissue engineering. For example, the non-woven PCL scaffold fabricated by PMG technology by Xu et al. [113] showed remarkable attachment, growth, and proliferation results for myoblasts. The fibre surface roughness and porosity of these scaffolds can be tuned by melting temperature to promote muscular tissue regeneration. Moreover, the PGS/PVA blended fibrous scaffold spun by PG possessed unique biocompatibility and non-toxicity [104]. The dermal fibroblast cells that adhered to these scaffolds showed superior cell viability, which is a promising material for soft tissue engineering. Kundu et al. [133] incorporated composite nanoclay and hydroxyapatite into PCL fibres by PG. The fabricated fibrous scaffolds had good cell viability and promoted osteogenic differentiation, calcium deposition, and collagen formation. Their results also showed that the osteogenic differentiation of mesenchymal stem cells (MSCs) was enhanced with the addition of PCL fibres. The PHA fibres spun by PG not only enhanced bone regeneration but also showed great application potential in soft tissue engineering such as nerve and cardiovascular [124]. Additional growth factors are not required of PHA scaffolds in tissue engineering, which is considered a unique advantage of PHA fibres. Heseltine et al. [123] achieved the efficient production of aqueous-based silk fibroin using PG. Osteocytes exhibited significant cellular activity and proliferation on these aligned silk fibroin fibres. The core-sheath fibres manufactured by core-sheath PG is a new fascinating strategy in tissue engineering. The hydroxyapatite-loaded sheath (PVA) provides the environment and conditions required for biological activities in tissue engineering, while the core (PCL) acts as a mechanical support [117].

Drug Delivery

Drug delivery systems are a critical component of disease treatment, playing a pivotal role in achieving optimal therapeutic outcomes. Traditional drug delivery methods, whether oral administration or intravenous injection, usually face the limitations of systemic administration, short-term and uncontrollable release efficacy, fast metabolism, low bioavailability, and the potential for causing drug resistance and cytotoxicity, etc. The new generation of drug delivery systems seeks to overcome these challenges by establishing delivery programs that are stable, controllable, and targeted.

Polymeric fibres, especially nanofibres, are one of the most promising carriers for drug delivery due to the high surface area-to-volume ratio, which allows high loading capacity and high encapsulation efficiency [188-190]. Encapsulating hydrophobic drugs into hydrophilic polymer fibres helps to solve the poor solubility of many drug molecules [191, 192]. The tunable characteristics of polymeric fibres such as fibre diameter, morphology, and porosity help to modulate the release rate for specific therapy. Moreover, controlled release at the action site maximises the effect of the drugs, achieving topical treatment and reducing drug dispersion [193, 194]. PG is considered a potential strategy for fibre drug delivery systems due to its highly controllable system parameters. Progesterone, an endogenous sex hormone that helps the development of the fetus and protects the endometrium during the female reproductive cycle, is widely used for the prevention of pre-term birth [195]. Progesterone was mainly administered by oral or parenteral injection, but these methods have the problem of rapid metabolism and inactivation before taking effect or causing some potential side effects [196].

Fibrous patches for vaginal administration are a promising therapeutic strategy. Brako et al. [155-157] and Cam et al. [121] manufactured progesterone-loaded fibrous constructs with mucoadhesion by PG, which proved to be a successful method for vaginal administration to the treatment of pre-term birth. Oral antidiabetic agent-loaded fibre mats having different release kinetics (burst release or sustained release) produced by PG showed significant effects of accelerating wound healing and reducing inflammation in diabetes treatment [146, 161]. Sustained release delivery systems were reported to exhibit more effective results. Majd et al. produced PVP-PCL core-sheath fibres by core-sheath PG, which showed excellent encapsulation efficiency and controlled release of tetracycline hydrochloride [114]. Core-sheath PG has great potential in the encapsulation and controlled release of growth factors, drugs, and peptides in polymer fibres in a more precise manner.

Wound Dressings

Once the skin is structurally or functionally deficient, its function as the body's protective barrier will be compromised. The invasion of bacteria, fungi, viruses, etc. on the damaged site leads to slow healing, wound infection, and even life-threatening [197]. Wound dressings are used to isolate the wound from pathogens and provide a suitable physiological environment for wound healing [198]. Compared with typical textile dressings, which take effects only by isolation and secretion absorption, fibre-based dressings show greater potential for wound healing [199-201]. The small pore size and high porosity of fibre mats maintain good air permeability while isolating microorganisms. The 3D structure of fibre mats, resembling that of ECMs, combined with their appropriate mechanical

strength, provides an ideal environment to support cell growth, adhesion, and proliferation [202]. The unique high surface area-to-volume ratio of fine fibres is the significant carrier for antibacterial agents and drugs, which has been discussed above. Through the material selection and 3D structure design of fibre products, polymer fibre-based dressings with excellent wound healing efficacy and good comfort were successfully fabricated by PG. With its inherent biocompatibility, bacterial cellulose (BC) is a fascinating candidate for wound dressings. The BC/PMMA binary fibres spun by PG not only overcame the difficulties of BC processing but also achieved the scalable production of natural polymer-based bandages [158]. The BC/PMMA bandages incorporated with metal nanoparticles have been proven to show excellent cell vitality and antibacterial properties, providing an attractive strategy for wound dressings [159]. Ahmed et al. [135, 136] studied the antimicrobial properties and cytotoxicity of cinnamon-containing PCL bandages manufactured by PG, demonstrating the prospects of this natural active substance-based bandage.

PG is also used in clinical imaging, diagnosis, therapy, etc. Mahalingam and his colleagues [127, 128] synthesised protein-coated polymer microbubbles—lysozyme-coated PVA microbubbles, using PG. The Au nanoparticles contained in these microbubbles have excellent chemical stability and biocompatibility, which has the potential for the application of intracellular probes. In addition, the Au nanoparticles can be used to make quantum dots (Q dots) to be imaged in a bimodal way in both fluorescence and ultrasound, which is a complementary technology for ultrasound imaging. These lysozyme-coated PVA microbubbles were demonstrated to have good biosensing abilities.

2.4.2 Filtration

With the development of industrialisation, particulate pollutants in the air have become a thorny environmental problem, threatening public health [203]. Airborne aerosol particles containing bacteria and viruses are one of the main transmission routes of many emerging infectious diseases (EIDs), such as the SARS-CoV-2 that is prevalent worldwide [204, 205]. Besides, water is also an important transmission medium of these tiny particulate pollutants [206]. Separating these pollutants from air/water using filter materials is a crucial process in air/water purification. Fibrous materials with very small diameters have large surface area-to-volume ratios, high porosity, and small pore size, becoming effective filtration pads [207]. PG is an efficient and facile method that can produce polymeric nanofibres with a diameter of less than 500 nm [95, 101, 112, 125, 137, 138, 150, 151, 157]. The unique surface effects of nanofibres effectively improve filtration efficiency. Filtration based on nanomaterials not only physically intercepts particles larger than the pore size through the sieve effect, but also captures extremely fine particles through the diffusion mechanism of the Brownian effect, or collides with these particles [203, 206, 208, 209]. In addition, gas slip occurs on the nanofibres, thereby reducing air resistance [210]. On the other hand, charged particles can be captured by electrostatic attraction with nanofibres [4, 149]. These nanofibre filters are promising to be used in healthcare facilities, electronic component manufacturers, pharmaceuticals, personal protective equipment, and food where superior air purification is desired [206]. Beaded fibres produced by PG, tailored through precise solution properties and processing parameter design, have shown significant potential as advanced filter media [109]. This is due to the fact that the beaded structure increases the

surface area of the filter and is beneficial to optimise the packing density. Moreover, the cavity structure caused by the beads further reduces the pressure drop by providing channels for airflow, which is an important criterion for evaluating filtration efficiency [149]. Wrinkled and porous fibres with a very high specific surface area are also typical products of PG, which can improve the filtration performance of filters [118, 124, 147, 204].

2.4.3 Energy Storage

The development of high-performance energy storage systems is a significant means to reduce the dependence on fossil fuels and promote the transition to clean energy. In addition to large specific surface area and unique surface effects, carbon nanofibres (CNFs) have considerable mechanical strength and excellent electrical conductivity, having great application potential in electrochemical energy storage [211]. CNFs are generally used in rechargeable batteries and supercapacitors as active electrode materials, conductive additives, and metal/metal oxide-loaded substrates [212, 213]. On one hand, carbonaceous materials with high specific surface area and porous structure are conducive to storing ions. On the other hand, reversible surface or near-surface reactions of the loaded metals/metal oxides improve charge storage [214]. Customised electrode materials with desired structures, sizes, morphologies, and compositions are of utmost importance for the development of superior energy storage systems. In addition, carbon nanotubes (CNTs) are also promising energy storage materials due to their higher electrical conductivity and larger surface area than CNFs [215, 216]. PAN is a material widely used to prepare CNFs due to its high carbon yield, high tensile strength, and relatively low price

[217]. The morphology of PAN fibres containing graphene oxide and graphene nanosheets prepared by PG highly depends on the processing parameters (rotational speed, working pressure, solution concentration, etc.) The mechanical properties and electrical conductivity of these fibres have been reported [119, 148]. Zhao et al. [120] used PG to prepare PAN nanofibres loaded with CNTs, achieving a 40% enhancement in specific capacitance along with improved reversibility. These characteristics make the material a promising candidate for rechargeable battery applications.

Regarding commercial applications, the fibre material market is vast in terms of market size and volume. In addition to the aforementioned uses, the aerospace, automotive, and apparel manufacturing sectors have significant shares in the fibre market. The rising need for lightweight components due to the increasing demand for automotive and commercial aviation is propelling the fibre materials market, specifically for those with high-strength modulus and lightweight properties. In addition, polymeric fibres are used in ultra-light clothing, fire-resistant and water-resistant textiles, and high-strength helmets, which also add to the rising demand for fibre materials in the commercial sector.

2.5 Research Gap

Since its inception, research on PG has developed rapidly, establishing a relatively complete processing framework and demonstrating significant potential. PG, emerging as a promising fibre manufacturing technology that can be expanded on a large scale, is likely to become a focal point in industrial fibre production. However, before it can be commercially adopted, addressing the consistency and reliability of the process is crucial. Although the introduction of

high-velocity airflow in PG greatly improves production efficiency, it tends to cause more beads or defects in the fibre than electrospinning. Enhancing the stability of the polymer fluid's motion state is the key to addressing this problem.

Additionally, in the existing literature, PG primarily involves the spinning of synthetic polymer/organic solvent solutions. The preparation of high-content natural polymer fibres remains to be discovered. Given the increasing emphasis on environmental sustainability, developing spinning techniques on natural materials and green solvents is a critical area for future research. Nonetheless, spinning fine biopolymer fibres presents significant challenges, with few successes even in the well-established field of electrospinning.

Addressing these issues will offer valuable insights into enhancing the performance of PG, expanding its application range, and ultimately facilitating its transition to industrial use.

3 Experimental Details

3.1 Spinning Apparatus Design

The spinning devices used in this study include conventional PG and nozzle-PG. The nozzle-PG setups were designed and hand-built by me, with the spinning vessels constructed by the UCL Mechanical Engineering Workshop. **Figure 3-1**a shows that the spinning vessel in the conventional PG setup is a cylindrical container, connected with a nitrogen gas inlet and an electrical motor. The vessel features 24 orifices, each with a diameter of 0.5 mm. In contrast, the nozzle-PG setup replaces these orifices with four external nozzles, each having an inner diameter of 0.5 mm and a length of 5 mm (**Figure 3-2**b). The spinning vessels have identical height and diameter (30 mm × 60 mm) in both setups.

Figure 3-2 presents an inverted nozzle-PG setup integrated with a coagulation bath, specifically designed for the wet spinning of biopolymers. Similarly, the system includes a nozzle-PG vessel fitted with eight external nozzles, connected to a nitrogen gas circuit and an electric motor for jet generation. The vessel chamber has dimensions of 30 mm in height and 60 mm in diameter, with each nozzle featuring an inner diameter of 0.3 mm and a length of 5 mm. Positioned beneath the inverted spinning vessel, the coagulation bath is mounted on an adjustable stage, enabling precise control of the air gap length.

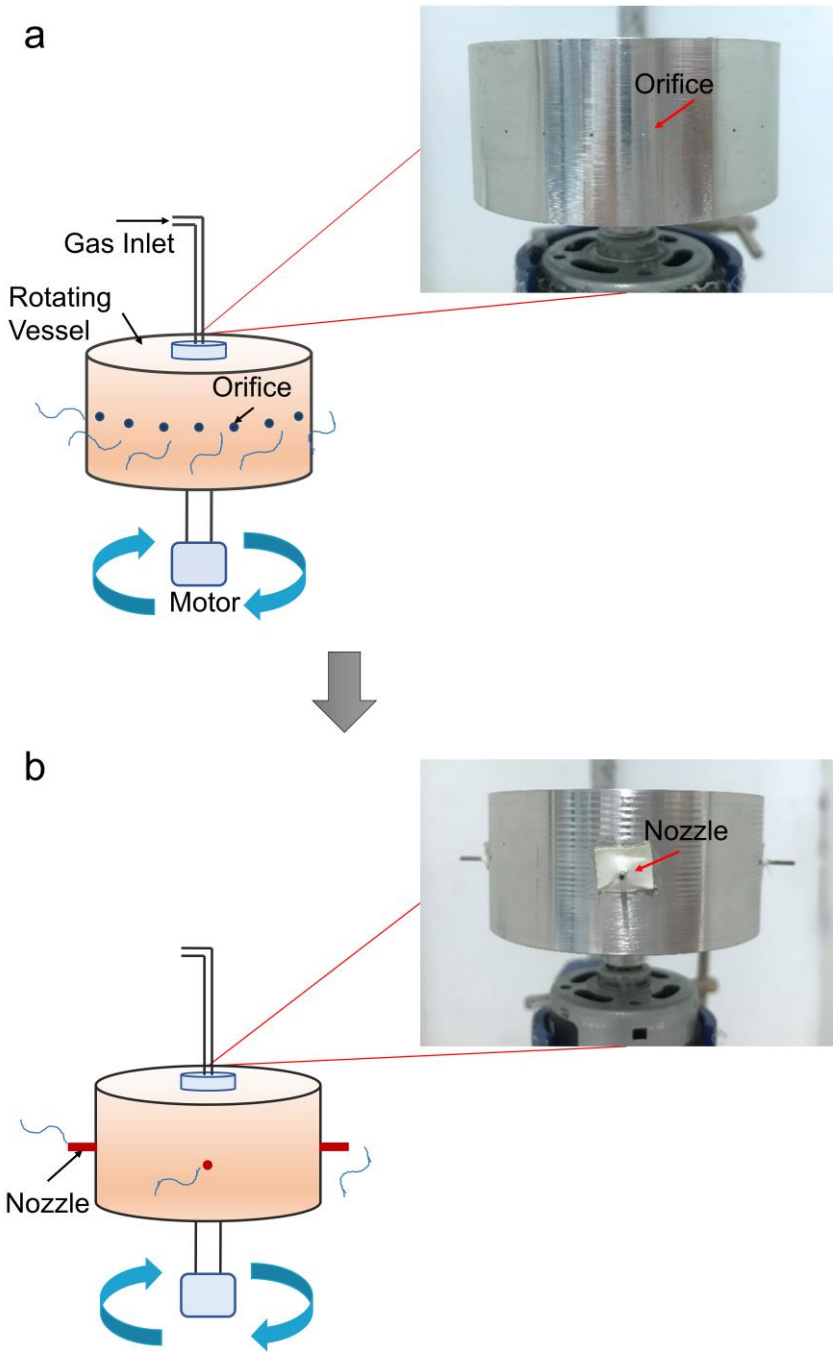

Figure 3-1 Schematic diagrams of (a) conventional pressurised gyration setup with 24 orifices and (b) nozzle-pressurised gyration setup with 4 external nozzles.

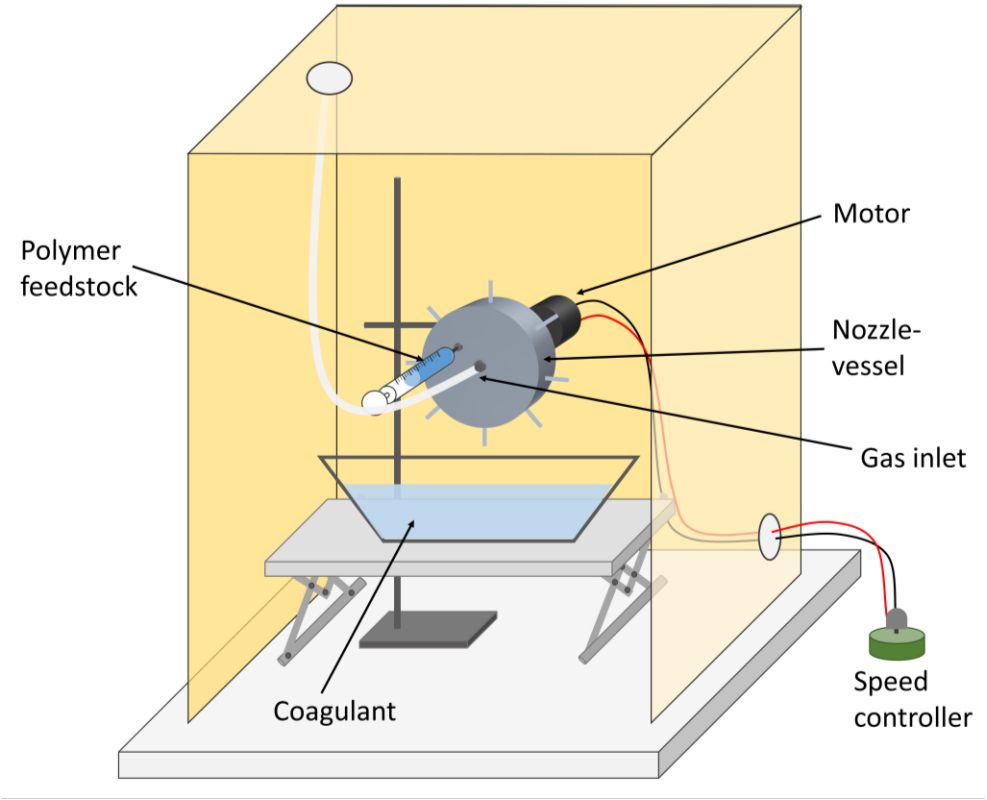

Figure 3-2 Schematic diagram of a modified nozzle-pressurised gyration setup incorporated with a coagulation bath.

3.2 Materials

3.2.1 Polymers and Chemicals

PCL (Mw ≈ 80,000 g/mol, CAS: 24980-41-4), PVP (Mw ≈ 1,300,000 g/mol, CAS: 9003-39-8), and PEO (Mw ≈ 200,000 g/mol, CAS: 25322-68-3) were obtained from Sigma-Aldrich (UK). Sodium alginate powders (Na-Alg, CAS: 9005-38-3) were obtained from Scientific Laboratory Supplies (UK).

The solvents used: ethanol absolute (CAS: 64-17-5) was purchased from VWR Chemicals (France). Chloroform (CAS: 67-66-3), 1-ethyl-3-methylimidazolium acetate (EMIM OAc, CAS: 143314-17-4) and dimethyl sulfoxide (DMSO, CAS:

67-68-5) were obtained from Sigma-Aldrich (UK). A mixture of EMIM OAc and DMSO with a weight ratio of 1:1 was used as the solvent for cellulose in this work. DMSO has been reported to be a good cosolvent for cellulose dissolution in ionic liquids [218].

Phosphate buffer saline (PBS), Tween 20 (CAS: 9005-64-5), glycerol (CAS: 56-81-5), potassium hydroxide (KOH, CAS: 1310-58-3), sodium chloride (NaCl, CAS: 7647-14-5), glacial acetic acid (CH3COOH, CAS: 64-19-7), sodium hypochlorite solution (NaClO, 6-14% active chlorine, CAS: 7681-52-9), sodium hydroxide (NaOH, CAS: 1310-73-2), concentrated 37.5% hydrochloric acid solution (HCl, CAS: 7647-01-0), and Luria-Bertani medium (#L7275) were acquired from Sigma-Aldrich (UK). Calcium chloride ($CaCl_2$, CAS: 10043-52-4) was purchased from Fisher Scientific (UK). Dulbecco's modified Eagle's medium (DMEM), fetal bovine serum (FBS), L-glutamine, and penicillin/streptomycin were purchased from Biochrom (Germany). All chemicals were of analytical grade and were used as received.

Curcumin (CUR, CAS: 458-37-7) was purchased from Cayman Chemical Company (USA). *Cinnamomum verum* in three different forms, ground cinnamon (GC), cinnamon essential oil (CEO), and cinnamaldehyde (CA) was provided by HDDES EXTRACTS PVT LTD (Sri Lanka). The gas chromatography-mass spectrometry (GC-MS) report of the CEO is shown in **Figure 3-3**. The GC-MS spectrum reveals that besides cinnamaldehyde-E, common antibacterial compounds such as eugenol and cinnamyl acetate were detected in CEO.

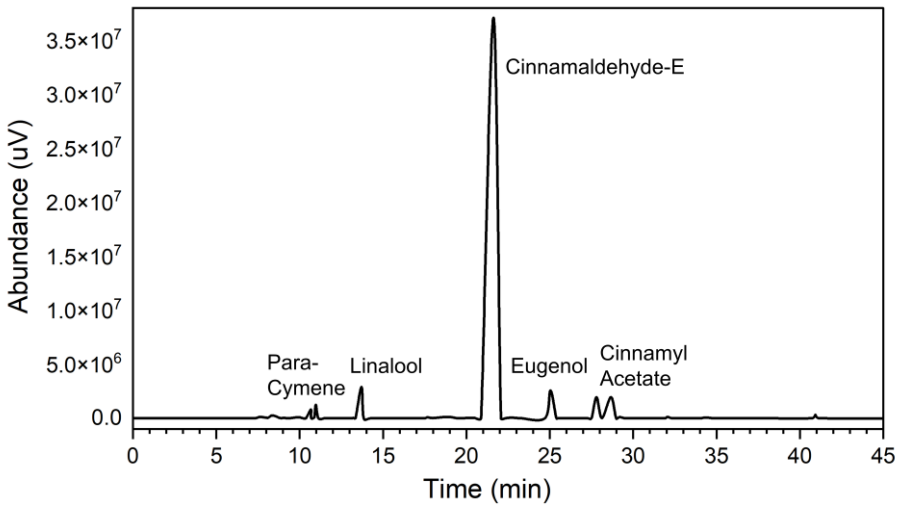

Figure 3-3 GC-MS results of the cinnamon essential oil used.

MF-Millipore™ mixed cellulose ester (MCE) membrane filters (pore size = 0.22 µm, diameter = 25 mm) were purchased from Sartorius (Germany). WST-1 Cell Proliferation Assay Kits were obtained from Cayman (USA).

3.2.2 Waste-Derived Cellulose

Seaweed Cellulose Derivation

Sugar kelp (*Laminaria hyperborea*) was provided by Marine Biopolymers Ltd, UK. The cellulose derived from this seaweed was a byproduct of Alg production. After the soluble alginate fraction was extracted, the insoluble cellulose fraction remained as a residual material. These residuals were dispersed in 0.5 M NaCl and washed thoroughly in water to remove any remaining soluble fractions and salts from the alginate extraction process. The material was subjected to high-pressure homogenisation without any further pretreatment following the procedure of Onyianta et al. [219], resulting in high aspect ratio cellulose nanofibrils. The average fibril width is 19 ± 5 nm and the fibril length is of several

micrometres, resulting in an aspect ratio greater than 100. Subsequently, free-flowing cellulose powders were prepared by a series of solvent exchange, filtration, and freeze-drying steps.

Animal Waste Cellulose Derivation

The raw cow manure sample was first dried in the open air, followed by oven drying at 105 °C overnight for disinfection. The dried cow manure crust was then ground and sieved to a smaller particle size. The nanocellulose extraction started with a bleaching process, where the dried cow manure particles were placed in an acidified 3 wt% NaClO solution at room temperature and stirred overnight for delignification of the material. The sample was then processed in a 1 wt% NaOH aqueous solution in the ambient with constant stirring for 2 h. An extra delignification process was used subsequently by placing the sample in the same NaClO solution as above for 2 h under continuous stirring. The material was washed vigorously in ultrapure water between each step by successive centrifugation and decantation. High aspect ratio cellulose nanofibrils were successfully obtained through this process, with an average fibril width of 12.8 ± 4.1 nm and an estimated fibril length greater than 1 µm. Subsequently, the above material underwent a series of solvent exchange, filtration, and freeze-drying steps to produce free-flowing dry cellulose flakes.

3.2.3 Spinning Solutions

PCL, PVP and PEO

PCL pellets were dissolved in chloroform and stirred magnetically at ambient temperature (~20 °C) for 24 h to obtain a homogeneous 15% (w/v) PCL solution.

15% (w/v) PVP solution and 15% (w/v) PEO solution were prepared by dissolving PVP and PEO powders in ethanol and distilled water, respectively, and processing under the same conditions.

Sodium Alginate

Na-Alg powders were dissolved in distilled water to prepare a series of Na-Alg feedstock with concentrations ranging from 1.0 to 3.5 wt%. Glycerol with a relative weight ratio of 1:10 to the polymer was added to the prepared solutions to improve the solution spinnability and reduce the brittleness of the resulting Alg products [220, 221].

Cellulose

The solid content of cellulose obtained above was dissolved in the EMIM OAc/DMSO mixture to form a series of cellulose solutions with concentration gradients (1, 1.5, 2, 2.5, 3 wt% for seaweed-derived cellulose and 2, 4, 6, 8, and 10 wt% for animal waste-derived cellulose). The dissolution process was promoted by gentle heating (≈ 40 °C) and prolonged mechanical stirring (≈ 48 h).

3.3 Fibre Preparation

3.3.1 PCL, PVP and PEO Fibres

Pressurised Gyration and Nozzle-Pressurised Gyration

For an individual spinning experiment, 3 mL of the polymer solution was loaded into the chambers in both PG and nozzle-PG (**Figure 3-1**) for spinning under the same conditions. Spinning was performed at a rotational speed of 13 000 rpm

under consistent ambient conditions (~20 °C temperature and ~50% relative humidity). The spinning parameters are listed in **Table 3-1** and **Table 3-2**.

Table 3-1 Spinning parameters for fibres produced using pressurised gyration and nozzle-pressurised gyration at a collection distance of 100 mm.

Polymer	**Fibre Production Method**	**Working Pressure [× 10^5 Pa]**
PCL	PG	1, 2, 3
	Nozzle-PG	1, 2, 3
PVP	PG	1, 2, 3
	Nozzle-PG	1, 2, 3
PEO	PG	1, 2, 3
	Nozzle-PG	1, 2, 3

Table 3-2 Spinning parameters for fibres collected at different distances in nozzle-pressurised gyration.

Polymer	**Working Pressure [× 10^5 Pa]**	**Collection Distance [mm]**
PCL	1	70, 100, 130
PVP	1	70, 100, 130
PEO	1	70, 100, 130

Electrospinning

The PVP solution was also used as the electrospinning solution. An 18G (diameter = 1.25 mm, Futongda Co., Ltd. China) needle and a PTFE capillary tube (outer diameter = 2 mm and inner diameter = 1.6 mm) were used. The 10 kV voltage was supplied by a DC power supplier (Glassman Europe Ltd., Tadley, UK). A grounded metal plate collector was used to collect the spreading fibres, with a distance to the needle tip of 150 mm. The flow rate was optimised as 0.2 mL/min. Each sample was taken by spinning for 3 mins.

Curcumin-loaded PVP Fibres

CUR was incorporated into a 12% (w/v) PVP solution, at a concentration of 1% (w/w) relative to the polymer. This solution was used as the feedstock for both the nozzle-PG and electrospinning processes to produce CUR-loaded PVP fibres. The nozzle-PG process was conducted under the following parameters: the rotational speed of 13 000 rpm, the working pressure of 1×10^5 Pa, and the collection distance of 100 mm. For the electrospinning process, the conditions included a voltage of 12 V, a flow rate of 0.1 mL/min, and a collection distance of 120 mm. The temperature and relative humidity were controlled at approximately 23 °C and 45%, respectively.

3.3.2 Alginate Fibres

The Na-Alg feedstocks were injected into the vessel chamber (**Figure 3-2**) with a syringe before spinning. In this work, nozzle-PG functioned as a jet generation apparatus, leading to the Na-Alg solution overflowing from the nozzles and forming spinning jets. Once these jets left the vessel, they underwent a stretching

process before their immersion in the coagulation bath. A 3.5 wt% $CaCl_2$ aqueous solution was prepared as the coagulant. The stretching time is related to the air gap length between the nozzle tip and the surface of the coagulation bath. All the spinning experiments were performed at ambient temperature of 20 - 25 °C and relative humidity of 45 - 50%. The resulting Alg gels were collected from the coagulant, preliminarily dried with absorbent tissue, and then oven-dried at 55 °C until completely dry.

GC was added into distilled water and was ultrasonicated for 90 min until the solids were uniformly dispersed. Subsequently, Na-Alg powders were added into the GC/water suspensions and mechanically stirred for 48 h. This process resulted in 3.2 wt% Na-Alg solutions containing GC at weight ratios of 1%, 2%, and 4% relative to the polymer. CEO/Na-Alg solutions and CA/Na-Alg solutions with identical ratios and concentrations were prepared following the same procedure, ensuring consistent preparation methods across all formulations. After the preliminary experiment, all the obtained solutions were subjected to the inverted nozzle-PG apparatus (**Figure 3-2**) with rotational speed of 11 000 rpm, working pressure of 2×10^5 Pa, and air gap length of 6 mm.

3.3.3 Cellulose Fibres

The solid content of cellulose obtained above was used as the feedstock for the inverted nozzle-PG apparatus (**Figure 3-2**). Finding the optimal system parameters is crucial for the formation of continuous spinning jets, as presented in **Figure 3-4**a. Insufficient rotational speed and working pressure may result in feedstock retention in the chamber, whereas excessive rotational speed and working pressure can lead to a jet split into droplets (**Figure 3-4**b).

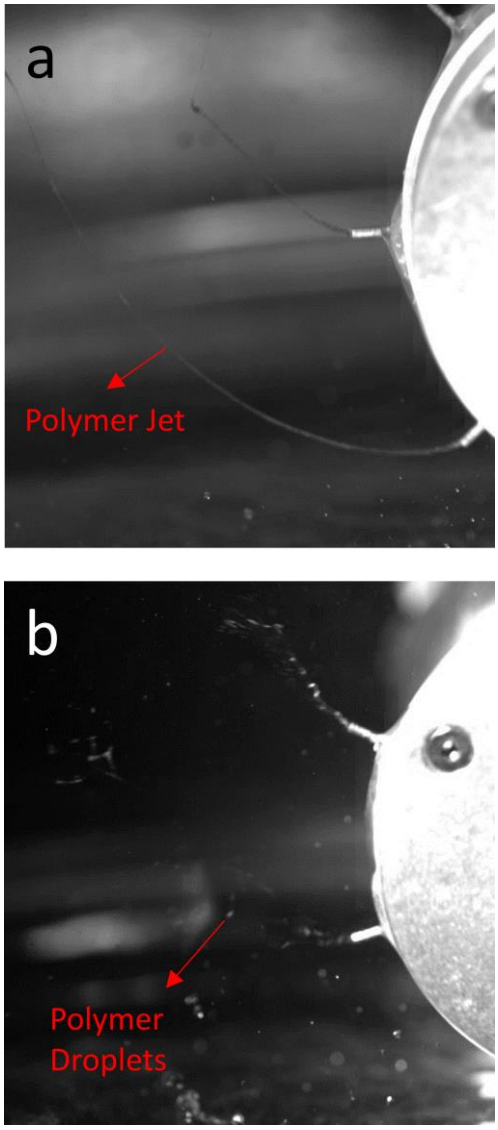

Figure 3-4 Digital photos of (a) continuous spinning jets and (b) droplets captured by a high-speed camera.

Following preliminary testing, the working conditions for seaweed-derived cellulose stock were as follows: the rotational speed of 12 000 rpm, the working pressure of 1×10^5 - 2×10^5 Pa, and the air gap length was 6-20 mm. For the animal waste-derived cellulose stock, the working conditions were determined as the rotational speed of 12 000 rpm, the working pressure of 1×10^5 - 3×10^5 Pa, and a fixed air gap length of 10 mm. The spinning was performed at ambient temperature (≈ 20 °C) and relative humidity of 45 - 55%. The cellulose solutions

were spun into the water bath and allowed to coagulate in water for 5 h. The water was replaced every hour to remove the solvent as much as possible. Afterwards, the cellulose samples were removed from the water and placed in an oven at 55 °C until completely dried. The preparation process is illustrated in **Figure 3-5**.

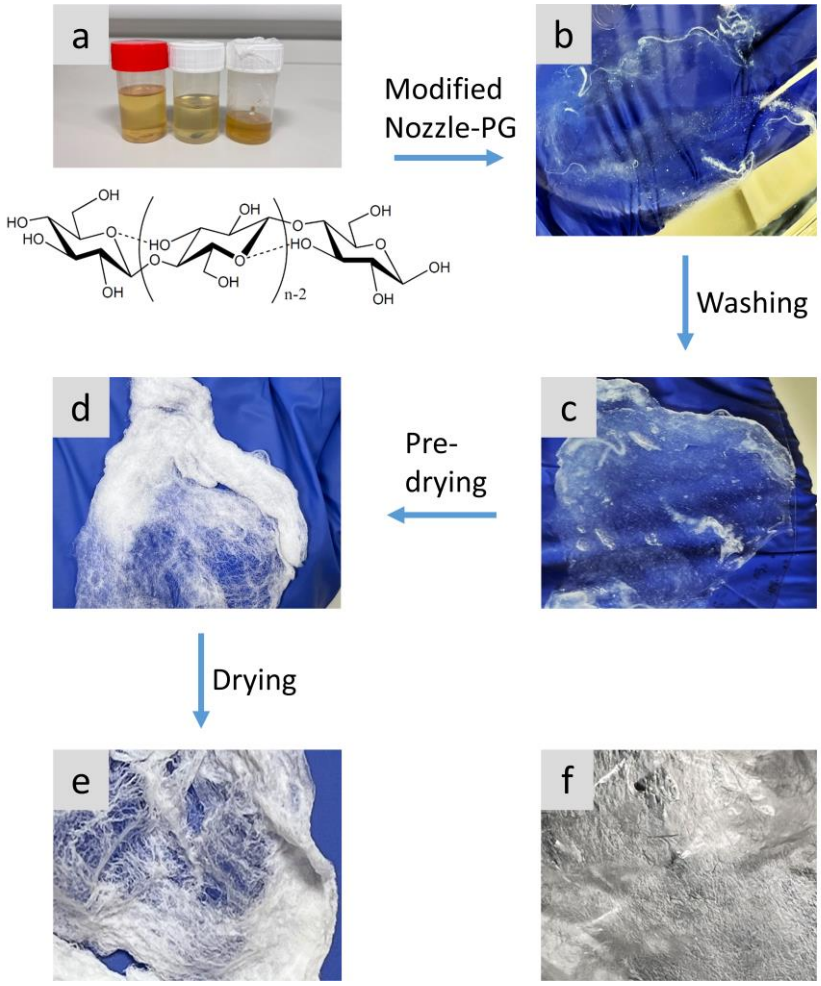

Figure 3-5 The preparation process of cellulose fibres and cellulose films: (a) cellulose solutions, (b, c) cellulose gels, (d, e) cellulose fibres before and after drying, respectively, and (f) cellulose films.

Table 3-3 summarises the spinning protocols used for fibre preparation via nozzle-pressurised gyration in this thesis.

Table 3-3 Summary of polymer solutions, system parameters, and experimental settings for fibre preparation using nozzle-pressurised gyration.

Polymer	**Solvent**	**Concentration**	**Speed [× 10^3 rpm]**	**Pressure [× 10^5 Pa]**	**Distance [mm]**	**Nozzle number and dimeter**	**Coagulation**
PCL	chloroform	15% (w/v)	13	1-3	70-130	4, Φ 0.5 mm	-
PVP	ethanol	13-15% (w/v)	13	1-3	70-130	4, 8, Φ 0.5 mm	-
PEO	distilled water	15% (w/v)	13	1-3	70-130	4, Φ 0.5 mm	-
SA	distilled water	1.0-3.5 wt%,	11	2	6	8, Φ 0.3 mm	3.5 wt% $CaCl_2$
Cellulose (seaweed-derived)	EMIM OAc and DMSO (1: 1, w/w)	1.0-3.0 wt%,	12	1-2	6-20	8, Φ 0.5 mm	water
Cellulose (animal waste-derived)	EMIM OAc and DMSO (1: 1, w/w)	2.0-10 wt%,	12	1-3	10	8, Φ 0.3 mm	water

3.4 Characterisation Methods

3.4.1 Solution Properties

The surface tension of the prepared polymer solutions was characterised by a Kruss Tensiometer (Germany) using the Du Nouy ring method. Before measurement, the tensiometer was calibrated with distilled water. The viscosity of the polymer solutions was measured using a Brookfield DV-III Ultra Viscometer (USA) with a small-sample adaptor attached to a SCV-18 spindle. All measurements were carried out three times for each sample at ambient temperature (~25 °C).

3.4.2 Scanning Electron Microscopy (SEM)

All fibres were imaged using a scanning electron microscope (SEM). Samples were coated using a Au sputtering machine to minimise charging effects before imaging. ImageJ (software) was used to measure the fibre diameter. The mean and the standard deviation of fibre diameter were calculated. The fibre diameter frequency distributions were plotted by OriginPro (software). OrientationJ (ImageJ plugin) was used to construct the distribution of fibre orientation and calculate the directional coherence coefficient of fibres. The coherence coefficient is an index between 0 and 1. A directional coherence coefficient close to 1 indicates a high fibre orientation [222].

3.4.3 Fourier Transform Infrared Spectroscopy (FTIR)

The chemical composition of the cellulose samples obtained was analysed using a Fourier transform infrared spectroscopy (FTIR) spectrometer at ambient

temperature. Each sample was scanned for 32 rounds between 4000-500 cm^{-1} at a resolution of 4 cm^{-1}, to obtain a reasonable signal-to-noise ratio. The samples were studied on diamond ATR.

3.4.4 Microwave Plasma Atomic Emission Spectroscopy (MP-AES)

The quantity of Na^{+} and Ca^{2+} in the obtained Alg samples was measured using microwave plasma atomic emission spectroscopy (MP-AES, Agilent Technologies 4210, USA). The Alg samples were dissolved in 6% (w/v) KOH aqueous solution. A concentrated 37.5% HCl solution was used to adjust the solution pH after proper dissolution of solids. The prepared solutions were then submitted to the MP-AES measurement.

3.4.5 X-Ray Measurements

X-ray diffraction (XRD) analysis was conducted on the cellulose samples. The measurement was performed on a STOE STADI-P diffractometer (Germany) with a Cu source ($K_{\alpha1}$ = 1.5406 Å and $K_{\alpha2}$ = 1.5444 Å), using a voltage of 40 kV and a current of 30 mA. The scanning rate was 5 s per step with a scanning step of 0.015°. The samples were scanned within the range of 10° - 45° (2θ). The collected data was analysed using the peak deconvolution method and fitted with the Gaussian function in OriginPro.

3.5 Mechanical Strength Testing

Ultimate tensile strength (UTS) calculations of fibre samples were performed in a specially designed homemade setup. In a testing procedure, fibrous materials were twined to get a thread with a 500 µm diameter. The thread ends were

secured to rubber clamps, one of which is fixed at the top and the other one attached to a load carrier. The maximum force that the threads will withstand was determined by adding 10 g incremental weights to the carrier at the bottom. The tensile strength was calculated based on the maximum applied load.

3.6 Absorption Properties

The liquid absorption properties of the cellulose samples in PBS solution (pH = 7.4) were investigated. Before the experiment, the initial weight of the dry samples was measured and denoted as w_0. Each sample was prepared in three duplications for parallel experiments. The weighed samples were soaked in the PBS solution and placed in a 37 °C incubator. At selected time points, the samples were removed from the PBS solution and blotted with absorbent tissue. The weight of the samples after absorbing liquid was measured and denoted as w_i. The percentage of liquid absorption (W%) was calculated according to **Equation 3-1**:

$$W\% = \frac{w_i - w_0}{w_0} \times 100\%$$

Equation 3-1

3.7 Drug Loading Efficiency

The CUR contents within the PVP fibres were quantified using a standard UV spectrophotometric assay at a wavelength of 427 nm, which was determined by the full wavelength scanning of a series of standard solutions. A 10 mg sample of the fibres was dissolved in 10 ml of PBS solution containing 2% (w/v) Tween 20 and analysed using a Jenway 7315 UV/Visible spectrophotometer (Bibby

Scientific, Staffordshire, UK) at 427 nm. Each sample was prepared in three duplications to ensure accuracy across parallel experiments. Drug encapsulation efficiency (EE) was determined by comparing the experimentally measured CUR content in 10 mg of fibres to the theoretical CUR content expected for that mass, expressed in **Equation 3-2**. The calibration curve presented in **Figure 3-6** was prepared in advance to support the cumulative drug release studies.

$$EE = \frac{w_{expt.}}{w_{theo.}} \times 100\%$$

Equation 3-2

where, $w_{expt.}$ is the experimental CUR content and $w_{theo.}$ is the theoretical CUR content.

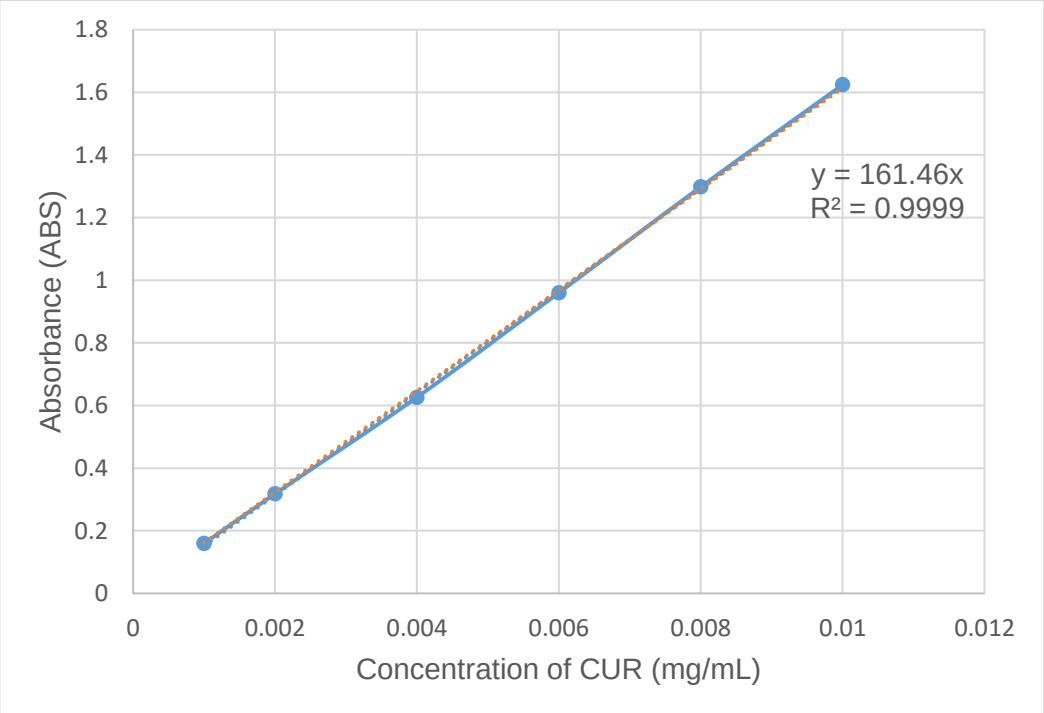

Figure 3-6 Calibration curve for curcumin dissolved in PBS.

3.8 In-Vitro Transdermal Release Study

10 mg of each CUR-PVP fibre sample was cut into a disc (diameter = 8 mm) and placed on the surface of an MCE membrane, which was then positioned within the Franz diffusion cell (**Figure 3-7**). The exposed edges of the membrane were sealed to prevent leakage. The top orifice of the donor cell (outer diameter = 9 mm) was covered with parafilm, with a small perforation to maintain pressure within the fibre system. The acceptor cell, with a volume of 4 mL, was maintained at a constant temperature of 37 °C to simulate physiological conditions. A magnetic stirrer was used to ensure thorough mixing of the CUR as it diffused through the membrane into PBS solution in the acceptor cell. 1 mL of solution was taken from the sampling port in intervals for concentration measurement, with 1 mL of PBS added into the solution immediately to maintain the solution volume. Each sample was prepared in three duplications to ensure accuracy across parallel experiments.

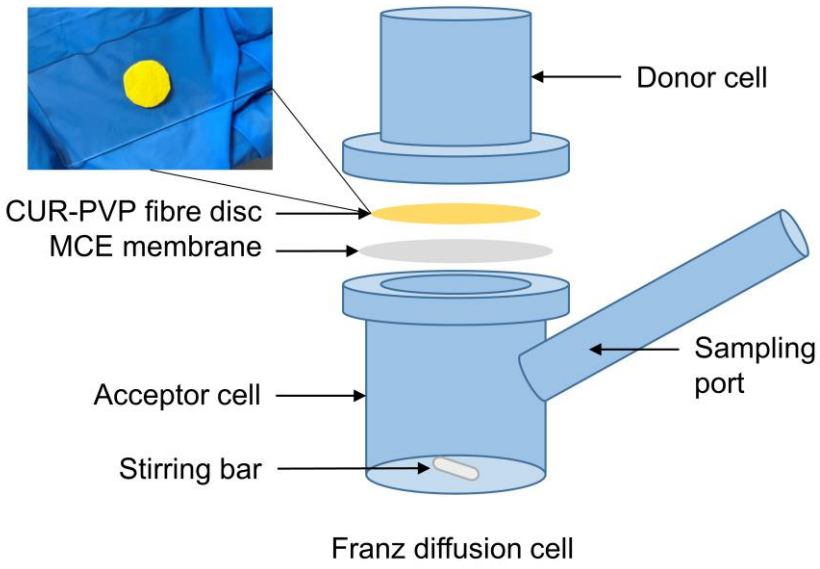

Figure 3-7 Schematic diagram of Franz diffusion cell apparatus and a digital image of a PVP-curcumin fibre disc.

3.9 In-Vitro Cytotoxicity Testing

The cytotoxicity tests of pure Alg and cinnamon-containing Alg fibrous samples were performed according to the ISO10993-5 standard. L929 mouse fibroblast cell line ATCC-NCTC clone 929:CCL1 was used [223]. All the samples were sterilised prior to the test. The test samples were prepared according to ISO standards with the 6 cm^2/mL sample-medium ratio and tested by WST-1 assay to examine their cytotoxic response. The test samples were immersed in a cell culture medium and kept at 37 °C for 72 h. The cell culture medium was composed of 90% DMEM, 10% FBS, 2 mM L-glutamine, and 100 IU/mL penicillin/streptomycin. The cells were seeded in a 96-well plate at 1×10^4 cells/well. Then the incubated cell culture media interacted with cells for 24 h. After 24 h, 10 µL WST-1 assay reagent was added to each well, and cells were incubated for 120 min. The 96-well plate (n = 3) was measured at 450 nm absorbance by an ELISA plate reader (SpectroStar nano, BMG Labtech). The non-reacted cell culture media was used as negative control and the 10% DMSO-90% medium was used as positive control.

3.10 Antibacterial Testing

The antibacterial activity of pure Alg and cinnamon-containing Alg fibrous samples was evaluated to determine their activity to inhibit biofilm formation. *Escherichia coli* (*E. coli*, ATCC, #25922) and *Staphylococcus aureus* (*S. aureus*, ATCC, #29213) bacteria strains were used. The bacterial solution (Luria-Bertani medium) was adjusted to 0.4 OD. The fibrous samples were placed into a 48-well plate and 0.5 mL bacteria suspension was added (n = 3). The samples were incubated for 24 h at 37°C in a shaker incubator. After 24 h, samples were

collected and kept in 1 mL of PBS solution. Then the test samples were ultrasonicated for 15 min. The collected PBS solution was serially diluted and 10 µL samples were cultivated to agar plates (n = 3). After 24 h, colony-forming units were counted and the antibacterial activity-antibiofilm formation was calculated. Additionally, after 24 h of incubation, the bacteria adhering to the surface were fixed in place and visualised by SEM. In the fixation procedure, the first cross-linking was performed with glutaraldehyde for 30 min. Then, incubation was carried out with serial alcohol solutions (50, 60, 70, 80, 90, 95, and 100%) for 15-min periods to gradually remove the water from the samples. All samples are Au-plated prior to SEM imaging [224].

4 Nozzle-Pressurised Gyration

4.1 Introduction

In recent decades, the enthusiasm for research on polymeric fibre spinning has remained unwavering. These efforts have been mainly focused on the reduction of fibre size and the increase of fibre yield. As the quality and quantity of the obtained fibres have increased to a satisfactory degree, much attention has been paid to the customisation of fibre structures and functions. Through technological innovation, polymeric fibres with uniform, beaded, hollow, core-sheath, and porous structures have been successfully prepared in laboratories [225-229].

Theoretically, an ideal uniform fibre means that there is no variation in the fibre diameter along the fibre length of individual fibre strands [230]. Compared with beaded fibres, uniform fibres show enhanced mechanical properties. Many reports have demonstrated that the presence of beads and defects on fibres considerably reduces the cohesion between fibres, resulting in lower Young's modulus, tensile strength, and elongation at break [231-233]. In addition, seeding cells on highly aligned fibre scaffolds tends to be more effective than that on randomly oriented fibre scaffolds, in order to achieve cell orientation control in tissue engineering [232, 234, 235]. This is related to the regular and defined orientation architecture of the natural ECMs found in tissues and organs [236]. The studies from Ottosson et al. and Norzain et al. have shown that the anisotropic orientation of fibres has significant impacts on cell adhesion mechanisms and promotes elongation and migration of fibroblasts along the fibre

direction [183, 237, 238]. The results suggest that the aligned fibre scaffold is a highly promising candidate for biomedical applications.

In this work, I develop a nozzle-PG setup for the first time. It effectively improves the uniformity and orientation of produced fibres. Although PG has demonstrated clear advantages over electrospinning in scaling up fibre production, it often comes at the cost of fibre uniformity and integrity, resulting in increased bead formation and structural defects. However, the introduction of nozzle-PG effectively addresses these limitations, offering a promising solution to enhance fibre quality while maintaining high production efficiency. In nozzle-PG, the nozzles work to direct the polymer fluid when it's ejected. I compare the differences in the morphology and alignment of fibres produced by PG with and without nozzles to demonstrate the advantage of nozzle-PG in producing uniform and aligned fibres. This work also reveals the effects of working pressure and collection distance on the fibre morphology obtained in nozzle-PG. Additionally, this technology is compared with electrospinning in terms of morphology, tensile strength, release behaviours of the resulting fibres, as well as fibre production rate, to thoroughly understand the distinct characteristics of each spinning method.

4.2 Solution Properties

The characteristics of PCL, PVP, and PEO spinning solutions are summarised in **Table 4-1**. Notably, even at the same concentration, the surface tension and viscosity of these polymer solutions can differ substantially, directly influencing their spinnability and will lead to differences in resulting spinning performance.

Table 4-1 Polymer type, concentration, solvent, surface tension and viscosity of the three solutions at ambient temperature.

Polymer	% (w/v)	Solvent	Surface Tension [mN/m]	Viscosity [mPa s]
PCL	15	Chloroform	32.7 ± 0.3	2065.0 ± 35.8
PVP	15	Ethanol	24.6 ± 0.2	751.8 ± 6.1
PEO	15	Distilled water	58.1 ± 0.4	2144.3 ± 74.9

4.3 Effects of Vessel Nozzle

Figure 4-1 illustrates the morphological differences in PCL fibres produced using PG with and without nozzles. It can be seen that under the same spinning parameters, nozzle-PG produced a PCL fibre mat without beads, while the PCL fibres obtained from the original PG were randomly arranged with large beads (**Figure 4-1**a, d). From the inset in **Figure 4-1**d, nozzle-PG fabricated PCL fibres with smoother and more uniform morphology than the PCL fibres produced by PG (**Figure 4-1**a). The fibre diameter distribution graphs (**Figure 4-1**b, e) illustrate that PCL fibres obtained from nozzle-PG had smaller fibre diameter and narrower diameter distribution than those obtained from PG, with a mean of 2.4 µm and a standard deviation of 1.2 µm. PG-produced PCL fibres have an average diameter of 3.9 ± 2.4 µm. In addition, PCL fibres produced by nozzle-PG had a larger orientation coherence (0.58) than that of PG fibres (0.36), indicating the higher alignment of fibres obtained from nozzle-PG.

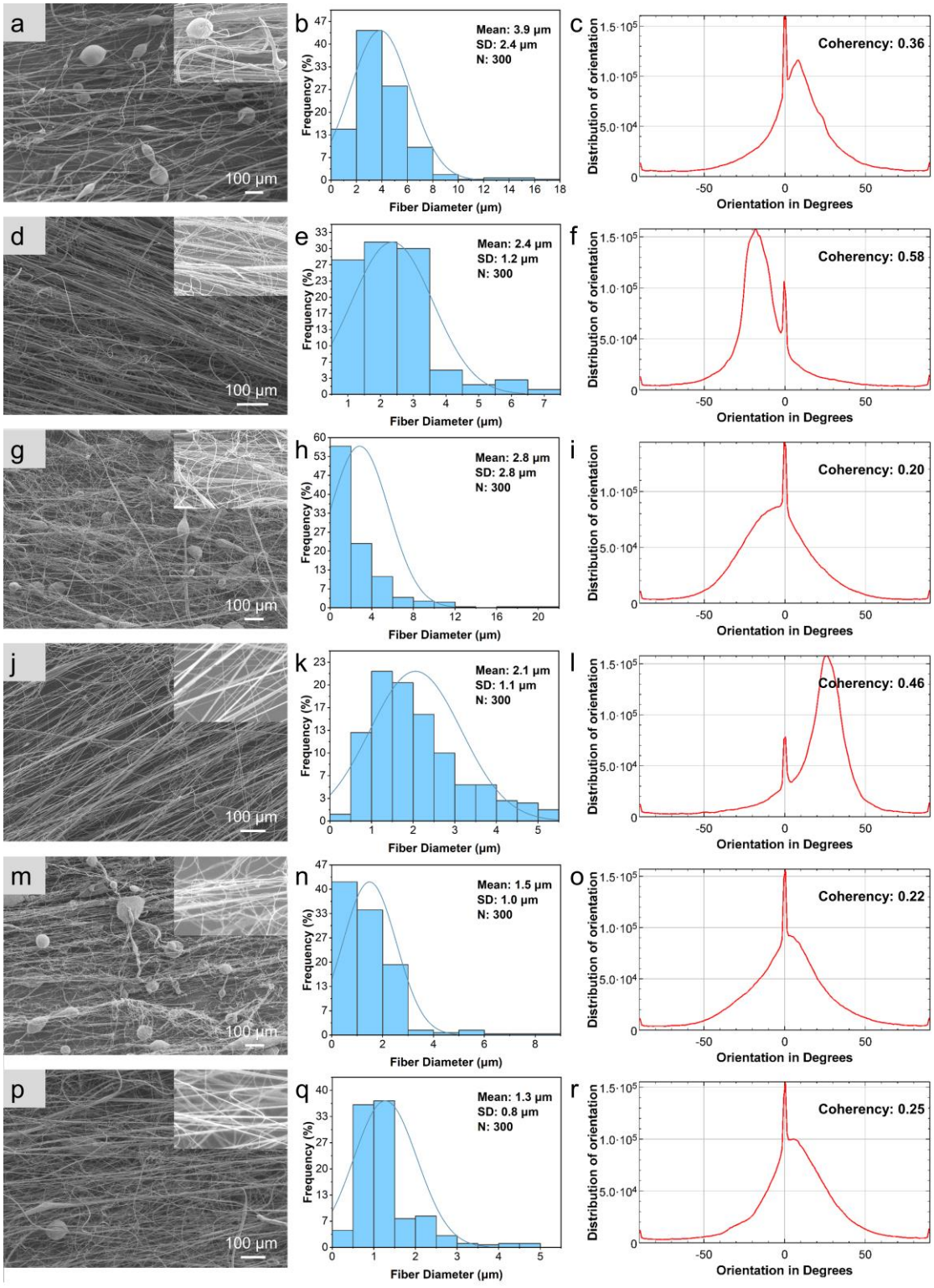

Figure 4-1 SEM images, fibre diameter distribution graphs and orientation distribution graphs of PCL fibres produced by (a-c) pressurised gyration, 1 × 10^5 Pa working pressure, (d-f) nozzle-pressurised gyration, 1 × 10^5 Pa working pressure, (g-i) pressurised gyration, 2 × 10^5 Pa working pressure, (j-l) nozzle-

pressurised gyration, 2 × 10^5 Pa working pressure, (m-o) pressurised gyration, 3 × 10^5 Pa working pressure, and (p-r) nozzle-pressurised gyration, 3 × 10^5 Pa working pressure. The insets show the high-magnification SEM images of fibres.

Similar results were obtained from the spinning under 2 × 10^5 Pa and 3 × 10^5 Pa pressures. PCL fibre mats fabricated by PG were randomly arranged with the presence of some thicker fibres and large beads (**Figure 4-1**g, m). While nozzle-PG produced PCL fibres with more aligned orientation and fewer beads (**Figure 4-1**j, p). The PCL fibres had diameters of 2.8 ± 2.8 µm and 2.1 ± 1.1 µm were produced by 2 × 10^5 Pa PG and nozzle-PG, respectively, suggesting that nozzle-PG enabled the manufacture of thinner and more uniform fibres. The orientation coherency coefficient of fibres produced by 2 × 10^5 Pa nozzle-PG (0.46) is closer to 1 than that of PG (0.20), indicating its higher alignment [239]. Similar results were acquired from the spinning under 3 × 10^5 Pa working pressure (**Figure 4-1**m-r). These results show that even under different working pressures, nozzle-PG always produced finer and more uniform PCL fibres with a higher fibre alignment than those obtained from the original PG.

These effects can be explained by the stability of spinning jets. Although the polymer solution undergoes a similar trajectory after moving out of the vessel in nozzle gyrospinning and nozzle-free gyrospinning, including jet necking, whipping, and formation of an anti-S shape jet path, the direction of the jet ejection and the flow state of the polymer solution are different [99, 240]. In PG, the gas outflow path from the orifices is jet-like (**Figure 4-2**a) [241]. In addition, turbulence occurs due to the chaotic change in pressure when the polymer fluid is ejected through the orifices [242]. This means that the polymer jets may be

formed at a certain angle to the central axis of the orifice and have different initial jet diameters (**Figure 4-2**b) [243]. This explains the lower alignment and uniformity of PG fibre products. However, when the fluid flows through the nozzles, it is subjected to the centrifugal force (F_{cent}), the static pressure (F_p), the viscous force (F_τ) and the surface tension (F_s) parallel to the axis of the nozzle, which help it move along the length of the nozzle (**Figure 4-2**c) [240]. Moreover, directing the liquid by nozzles helps to stabilise the flow state of the polymer flow and form stable spinning jets [244]. As a result, the polymer jets leave the nozzle in a more stable flow state and tend to move along the nozzle axis under the action of inertia, thereby improving the alignment and uniformity of fibres.

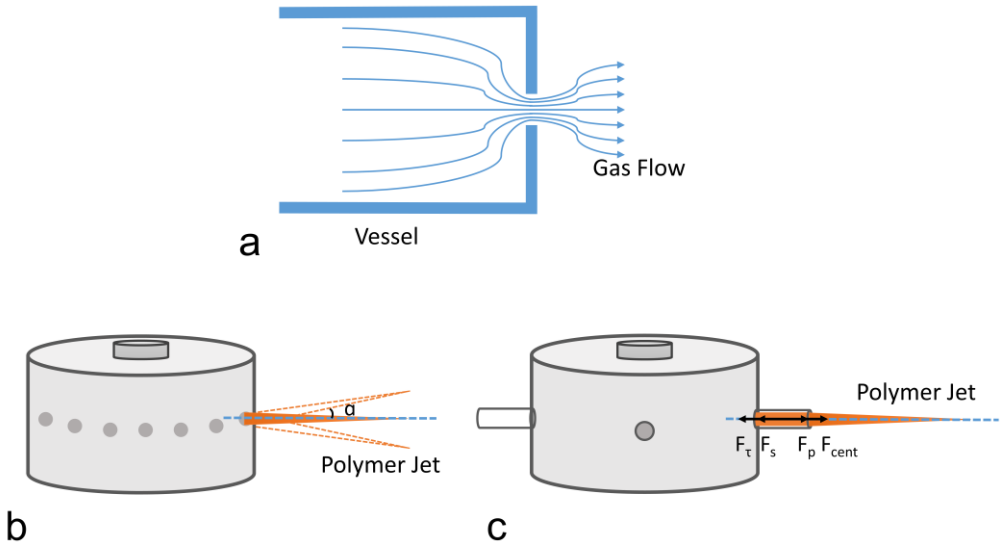

Figure 4-2 Diagrammatic representation of (a) gas flows through an orifice and the liquid flow ejected from (b) orifices in pressurised gyration and from (c) nozzles in nozzle-pressurised gyration, respectively.

The same experiment was carried out at 15% (w/v) PVP/ethanol. The results are shown in **Figure 4-3**.

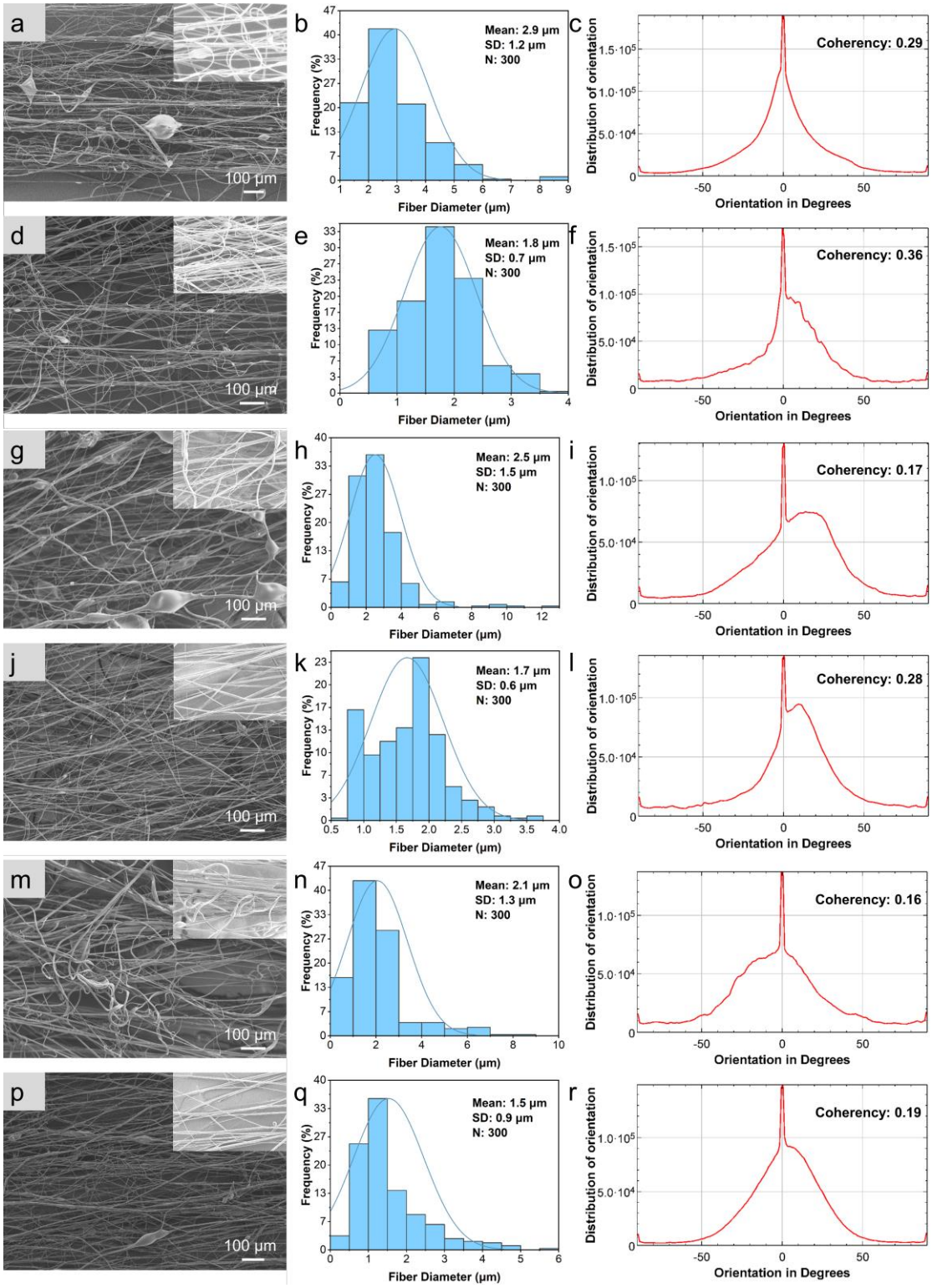

Figure 4-3 SEM images, fibre diameter distribution graphs and orientation distribution graphs of PVP fibres produced by (a-c) pressurised gyration, 1 × 10^5 Pa working pressure, (d-f) nozzle-pressurised gyration, 1 × 10^5 Pa working pressure, (g-i) pressurised gyration, 2 × 10^5 Pa working pressure, (j-l) nozzle-

pressurised gyration, 2 × 10^5 Pa working pressure, (m-o) pressurised gyration, 3 × 10^5 Pa working pressure, and (p-r) nozzle-pressurised gyration, 3 × 10^5 Pa working pressure. The insets show the high-magnification SEM images of fibres.

Figure 4-3a and d are the SEM images of PVP fibres produced by PG and nozzle-PG at 1 × 10^5 Pa working pressure, respectively. PG produced a PVP fibre mat containing large beads. In contrast, the PVP fibre mat fabricated by nozzle-PG only had some small beads. The effects of vessel geometry played a key role in the fibre diameter value. PVP fibres with a diameter of 2.9 ± 1.2 μm were produced at 1 × 10^5 Pa with PG, while nozzle-PG under the same working pressure generated finer and more uniform fibres with a diameter of 1.8 ± 0.7 μm. In addition, PVP fibres processed by nozzle-PG also showed better fibre alignment with a larger orientation coherency coefficient (0.36) than that of PG (0.29) at the same pressure. These encouraging results were replicated in the 2 × 10^5 Pa and 3 × 10^5 Pa spinning (**Figure 4-3**g-i and m-r, respectively). Nozzle-PG always produced finer and more aligned PVP fibres with fewer and smaller beads than PG, even if the working pressure changed.

Water-soluble polymer PEO was also spun using PG and nozzle-PG (**Figure 4-4**). Nozzle-PG successfully produced PEO nanofibres (172 ± 67 nm) with “ideal” morphology—smooth, uniform and of better alignment than the PEO nanofibres obtained by PG (198 ± 102 nm) under 3 × 10^5 Pa working pressure, as shown in **Figure 4-4**m-r. In addition, no beads were observed in PEO nanofibres fabricated by nozzle-PG. The nozzle-PG-produced PEO nanofibres also had narrower distributions of fibre orientation (**Figure 4-4**f, l, r) than those of PEO nanofibres produced by PG (**Figure 4-4**c, i, o), indicating their higher fibre alignment.

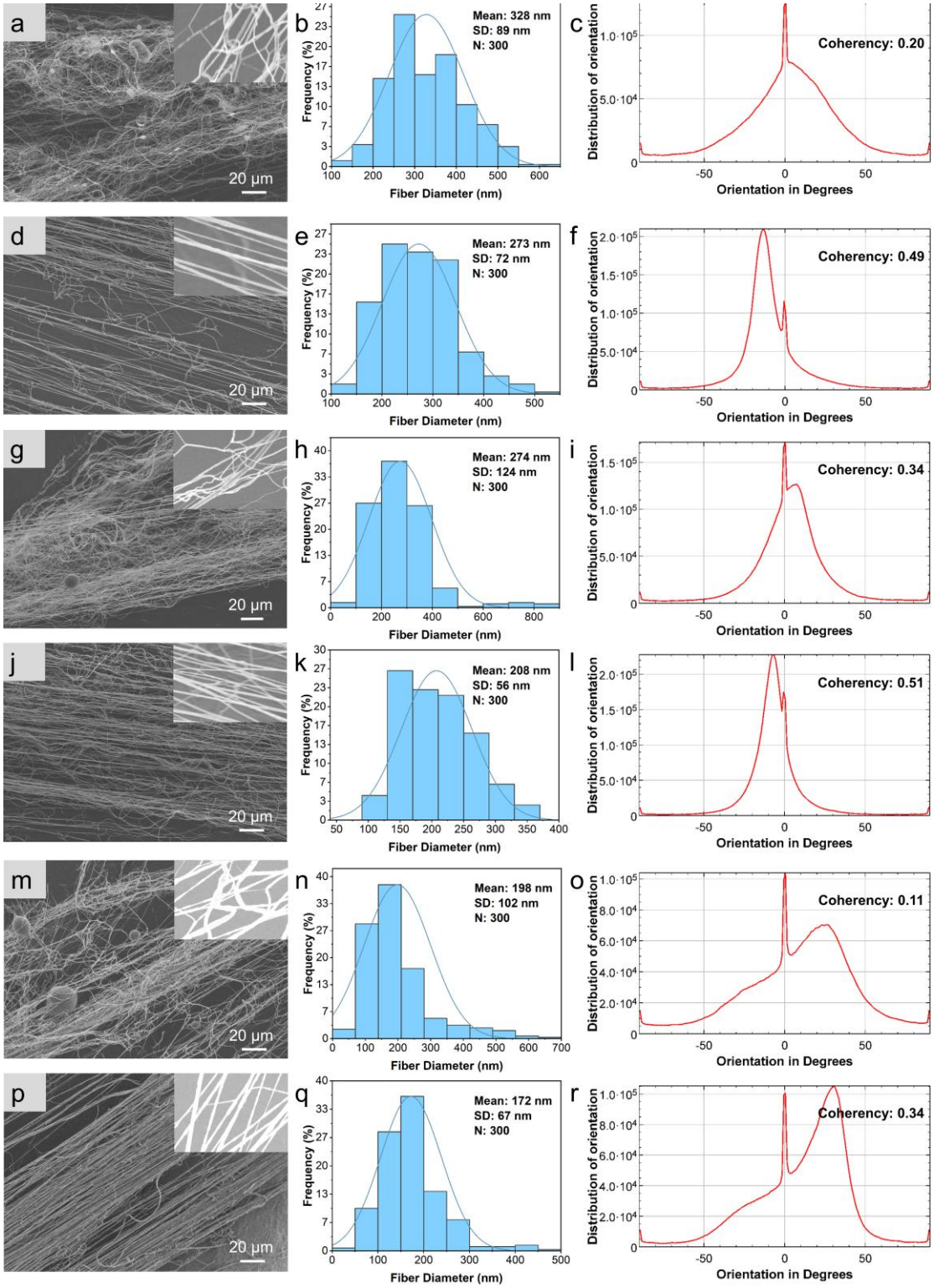

Figure 4-4 SEM images, fibre diameter distribution graphs and orientation distribution graphs of PEO fibres produced by (a-c) pressurised gyration, 1 × 10^5 Pa working pressure, (d-f) nozzle-pressurised gyration, 1 × 10^5 Pa working pressure, (g-i) pressurised gyration, 2 × 10^5 Pa working pressure, (j-l) nozzle-

pressurised gyration, 2 × 10^5 Pa working pressure, (m-o) pressurised gyration, 3 × 10^5 Pa working pressure, and (p-r) nozzle-pressurised gyration, 3 × 10^5 Pa working pressure. The insets show the high-magnification SEM images of fibres.

4.4 Effects of Working Pressure

Through the comparison of fibres produced under different working pressures shown in **Figure 4-1**, **Figure 4-3**, and **Figure 4-4**, the influence of working pressure on the fibre morphology and fibre alignment can be deduced. The alignment and uniformity of PCL fibres significantly declined with the increase in working pressure from 1 × 10^5 Pa to 3 × 10^5 Pa. Meanwhile, the fibre diameter decreased accordingly from 3.9 μm to 1.5 μm in PG, and from 2.4 μm to 1.3 μm in nozzle-PG. Similarly, with this pressure increase, the PVP fibre diameters slightly decreased from 2.9 μm to 2.1 μm and from 1.8 μm to 1.5 μm in PG and nozzle-PG, respectively. The PEO fibre diameters decreased from 328 nm to 198 nm and from 273 nm to 172 nm in PG and nozzle-PG, respectively. While their fibre uniformity and fibre alignment significantly decreased with the pressure increasing. A higher working pressure is generally preferred in PG to produce finer fibres, while it also leads to lower fibre alignment and the presence of beads. This occurs because increased pressure promotes additional stretching of the spinning jets, resulting in finer fibres [110]. However, the intensified gas flow also heightens the instability of spinning jets, causing bead formation and poor fibre alignment. Thus, increasing working pressure can be counterproductive when aiming to produce unidirectional fibres.

4.5 Effects of Collection Distance

The effects of collection distance on fibre morphology are presented in the SEM images in **Figure 4-5**. When the collection distance was 130 mm, randomly oriented PCL fibres with large beads and a small diameter (1.3 ± 0.9 µm) were collected. Thicker PCL fibres (2.7 ± 1.4 µm) were collected at the 70 mm distance. The collection distance of 100 mm led to the best PCL fibres with pronounced fibre morphology and alignment, with a fibre diameter of 2.4 ± 1.2 µm (**Figure 4-1**d-f). It has been known that the spinning jet in gyrospinning undergoes stretching before reaching the collector, during which the diameter of the jet decreases monotonously with the increase of movement distance [99]. Thus, it can be expected that collection distance has significant effects on fibre diameter. The polymer jet cannot be stretched sufficiently at a small collection distance, forming short and thicker fibres. Conversely, when the collection distance is excessively long, it will cause jet rupture, or fibres fail to deposit on the collector [92, 245]. In addition, collection distance determines solvent evaporation, thus affecting fibre morphology. This effect may lead to different results in different polymer solution systems.

Similar results were obtained from the spinning of PVP at different collection distances (**Figure 4-5**g-l). PVP fibres collected at 70 mm, 100 mm and 130 mm distances had diameters of 2.1 ± 0.7 µm, 1.8 ± 0.7 µm, and 1.3 ± 0.9 µm, respectively. This result shows that a longer collection distance tends to produce finer PVP fibres. However, PVP fibres with lower alignment were collected with the distance increase. The 130 mm collection distance resulted in the randomly arranged PVP fibres with an orientation coherency coefficient of 0.23. The PVP

fibres collected at the 70 mm and the 100 mm distance were highly anisotropic, having narrower orientation distributions and higher orientation coherency coefficients (0.42 and 0.36, respectively).

In **Figure 4-5**, some small beads were presented as a by-product of the spinning process. The formation of beads can be the result of multiple factors, among which polymer molecular weight and polymer chain entanglement are the important ones [95, 98, 225]. A molecular weight that does not provide sufficient chain entanglement results in the formation of beads. For a given molecular weight, the degree of chain entanglement increases with the increase of polymer concentration [105]. Thus, a high polymer concentration helps the production of smooth and uniform fibres, while a low concentration generally promotes bead formation [95]. The bead formation is also related to centrifugal force. Beads are produced when centrifugal force is insufficient to overcome surface tension before it reaches the collector [96]. This is the main reason for the beaded structure in fibres that are generated at a low rotational speed. In PG and nozzle-PG, the application of high-pressure nitrogen flow can enhance the instability of the flow state of the polymer jets, promoting the formation of beads [99, 225]. The collection distance also affects bead formation. At a short collection distance, the solvent is not able to evaporate fully, and solvent droplets remain on the fibre chains. These solvent droplets can prevent proper mixing of the polymer during jet drying, resulting in the formation of beads [15]. When the collection distance is too long, excessive stretching causes jet rupture [246]. Thus, the polymer jets break up into small droplets. These droplets eventually deposit on the collector, forming polymer beads on fibres.

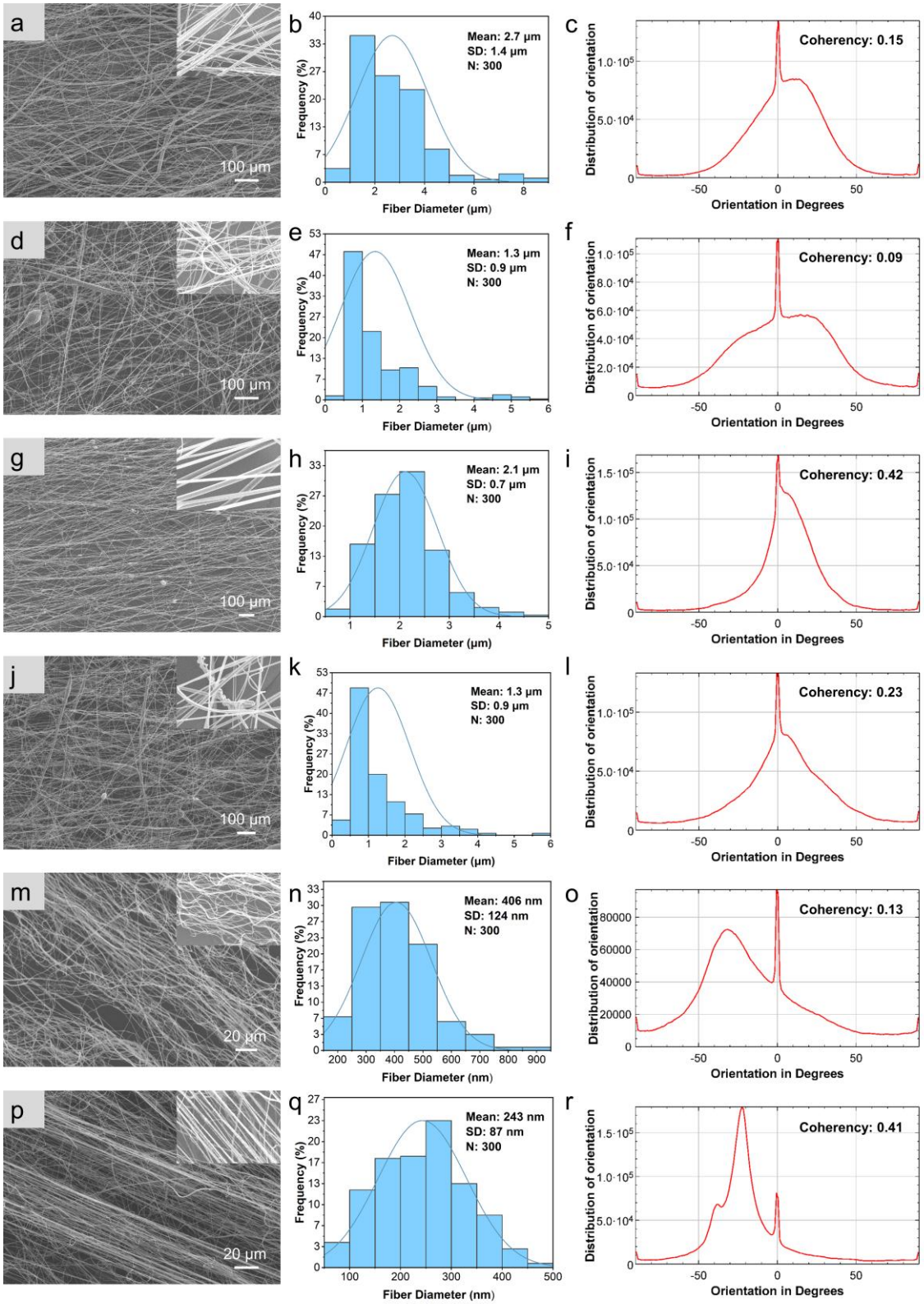

Figure 4-5 SEM images, fibre diameter distribution graphs and orientation distribution graphs of PCL fibres collected at (a-c) 70 mm and (d-f) 130 mm, PVP fibres collected at (g-i) 70 mm and (j-l) 130 mm, and PEO fibres collected at (m-

o) 70 mm and (p-r) 130 mm, in 1 × 10^5 Pa nozzle-pressurised gyration. The insets show the high-magnification SEM images of fibres. The results of PCL, PVP, and PEO fibres collected at the 100 mm distance are shown in **Figure 4-1**d-f, **Figure 4-3**d-f, and **Figure 4-4**d-f.

However, the results show some differences for water-soluble polymer PEO. As shown in **Figure 4-5**m-r, the PEO nanofibres collected at the 130 mm distance not only showed the smallest diameter and greatest uniformity (243 ± 87 nm) than PEO nanofibres collected at the 70 mm distance (406 ± 124 nm) and the 100 mm distance (273 ± 72 nm) but also had significantly aligned arrangement. Different from PCL fibres and PVP fibres, increasing collection distance in nozzle-PG produced PEO nanofibres with a highly unidirectional arrangement, since it's more difficult for pure water to fully evaporate compared with organic solvents [247]. The spinning jets experience air resistance when travelling in the air, during which the solvent undergoes forced convective mass transfer on the jet surface [248]. Subsequently, the solvent evaporates to form dry fibres. The time required for this process increases as solvent volatility decreases. Thus, for aqueous solvents which have relatively low volatility, a longer collection distance is desired to ensure proper fibre drying. In addition, it will extend the jet elongation so as to reduce the fibre diameter, especially for polymers with high flexibility and high ductility such as PEO.

4.6 Fibre Production Rate

Substantial fibre productivity is an essential prerequisite for the industrialisation and commercialisation of fibre manufacturing strategies. While electrospinning remains the most advanced and widely adopted method for fibre production, it

still faces significant limitations when it comes to scaling up. PG and its sister technologies have been developed in response to this challenge, aiming to realise the scale-up of fibre production. **Figure 4-6** highlights the notably higher fibre production rates of PG and nozzle PG compared to conventional electrospinning, showcasing their potential for more efficient large-scale fibre manufacturing.

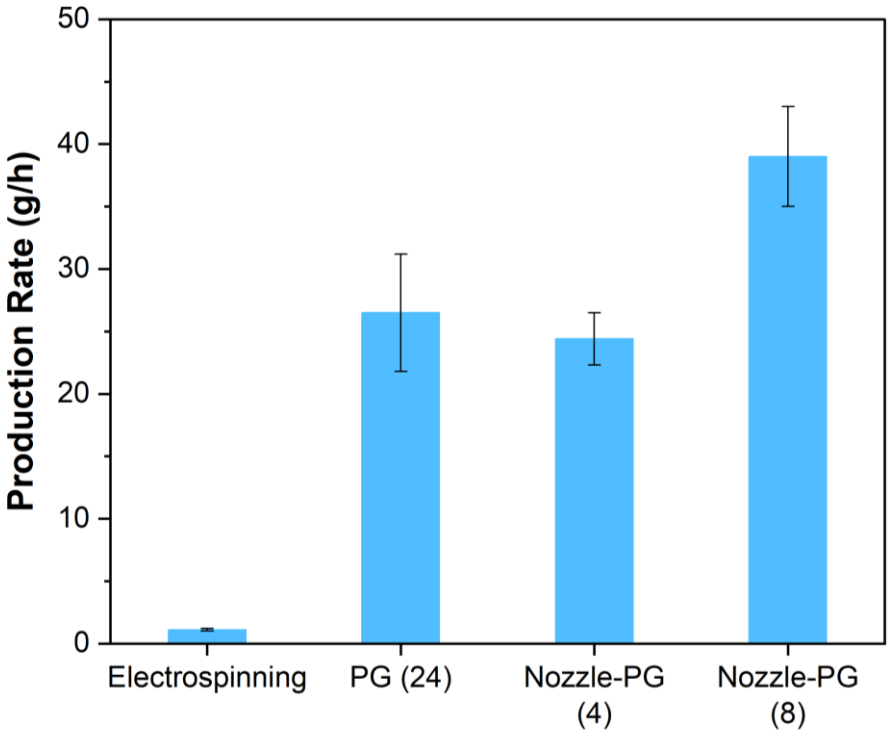

Figure 4-6 Fibre production rate of electrospinning, pressurised gyration with 24 orifices and nozzle-pressurised gyration with 4 and 8 nozzles.

In this study, electrospinning yielded only 1.1 ± 0.1 g of PVP fibres per hour, which falls well below the requirements for industrial-scale production. In contrast, PG and nozzle-PG demonstrated fibre production rates up to twenty times greater. Specifically, PG produced 26.5 ± 4.7 g PVP fibres per hour, while nozzle-PG achieved a fibre production rate of 24.4 ± 2.1 g/h with four nozzles and 39.0 ± 4.0

g/h with eight nozzles, respectively. Notably, the optimised eight-nozzle vessel used in this work produced a significantly higher yield than the four-nozzle version, highlighting its greater potential for scalable fibre manufacturing. These findings confirm that optimising the spinning vessel is both effective and beneficial for enhancing fibre productivity.

Moreover, it was observed that, despite having fewer liquid channels, nozzle-PG not only further enhanced fibre productivity but also demonstrated a more stable production rate compared to PG. This improvement may be attributed to the reduction in solution loss in nozzle-PG. In the PG process, solution flow instability often led to the aggregation and deposition of the polymer solution at the orifices, rather than the formation of fibres (**Figure 4-7**a), thereby significantly decreasing fibre yield. In contrast, nozzle-PG overcame this issue by improving the flow stability of the spinning jets, which were better directed by the nozzle. This enhanced flow stability contributed to more efficient fibre production and mitigated solution loss, further increasing the reliability of the nozzle-PG process, as shown in **Figure 4-7**b.

Besides the superior production rate, by eliminating the need for high-voltage electricity, PG offers economic benefits through lower energy consumption, reported by Amarakoon et al. [249]. Specifically, the energy consumption per spin of 1 mL of polymer solution is 5.19×10^5 J for PG, in contrast to 9.15×10^5 J for electrospinning, underscoring the superior efficiency and scalability of PG.

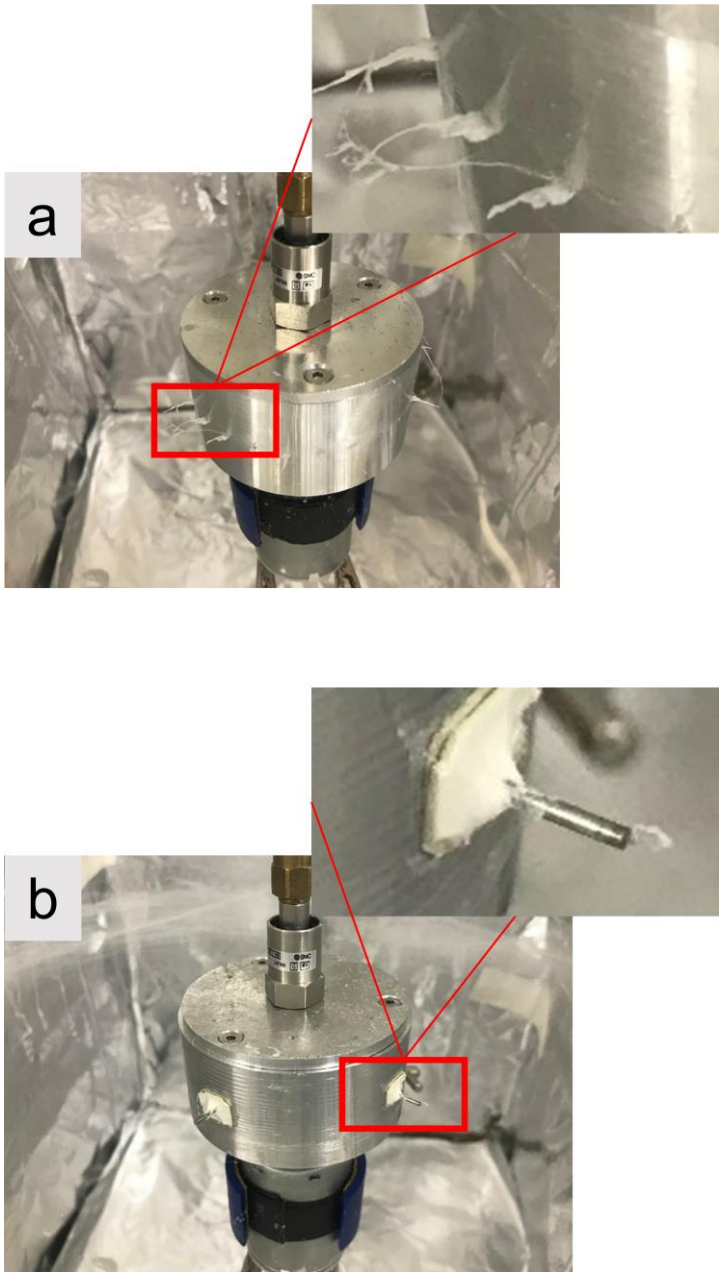

Figure 4-7 The deposition of solidified polymers in (a) pressurised gyration and (b) nozzle-pressurised gyration setups.

4.7 Mechanical Strength

Tensile strength is critical for evaluating the performance of polymeric fibres, as it directly influences their mechanical functionality and indirectly affects their biochemical and other characteristics, especially when used as tissue scaffolds.

Fibres fabricated through different technologies may exhibit differing tensile strengths due to variations in factors such as fibre size, morphology, alignment, and the presence of defects. These variations can significantly impact the overall mechanical properties of fibres, including their strength, flexibility, and durability. As such, tensile strength serves as a key indicator of a fibre's suitability for specific applications, particularly those requiring high mechanical resilience.

The ultimate tensile strength of PVP fibres fabricated by electrospinning, PG, and nozzle-PG was compared in **Figure 4-8**. The PVP fibres obtained from different methods had a tensile strength of 1 − 3 MPa, which is consistent with the data in the literature [250-252]. This correlation indicates that the test results are logical and reliable, reinforcing the validity of the findings. Under identical testing conditions, PVP fibres produced by nozzle-PG demonstrated superior mechanical strength compared to electrospun fibres, exhibiting ultimate tensile strengths of 2.9 ± 0.8 MPa and 1.9 ± 0.6 MPa, respectively, which aligns with our expectations. Electrospun fibres, characterised by a random orientation, possess isotropic properties, resulting in uniform mechanical behaviour in all directions. In contrast, highly aligned fibres from nozzle-PG concentrate strength along a specific axis, thus exhibiting the greatest tensile strength along the fibre length [253, 254]. The anisotropic mechanical properties of aligned fibres help distribute stress efficiently along the fibre length, minimising the risk of failure under tensile loads, and allowing for tailored performance based on the specific needs of the application. However, the relatively aligned fibres prepared by PG exhibited an unexpectedly low ultimate tensile strength of 1.2 ± 0.5 MPa, likely attributable to the presence of beads in fibres [255].

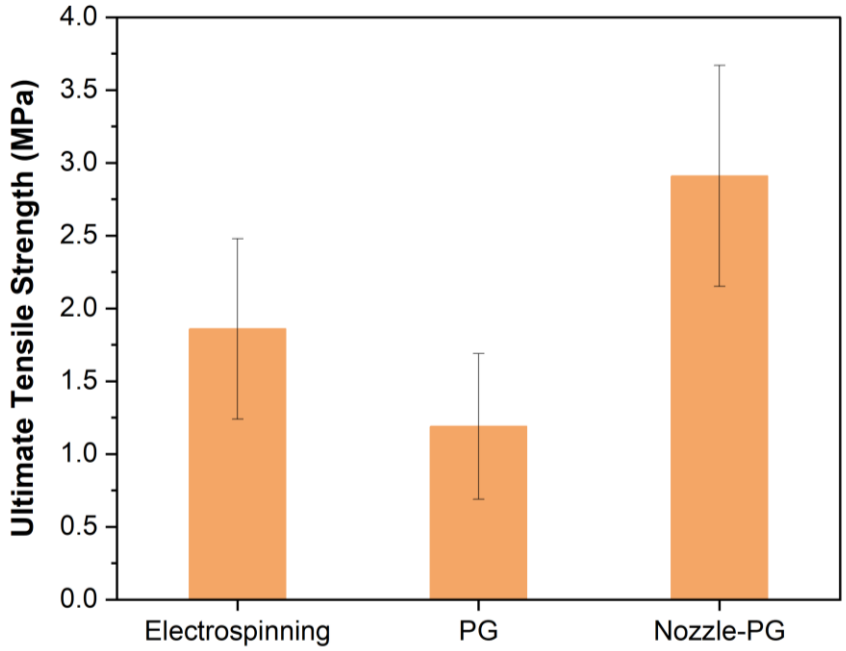

Figure 4-8 Ultimate tensile strength of PVP fibres produced by electrospinning, pressurised gyration, and nozzle-pressurised gyration.

4.8 Drug Encapsulation Efficiency and Release Analysis

Drug loading and release capacity are also important properties of polymeric fibres when used as biomaterials, as these fibres often serve as carriers for specific drugs or bioactive substances that modulate the biological activities of cells or tissues. In this work, PVP fibres loaded with CUR were used as a model system to investigate the effects of fibre fabrication technologies on drug loading efficiency and release profiles.

Figure 4-9 demonstrates the total encapsulation efficiency of CUR in the PVP fibres produced by electrospinning, PG, and nozzle-PG. The results show no significant differences in drug loading efficiency among the three fibre fabrication technologies. The highest efficiency at 77.4 ± 2.6% was achieved by nozzle-PG, while electrospinning and PG exhibited similar efficiencies of 73.3 ± 3.5% and

73.3 ± 4.5%, respectively. These findings suggest that all three methods perform comparably in terms of drug loading capacity. Notably, nozzle-PG exhibited the smallest intergroup variation in encapsulation efficiency, indicating a more stable and reliable encapsulation process. This enhanced consistency can be attributed to the improved jet stability conferred by the introduction of nozzles, which reduces the fluctuations typically encountered in nozzle-free PG systems.

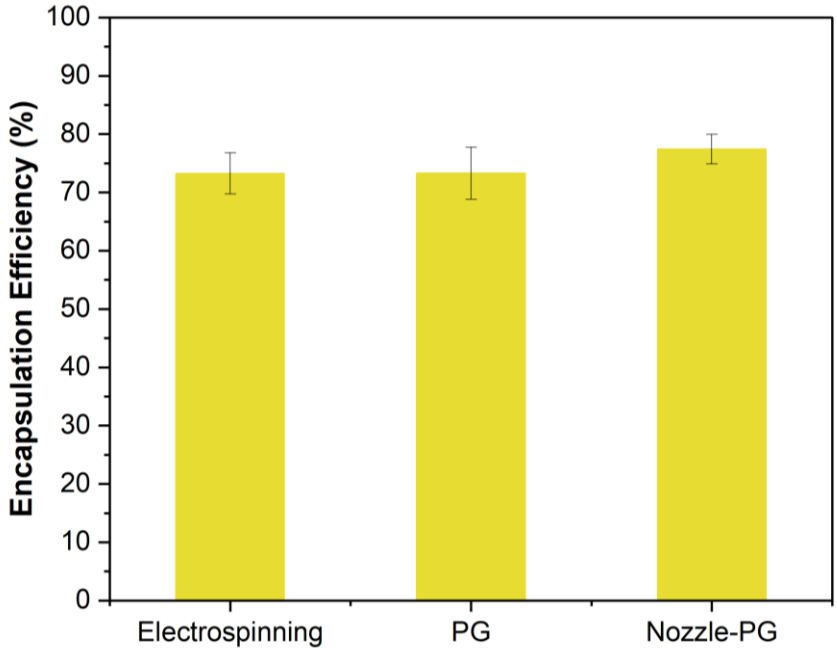

Figure 4-9 Drug encapsulation efficiency of PVP-curcumin fibres produced by electrospinning, pressurised gyration, and nozzle-pressurised gyration.

The transdermal release profiles of free CUR and CUR encapsulated within PVP fibres are presented in **Figure 4-10**. The drug-loaded fibres demonstrated significantly enhanced CUR release compared to the free drug. All three CUR-encapsulated PVP fibres achieved a release rate exceeding 60% over a 120-h transdermal test period, whereas free CUR exhibited a release rate of only 0.7%. CUR, known for its potent anti-inflammatory and antioxidant properties, suffers

from extremely low water solubility, leading to poor pharmacokinetic performance [256]. Encapsulating CUR within hydrophilic PVP fibres effectively improves its solubility and facilitates its release. Additionally, PVP fibres possess a high surface area-to-volume ratio and porosity, which reduces drug molecule aggregation and increases drug exposure, leading to the enhanced dispersion and diffusion of CUR molecules. Moreover, when embedded in the polymer matrix, CUR remains in an amorphous state rather than its crystalline form. The amorphous state is associated with higher solubility and a faster dissolution rate, thereby improving the drug's bioavailability [257]. Thus, hydrophilic polymer fibres provide an efficient delivery system for poorly water-soluble drugs.

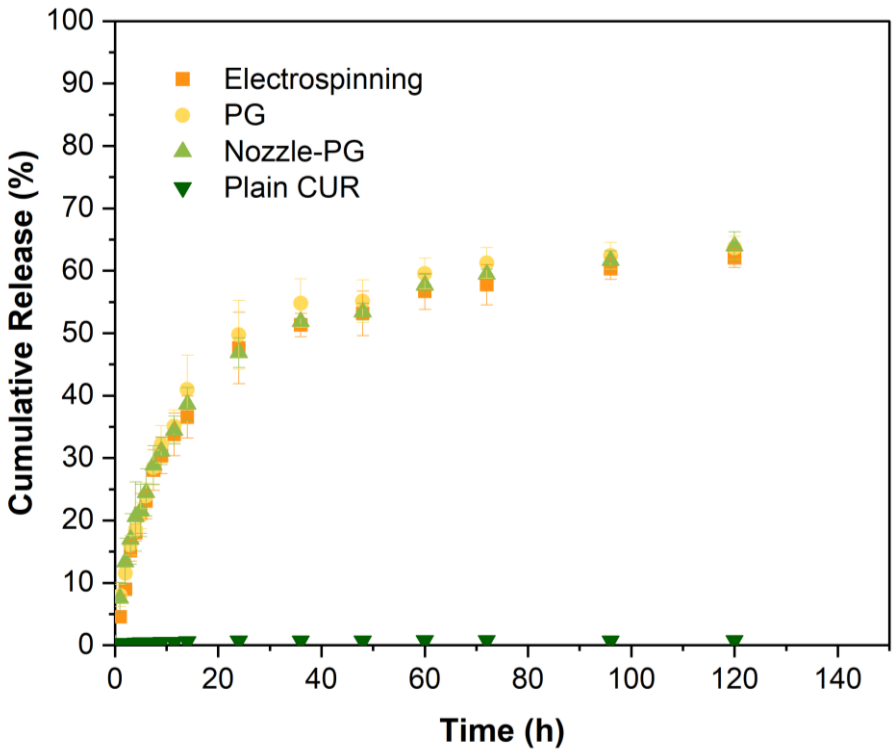

Figure 4-10 Transdermal release of curcumin from PVP fibres produced by electrospinning, pressurised gyration, and nozzle-pressurised gyration.

This study also demonstrated that fibres produced by PG and nozzle-PG achieved release efficiencies comparable to those of electrospun fibres, with release rates of 63.7 ± 1.9%, 64.0 ± 2.3%, and 62.1 ± 1.6%, respectively. These findings highlight the effectiveness of PG and nozzle-PG as viable alternatives to electrospinning for the fabrication of drug-loaded fibres with efficient release profiles.

Moreover, nozzle-PG offers distinct advantages over electrospinning in preserving the integrity of sensitive biological materials, such as enzymes, antibodies, and growth factors when used in fabricating drug delivery systems. The high-voltage electric fields applied in electrospinning can potentially degrade or denature these delicate substances. Nozzle-PG avoids such harsh conditions, thereby maintaining the functional properties of bioactive molecules. This characteristic makes nozzle-PG a highly suitable technique for applications that require the encapsulation or processing of sensitive biomolecules.

4.9 Conclusions

In conclusion, this research highlights significant advancements in PG, a scalable method for fibre production. The development of nozzle-PG offers notable improvements in fibre morphology, alignment, and production efficiency. This innovative technique facilitates the efficient formation of uniform and highly aligned fibres through a straightforward one-step process. These fibres exhibit comparable performance to electrospun fibres in terms of mechanical strength and drug release while achieving a fibre production rate of more than twenty times higher than electrospinning. Given its scalability, nozzle-PG emerges as a highly

promising technology for industrial-scale applications, paving the way for future innovations in fibre production and its diverse applications.

Moreover, the high fibre alignment achieved through nozzle-PG broadens its application potential. The parallel orientation of these fibres mimics the structure of natural tissues, such as the cornea, heart, nerves, and skeletal muscles, which facilitates cell adhesion, migration, and proliferation. Combined with its high tensile strength, nozzle-PG fibres are considered an encouraging candidate for tissue engineering scaffolds. Additionally, the highly uniaxially oriented fibres have the potential to control electrical diffusion, positioning them as a promising material for the production of advanced biosensors.

Overall, nozzle-PG has the potential to be a transformative technology in fibre production, offering a scalable method for generating high-performance fibres with broad applications in tissue engineering, drug delivery, and sensor technologies.

5 Nozzle-Pressurised Gyration for Biopolymer Spinning

5.1 Introduction

The extensive utilisation of polymer materials in diverse domains is well acknowledged. Presently, commercial polymer materials are predominantly petroleum-based synthetic polymers, also known as plastics. However, the challenge of plastic pollution is increasingly pressing, inflicting significant harm on ecosystems and human health. Global annual production of plastics surged from 1.5 million metric tons in 1950 to 390 million metric tons in 2021 [258]. While merely 20% of the resulting plastic waste is effectively managed, the majority ends up in landfills or the natural environment [259, 260]. The development of natural polymers, such as alginate, is perceived as a viable strategy to mitigate the challenges associated with the over-reliance on crude oil and plastic pollution [261].

This work performs ion exchange of Na-Alg by introducing a coagulation bath in nozzle-PG to produce Alg fibres. It is noted that high-molecular-weight Na-Alg solutions, even at a relatively low concentration (< 5 wt%), are significantly viscous, exhibiting a pronounced solid-like behaviour that complicates their processing [266]. The high working pressure applied in nozzle-PG effectively mitigates the viscous effects of Na-Alg solutions during spinning, facilitating the formation of continuous jets. Additionally, given the exceptional fibre production efficiency of nozzle-PG, this strategy stands out as a promising approach for the scaling up of Alg fibre production, compared with common methods like electrospinning and wet spinning. This study investigates the intricate interplay

between the solution properties/processing parameters and the resulting product in the modified nozzle-PG, providing a well-defined roadmap for producing desired Alg products. *Cinnamomum verum* is incorporated into Alg fibres using the modified nozzle-PG setup to explore their potential as antibacterial patches, highlighting a crucial aspect of these natural cinnamon-Alg fibrous patches as advancing biomaterials.

5.2 Solution Properties

Table 5-1 presents the surface tension and viscosity results of Na-Alg aqueous solutions. Notably, the acquisition of accurate surface tension data for the Na-Alg solutions with concentrations higher than 3.0 wt% was difficult, attributable to the pronounced influence of the measurement technique on surface tension determinations in highly viscous solutions, as reported by Lee [267]. As the concentration of Na-Alg increases from 1.0 wt% to 3.5 wt%, the viscosity escalates dramatically from 542.9 ± 1.2 mPa s to 67,873 ± 801 mPa s. This pronounced sensitivity of Na-Alg solution viscosity to concentration poses challenges for its processing via electrospinning. However, the high working pressure utilised in nozzle-PG effectively facilitates its spinning, offering a practical solution to these difficulties.

Table 5-1 Solution properties of Na-Alg solutions at different polymer concentrations.

Concentration [wt%]	**Surface Tension [mN/m]**	**Viscosity [mPa s]**
1.0	22.0 ± 0.9	542.9 ± 1.2

1.5	36.6 ± 1.1	2042 ± 37
2.0	58.5 ± 0.7	6783 ± 161
2.5	68.6 ± 1.1	13949 ± 164
3.0	-	27330 ± 251
3.2	-	51328 ± 508
3.5	-	67873 ± 801

5.3 Crosslinking of Alginate

In this work, Alg samples with different structures and morphologies were produced through a method based on the dry-jet wet spinning principle. Specifically, nozzle-PG was used to extrude the Na-Alg solutions into the ambient air, where the Na-Alg jets underwent stretching within the air gap (dry jet formation, **Figure 5-1**a). Subsequently, Alg gels with a more stable semi-solid structure formed in the $CaCl_2$ coagulation bath (wet spinning process, **Figure 5-1**b). Nozzle-PG, serving as a jet generator, has processing parameters such as rotational speed and working pressure that significantly influence jet formation and jet structure. Generally, increasing the rotational speed and working pressure of nozzle-PG is conducive to shortening the jet formation time and reducing the jet diameter, thus forming more and finer jets in a specific time [268]. The air gap length determined the degree of jet stretching. A longer air gap favoured sufficient stretching of the jets but may lead to relaxation of the polymer jets or jet rupture.

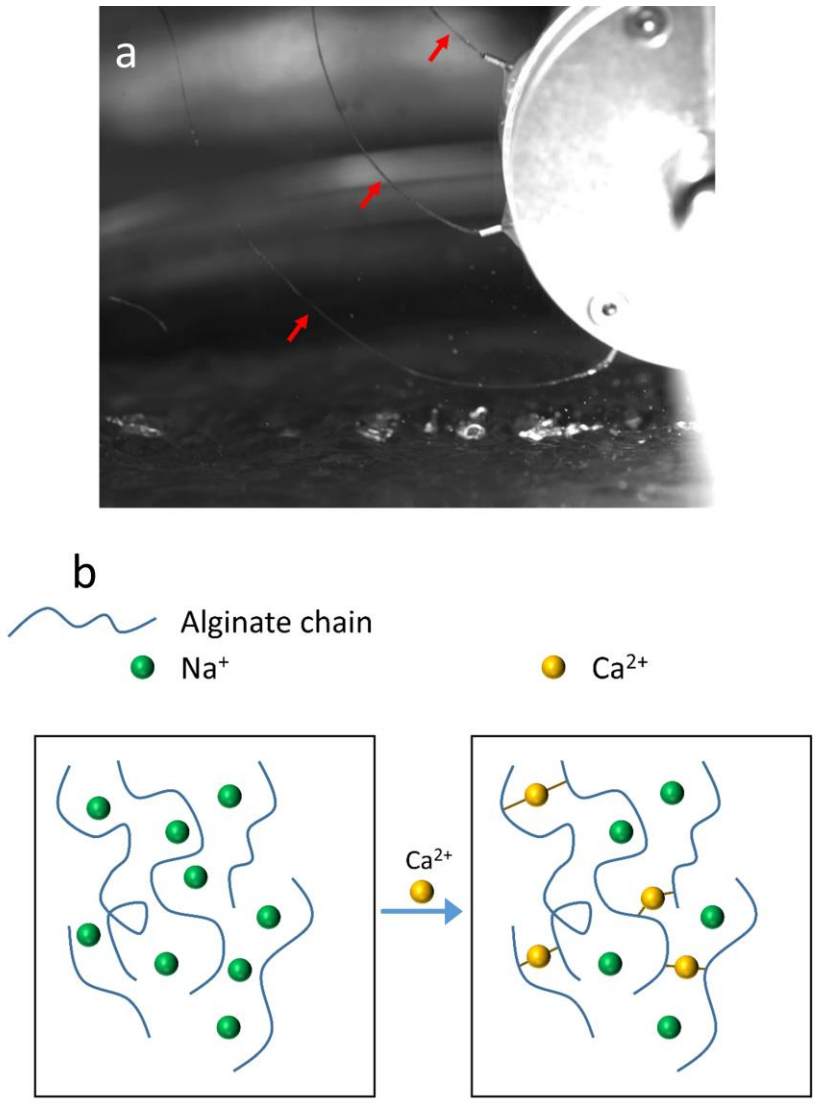

Figure 5-1 (a) Na-Alg solution jetting in nozzle-pressurised gyration and (b) crosslinking process of Alg chains in the Ca^{2+}-riched coagulation bath.

The divalent cations (Ca^{2+}) in the coagulation bath played a pivotal role in the eventual formation of Alg gels. When Na-Alg solutions were extruded into the Ca^{2+}-riched coagulation bath, Ca^{2+} selectively combined with the guluronic acid (G) blocks of the Alg chain, due to the higher degree of coordination with divalent ions of G blocks [269]. Thus, an ion exchange between Na^{+} and Ca^{2+} occurred. Ca^{2+} helped to bind adjacent Alg chains together in the cross-linked “egg-box” model, resulting in a robust gel network (**Figure 5-1**b) [270].

Figure 5-2 reveals that the Ca content of the Alg samples increases from 1.1 wt% to 12.2 ± 0.9 wt% after crosslinking, demonstrating the binding of Ca^{2+} to Alg chains while part of Na^{+} is released from the Alg system. Therefore, controlling the gelation rate is beneficial to achieve a more uniform gel matrix with enhanced mechanical strength.

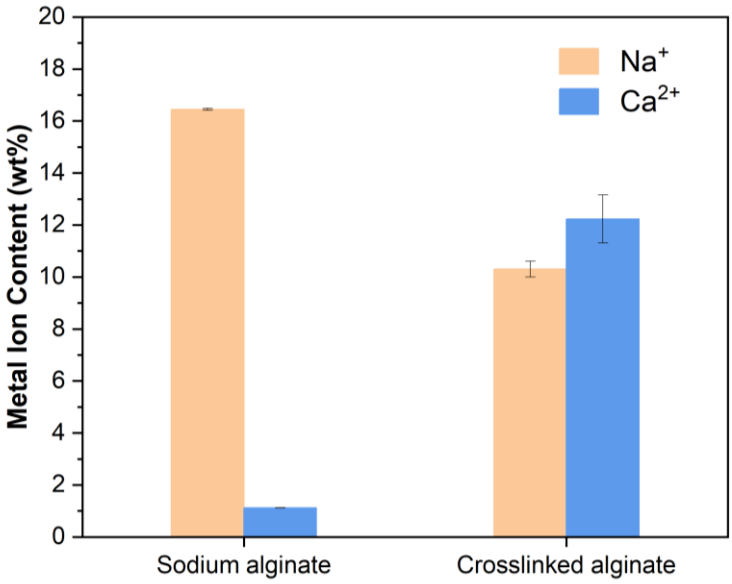

Figure 5-2 The content of Na^{+} and Ca^{2+} in Na-Alg and the crosslinked Alg samples, determined by microwave plasma atomic emission spectroscopy (MP-AES).

5.4 Effects of Solution Properties

To investigate the spinnability of Na-Alg solutions and their impacts on the morphology of Alg samples produced, Na-Alg solutions with concentrations ranging from 1.0 wt% to 3.5 wt% were processed using modified nozzle-PG. Apart from the solution concentration, all other processing parameters were kept consistent: rotational speed of 11 000 rpm, working pressure of 1×10^5 Pa, and air gap length of 6 mm. **Figure 5-3** illustrates a marked alteration in the

morphology of the obtained Alg samples correlating with an increase in solution concentration.

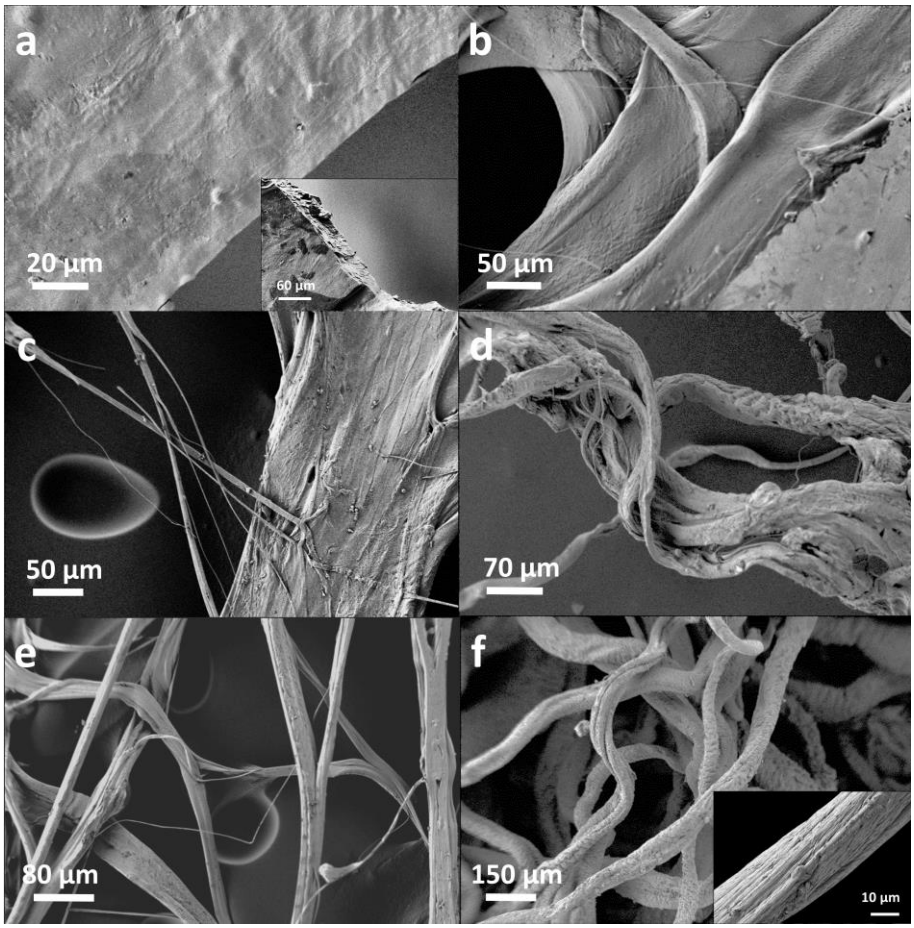

Figure 5-3 SEM images of Alg samples produced from Na-Alg solutions with concentrations of (a) 1.0 wt%, (b) 1.5 wt%, (c) 2.0 wt%, (d) 2.5 wt%, (e) 3.0 wt%, and (f) 3.5 wt%.

The Na-Alg solution with a concentration of 1.0 wt% formed a smooth and non-porous Alg film with an average thickness of approximately 30 µm after nozzle-PG processing (**Figure 5-3**a). When the Na-Alg concentration increased to 1.5 wt%, the Alg product evolved into a broad ribbon structure (**Figure 5-3**b). As the concentration continued to increase, more filamentous structures formed in the resulting samples, though some broad ribbons or large clumps persisted (**Figure**

5-3c, d). Upon the Na-Alg solution reaching a concentration of 3.0 wt%, these ribbon-shaped products and clumps dissipated entirely, yielding Alg fibres. Accordingly, with the concentration increasing from 3.0 wt% to 3.5 wt%, the obtained Alg fibres transitioned from flat (**Figure 5-3**e) to cylindrical (**Figure 5-3**f) in shape.

The pronounced difference in the structure of obtained Alg products is predominantly attributed to the difference in rheological properties engendered by the solution concentration. The rapid increase of solution viscosity with its increasing concentration is a remarkable feature of Na-Alg solution, accompanied by a significant reduction in its fluidity [271]. Therefore, the 1.0 wt% Na-Alg solution had the best liquid fluidity, and when it entered the coagulation bath, the Na-Alg phase quickly flowed and dispersed into a uniform film before gelation occurred. Thus, an Alg film with a smooth surface formed in this scenario. However, when the viscosity increased gradually with the increase of solution concentration, the fluidity of the Na-Alg solutions correspondingly deteriorated. After being immersed in the coagulation bath, these Na-Alg jets, hindered by their reduced mobility, predominantly preserved the elongated structure they adopted upon emerging from the nozzle tips. The high viscosity also prevented the infiltration of Ca^{2+} from the coagulant into the central area of the Na-Alg solution. Consequently, gelation initially occurred on the surface of the Na-Alg phase, obstructing the dispersion of the Na-Alg solution within the coagulation bath. Hence, the morphology of the resulting Alg samples evolved from a thin film to a ribbon-like structure, ultimately obtaining a filamentous form at the concentration of 3.0 wt%. It can be concluded that to produce Alg fibres with well-defined filamentous structures, the preparation of Na-Alg solutions that meet the critical

rheological properties is the key. The correlation between the solution viscosity and the resulting Alg structure is revealed in **Figure 5-4**. Na-Alg solutions with a concentration above 4.0 wt% are difficult to process due to their excessive viscosity.

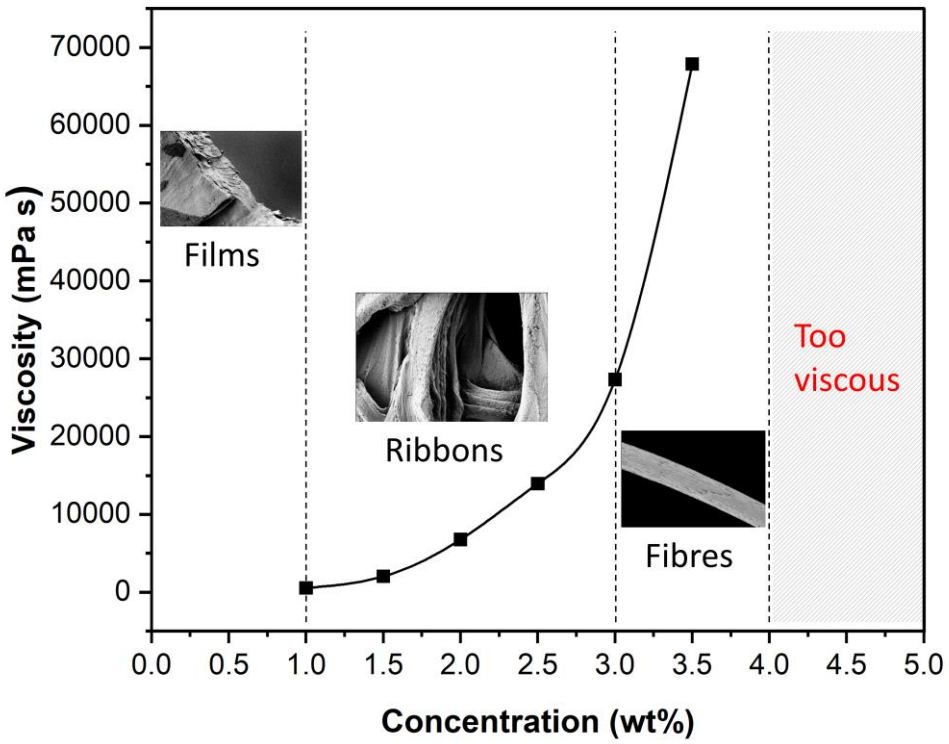

Figure 5-4 The viscosity profile of Na-Alg solutions and the structures of corresponding Alg products.

5.5 Effects of System Parameters

To further enhance the quality of the Alg products, the impact of different processing parameters in nozzle-PG on fibre morphology was explored in this section. In this study, Na-Alg solutions spun without pressure failed to overcome their surface tension and remained confined within the chamber. This scenario indicates the significance of high working pressure applied in nozzle-PG to

effectively process highly viscous solutions. With the increase of working pressure, the kinetic energy of the spinning jet increases accordingly, which facilitates additional stretching and refinement of the jet [268]. Additionally, a high working pressure shortens the time required for jet formation, thereby improving the spinning efficiency of nozzle-PG [268]. Similarly, the rotational speed affects the fibre formation by influencing the motion state of the jet. Only when the rotational speed reaches the critical value, the solutions can be ejected to form spinning jets. The Na-Alg solution processed under low-speed spinning (< 9 000 rpm) was subjected to decreased production efficiency and led to the waste of feedstock due to insufficient kinetic energy.

Therefore, weighing the synergistic effect of working pressure and rotation speed is pivotal to producing Alg fibres via nozzle-PG, intending to attain optimal product morphology and production efficiency. In the context of this research, by setting the system parameters to the working pressure of 2×10^5 Pa, the rotational speed of 11 000 rpm, and the air gap length of 6 mm, the desired Alg fibres with an average diameter of approximately 10 µm were successfully produced using 3.2 wt% Na-Alg solution (**Figure 5-5**). The inset in **Figure 5-5**a provides a microscopic depiction of the Alg fibre surface.

The Alg fibre exhibited prominent striations along the longitudinal axis on the surface. The formation of these grooves can be attributed to the uneven diffusion of the coagulant on the jet surface in wet spinning [272]. A pronounced viscosity difference between the Na-Alg solution and the Ca^{2+} coagulant impeded biphasic diffusion, resulting in the formation of deeper grooves on the surface. Conversely, the small viscosity difference between the low-concentration Na-Alg solution and

the coagulant was conducive to the fluidity and diffusion of the Na-Alg phase in the coagulation bath, thus forming an Alg product with a smoother surface (**Figure 5-3**a). In terms of fibre size and morphology, there was no significant difference observed between the cinnamon-containing Alg and the pure Alg samples when the polymer concentration and the processing parameters were kept consistent.

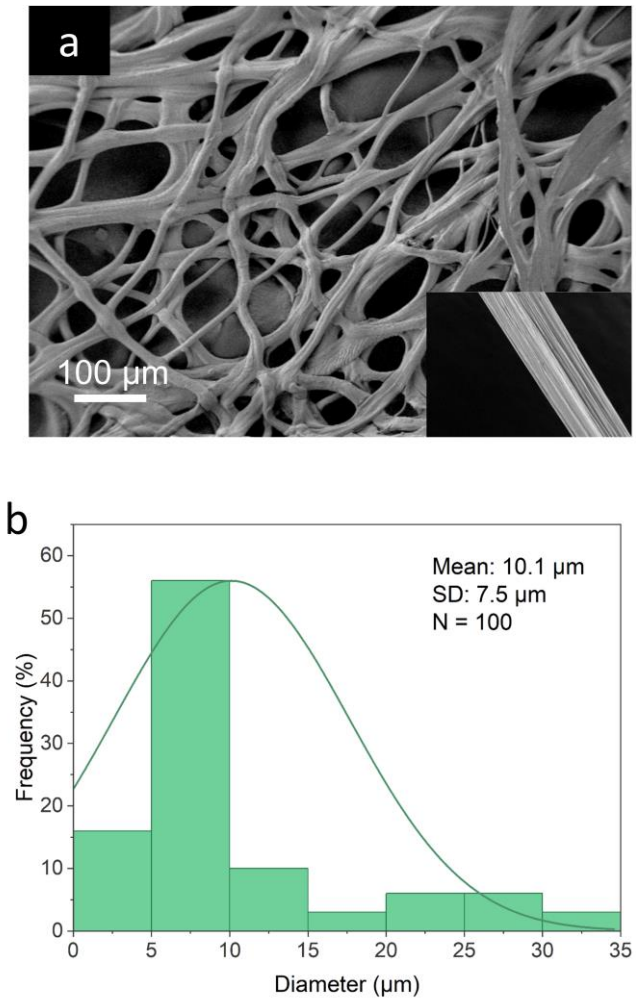

Figure 5-5 SEM image and diameter distribution of Alg fibrous patches produced by modified nozzle-pressurised gyration under the processing conditions of 3.2 wt% of Na-Alg solution, working pressure of 2×10^5 Pa, rotational speed of 11 000 rpm, and air gap length of 6 mm.

In conventional PG methodologies, higher pressures and rotational speeds are generally favoured to enhance fibre morphology and yield. Yet, the results from our experiments elucidated the negative impacts of excessively high pressure and rotational speed on the manufacturing of Alg fibres using this method. Such outcomes might stem from a discord between the balance of jet formation and its solidification rate. Within the coagulation bath, the double diffusion of Ca^{2+} and Na^{+} ions leads to the cross-linking interaction between the Ca^{2+} ions and Alg chains, resulting in the solidification of fibres. Therefore, the time required for the solidification process includes diffusion time and cross-linking time, which is longer than normal ionic bond formation. According to Yan et al. [273] when certain assumptions are met, the diffusion process can be expressed by **Equation 5-1**:

$$\frac{M_t}{M_\infty} = 1 - \sum_{n=0}^{\infty} \frac{8}{(2n+1)^2\pi^2} \exp\left[\frac{-D(2n+1)^2\pi^2 t}{l^2}\right]$$

Equation 5-1

where, *l* is half of the fibre diameter, M_t is the percentage of Ca^{2+} diffusing into the fibre at time *t*, M_∞ is the percentage of Ca^{2+} diffusing into the fibre after diffusion, and *D* is the diffusion coefficient.

The value of the intermediate stage of diffusion, specifically when $\frac{M_t}{M_\infty} = 0.5$, is recognised as the actual diffusion coefficient. At this juncture, **Equation 5-1**can be simplified to:

$$D = 0.0492\frac{l^2}{t}$$

Equation 5-2

In **Equation 5-2**, a relationship is established among the diffusion coefficient, the diffusion time, and the fibre diameter. This relationship provides valuable insights into the dynamic behaviour of jet coagulation processes.

After analysing the solution properties and system parameters, as well as considering the results of preliminary experiments, the optimal spinning conditions were defined as follows: the Na-Alg concentration of 3.2 wt%, the rotational speed of 11 000 rpm, the working pressure of 2×10^5 Pa, and the air gap length of 6 mm. This protocol was applied to process Na-Alg solutions containing natural cinnamon substrates, resulting in the production of cinnamon-containing Alg fibrous patches for evaluating cell viability and antibacterial properties. The specifics of each sample are listed in **Table 5-2**.

Table 5-2 Solution properties, average fibre diameter, and acronym of Alg and cinnamon-containning Alg samples. The concentration of Na-Alg remained constant at 3.2 wt%.

Cinnamon Source	**Cinnamon Concentration [w/w%]**	**Average Fibre Diameter [µm]**	**Acronym**
-	0	10.1 ± 7.5	Alg
Ground cinnamon	1	12.8 ± 7.6	Alg-GC1
Ground cinnamon	2	12.9 ± 6.0	Alg-GC2
Ground cinnamon	4	13.5 ± 8.0	Alg-GC4
Cinnamon essential oil	1	12.2 ± 7.8	Alg-CEO1

Cinnamon essential oil	2	12.6 ± 5.0	Alg-CEO2
Cinnamon essential oil	4	13.5 ± 7.7	Alg-CEO4
Cinnamaldehyde	1	14.8 ± 8.0	Alg-CA1
Cinnamaldehyde	2	12.6 ± 6.0	Alg-CA2
Cinnamaldehyde	4	12.9 ± 6.9	Alg-CA4

5.6 Cytotoxicity Features

The indirect cytotoxicity test of pure Alg and cinnamon-containing Alg samples was conducted using the WST-1 assay, following the ISO 10993-5 standard for medical devices. The results highlighted the exceptional biocompatibility of Alg as a promising biomaterial with its fibrous patches retaining a cell-friendly nature [274]. As shown in **Figure 5-6**, the pure Alg fibrous patches exhibited a cell viability of 94 ± 2.8% compared to the negative control, confirming their non-toxic and biocompatible properties. In contrast, the positive control treated with DMSO showed a significantly lower cell viability of 31 ± 7.8%, underscoring the sensitivity of the L929 cell line and validating the test system [275]. These findings reinforce Alg's suitability for biomedical applications, particularly in wound healing and tissue engineering, where biocompatibility is a critical requirement.

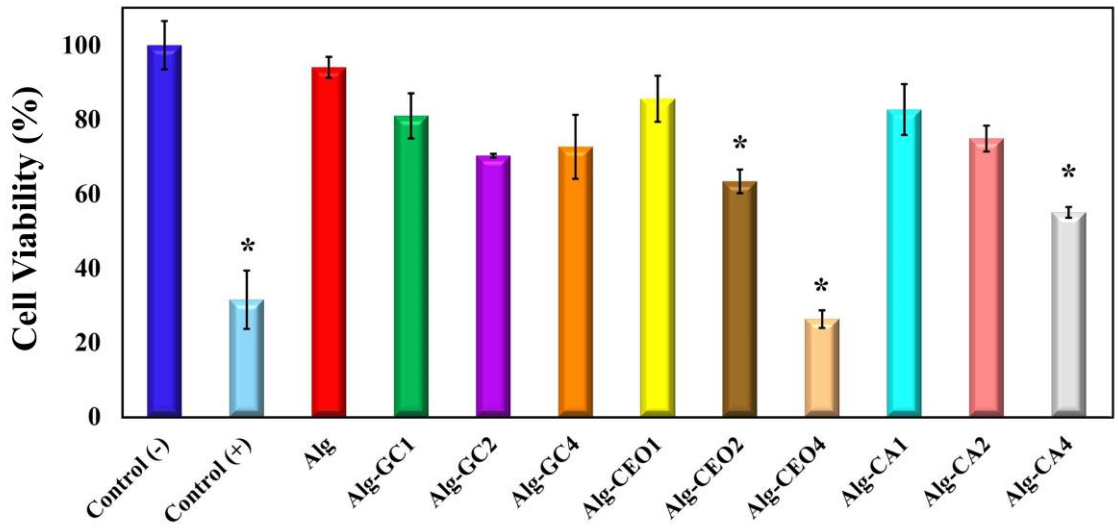

Figure 5-6 Cell cytotoxicity test results of Alg and cinnamon-containing Alg fibrous samples with the different concentrations (1%, 2%, and 4%, w/w) of ground cinnamon, cinnamon essential oil, and cinnamaldehyde, (Alg, Alg-GC1, Alg-GC2, Alg-GC4, Alg-CEO1, Alg-CEO2, Alg-CEO4, Alg-CA1, Alg-CA2 and Alg-CA4, respectively). (* indicates the statistically significant difference $p<0.005$)

Additionally, it was determined that when GC was added to Alg fibrous patches, cell proliferation did not show toxicity at all concentration values. The cytotoxicity limit is defined by the ISO standard as below 70% cell viability. Alg-GC1, Alg-GC2, and Alg-GC4 fibrous patch sample groups showed above 70% cell viability compared to negative control. Ahmed and coworkers [263] also reported that the cinnamon powder extracts do not exhibit cytotoxic effects on L929 fibroblast cells.

Figure 5-6 also reveals the cytotoxic effect of CEO as its concentration increased in the Alg samples. The Alg-CEO1 sample group demonstrated 86 ± 6.2% cell viability compared to the negative control, indicating good biocompatibility at lower concentrations. However, at higher concentrations, the Alg-CEO2 and Alg-CEO4 sample groups exhibited significantly reduced cell viability of 63 ± 3.2%

and 26 ± 2.4%, respectively, reaching the cytotoxicity limit defined by ISO standard. This indicates that excessive CEO concentrations compromise cell compatibility, likely due to the bioactive compounds in the essential oil that can disrupt cellular integrity at higher doses. A similar trend was observed with the CA groups, though cytotoxicity was less pronounced at lower concentrations. The Alg-CA1 and Alg-CA2 sample groups displayed cell viabilities of 83 ± 6.9% and 75 ± 3.5%, respectively, maintaining acceptable biocompatibility. However, at the highest concentration, the Alg-CA4 sample group exhibited a toxic effect, showing a marked decline in cell viability to 55%.

These findings suggest that while both CEO and CA have promising applications due to their bioactive properties, careful control of their concentrations is essential to maintain biocompatibility. Lower concentrations can be effectively incorporated into Alg-based biomaterials for therapeutic applications, while higher concentrations should be avoided to prevent cytotoxic effects.

In this study, the pure Alg, Alg containing 1%, 2%, and 4% (w/w) GC, Alg containing 1% (w/w) CEO, and Alg containing 1% and 2% (w/w) CA fibrous patches were determined to be cell-friendly and have the potential to be used as biomaterials.

5.7 Antibacterial Features

Alg, Alg-GC1, Alg-GC2, Alg-GC4, Alg-CEO1, Alg-CEO2, Alg-CEO4, Alg-CA1, Alg-CA2, and Alg-CA4 fibrous patch sample groups were tested against gram-negative *E. coli* (ATCC 25922) and gram-positive *S. aureus* (ATCC 29213) bacteria species. The antibacterial tests were applied according to the biofilm

formation determination assay. The results were reported in terms of adhered colony-forming units (**Figure 5-7**) and microscopic evaluations of adhered bacteria fixation (**Figure 5-8**).

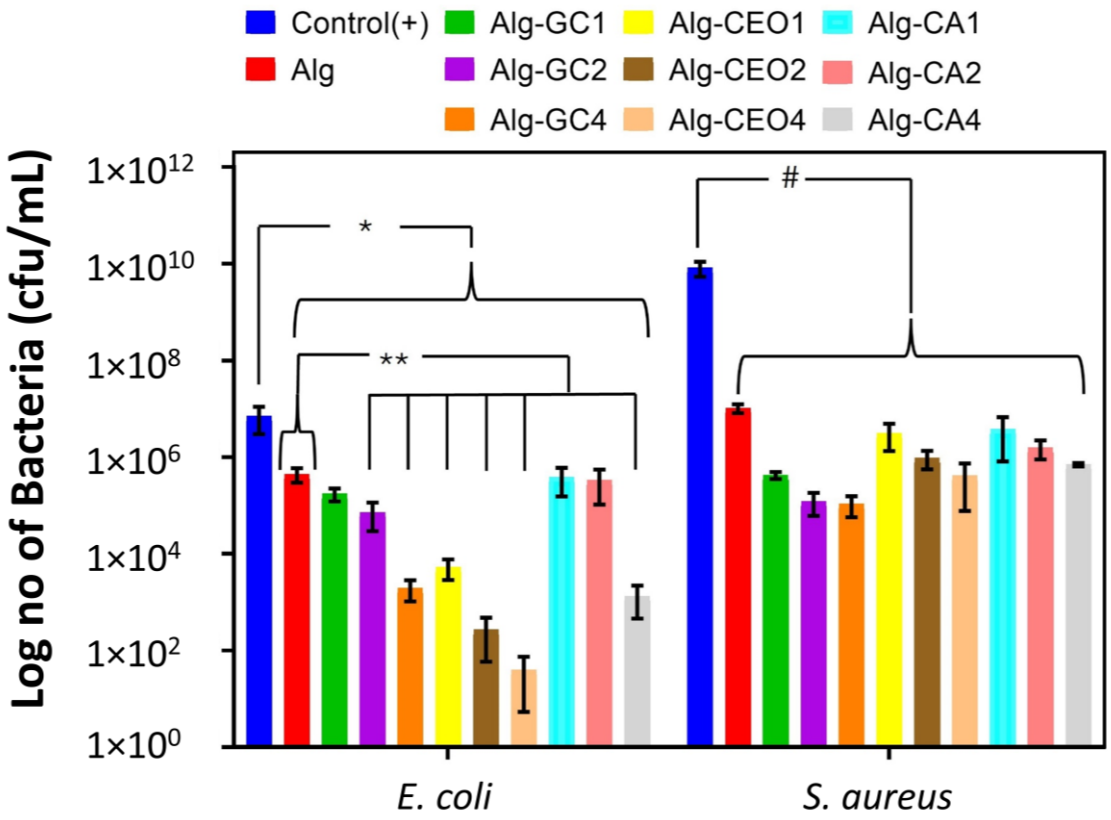

Figure 5-7 Antibacterial test results of Alg and cinnamon-containing Alg fibrous samples with the different concentrations (1%, 2%, and 4%, w/w) of ground cinnamon, cinnamon essential oil, and cinnamaldehyde, (Alg, Alg-GC1, Alg-GC2, Alg-GC4, Alg-CEO1, Alg-CEO2, Alg-CEO4, Alg-CA1, Alg-CA2 and Alg-CA4, respectively) against gram-negative *E. coli* (ATCC 25922) and gram-positive *S. aureus* (ATCC 29213) bacteria species. (*, ** and # indicate the statistically significant difference $p<0.005$)

The antibacterial test results showed that a decrease in bacterial adhesion and biofilm formation was detected at least log 1 in all groups for both gram-negative

E. coli (ATCC 25922) and gram-positive *S. aureus* (ATCC 29213) bacteria species. It was determined that increasing cinnamon concentrations increased the antibacterial activity in all 3 cinnamon groups (Alg-GC, Alg-CEO, and Alg-CA). On the other hand, antibacterial tests showed results consistent with cellular tests. All the sample groups exhibited statistically significant antibacterial activity against the control group for *E. coli* (ATCC 25922). It was determined that the dose-dependent increase of active ingredient concentration reduced bacterial activity by log 5 for Alg-CEO4, log 4 for Alg-CEO2, and log 3 for Alg-CA4. However, they also had a toxic effect on healthy cells of *E. coli* bacteria species. GC-MS spectrum (**Figure 3-3**) showed that CEO contained antibacterial compounds eugenol, cinnamyl acetate, and cinnamaldehyde-E. These data indicate that the high antibacterial effect of CEO compared to CA can be attributed to the synergistic effect of cinnamaldehyde-E, eugenol, cinnamyl acetate, and other chemical compounds. Additionally, this synergistic effect resulted in cytotoxicity in high-concentration CEO sample groups. It was determined that Alg-GC sample groups showed antibacterial activity at all concentrations without any cytotoxic response. Alg-GC1, Alg-GC2, and Alg-GC4 fibrous patch sample groups showed log 1, log 2, and log 3 decrease in biofilm formation against *E. coli* bacteria species, respectively. Additionally, Alg-GC2, Alg-GC4, Alg-CEO1, Alg-CEO2, Alg-CEO4, and Alg-CA4 fibrous patch sample groups exhibited a statistically significant decrease on biofilm formation of *E. coli* compared to Alg ($p<0.005$). Moreover, statistically significant antibacterial activity was also determined for *S. aureus* bacteria species for all sample groups compared to the control group ($p<0.005$). The number of adhered bacteria decreased up to log 5 for GC-included sample groups (Alg-GC1, Alg-GC2, Alg-

GC4). Notably, distinct antibacterial effects were observed between Alg-CEO and Alg-GC formulations. Specifically, Alg-CEO exhibited the strongest antibacterial activity against gram-negative *E. coli*, while Alg-GC demonstrated superior antibacterial efficacy against gram-positive *S. aureus*. These differences can be attributed to the unique components of each formulation and their respective antibacterial mechanisms. CEO primarily contains lipophilic compounds such as cinnamaldehyde, eugenol, and linalool. These compounds can effectively penetrate and disrupt the lipid membranes of gram-negative *E. coli*, leading to increased membrane permeability and cell death. In contrast, GC has a significantly lower concentration of cinnamaldehyde and contains additional non-volatile components, such as cinnamic acid and tannins. These non-volatile substances exert their antibacterial effects primarily against gram-positive *S. aureus* by interfering with cell wall synthesis and integrity, leading to the leakage of cellular contents and cell death. These findings highlight the potential for tailored applications of these cinnamon-containing Alg fibres depending on the bacterial target.

Biofilm formation and antibacterial activity of fibrous patches are also evaluated by SEM micrographs (**Figure 5-8**). The results showed similar results with the biofilm formation determination tests. Alg-GC1, Alg-GC2, Alg-GC4, Alg-CEO1, Alg-CA1, and Alg-CA2 fibrous patch sample groups showed less bacterial adhesion than Alg sample group for both *E. coli* and *S. aureus* bacteria species as is shown in **Figure 5-8**. It was also observed in SEM images that gram-positive *S. aureus* bacterial species adhered to the fibrous patch sample surfaces more than gram-negative *E. coli* bacterial species. The results were supported by the antibacterial activity of cinnamon as reported in the literature [263, 276].

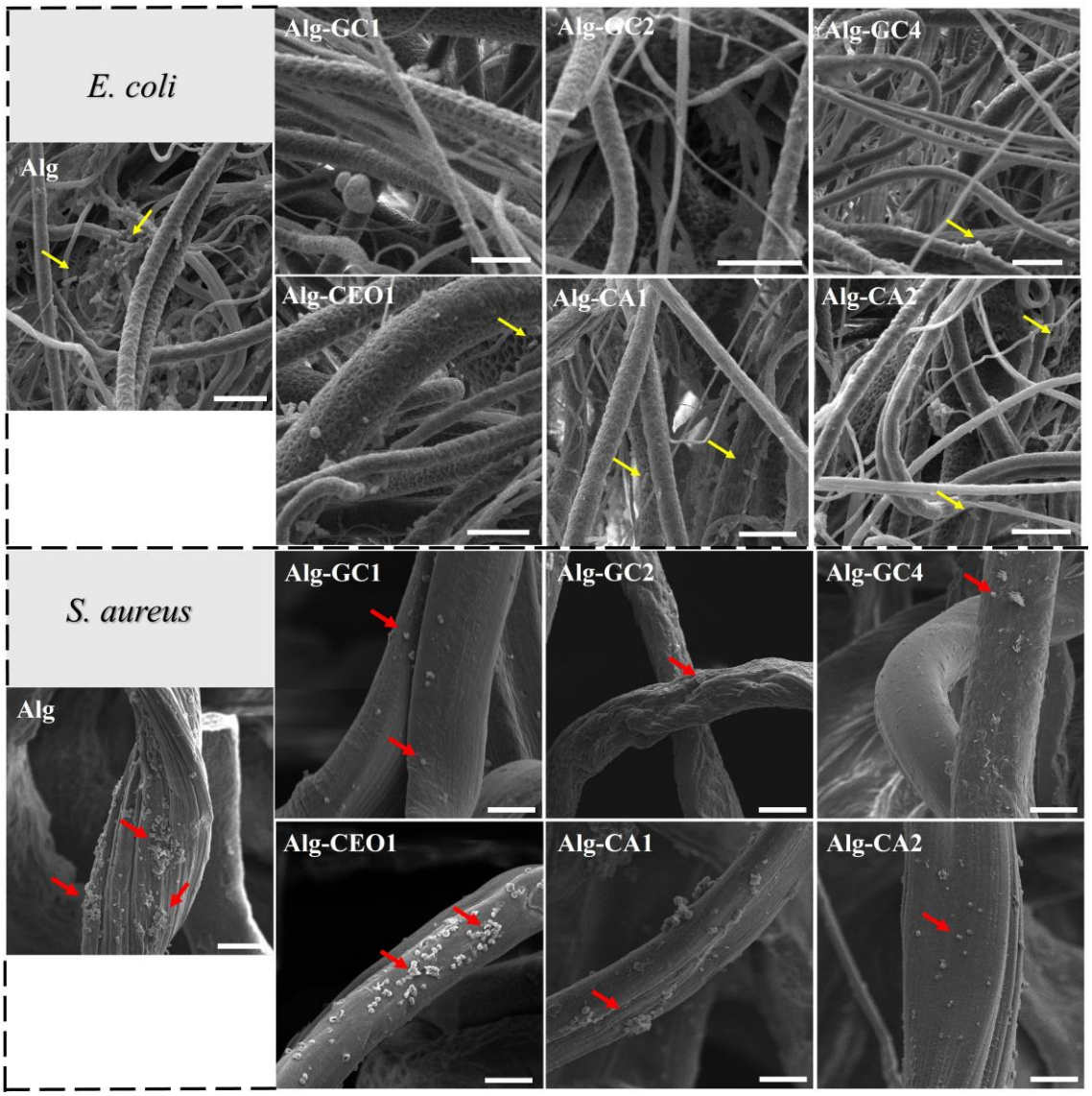

Figure 5-8 SEM images of fibrous patches with adhered *E. coli* and *S. aureus* bacteria species on cinnamon-containing Alg fibrous samples with 1%, 2%, and 4% (w/w) of ground cinnamon, 1% (w/w) of cinnamon essential oil, and 1% and 2% (w/w) of cinnamaldehyde, (Alg-GC1, Alg-GC2, Alg-GC4, Alg-CEO1, Alg-CA1, and Alg-CA2, respectively). Yellow arrows indicate *E. coli* and red arrows indicate *S. aureus* bacteria species. (Scale bar = 10 µm)

Natural components, especially cinnamon, and its derivatives, are important antibacterial agent candidates with different strategies that inhibit bacterial cell

division, ATPase activity, quorum sensing (QS) contact, membrane porins or alter bacterial cell membrane permeability [277]. The synergistic effect of these features is used to create common solutions to the differences in the membrane structures of gram-negative and gram-positive bacteria.

According to the antibacterial activity results of *E. coli* and *S. aureus*, Alg-GC4 and Alg-CEO1 show great potential as antibacterial wound dressing candidates with high antibacterial activity against both gram-negative and gram-positive bacteria species and high cell compatibility.

5.8 Conclusions

In this study, an innovative Alg fibre processing approach based on nozzle-PG was developed. This method combines the high production efficiency of nozzle-PG with the adaptability of wet spinning for Alg materials, offering a scalable, cost-effective, and straightforward pathway for Alg fibre production. By meticulously adjusting the solution concentration and processing parameters associated with nozzle-PG, a comprehensive protocol for producing Alg fibres using this innovative method was established. As a result, Alg fibrous patches with a fibre diameter of approximately 10 μm were successfully produced. Subsequently, three *Cinnamomum verum* substances were incorporated in the resulting Alg fibrous samples. When incorporated with *Cinnamomum verum*, the resulting Alg fibrous patches demonstrated exceptional antibacterial activity against both gram-negative and gram-positive bacterial species, showcasing a dosage-dependent response. Higher cinnamon content enhanced antibacterial efficacy but also led to increased cytotoxicity. Remarkably, even the pure Alg patches displayed considerable antibacterial properties and significant

biocompatibility, underscoring their potential as standalone biomaterials for biomedical applications. While the inclusion of *Cinnamomum verum* significantly bolstered antibacterial performance, their cytotoxic effects at higher concentrations necessitate cautious optimisation for safe biomedical use. These findings establish this innovative Alg fibre processing technique, combined with the potent bioactivity of cinnamon extracts, as a promising platform for creating advanced antibacterial biomaterials with applications ranging from wound dressings to infection-resistant medical devices.

6 Exploring Sustainable Sources for Nozzle-Pressurised Gyration

6.1 Introduction

Dairy farm waste such as cow manure/dung is a major threat to the environment especially in polluting water bodies and contributing to waterborne diseases and public health hazards [278]. Effective methods for recycling and repurposing these wastes are imperative. In regions where agriculture and animal husbandry prevail, animal waste finds utility as crop fertilizer, fuel, or house insulation material. Recently, there is growing interest in recovering valuable substances from these waste materials for refinement into high-value products, thereby finding applications across diverse fields such as packaging, energy, electronics, and biomedicine [279]. Considering the significant cellulose (1.6-23.5%), hemicellulose (1.4-12.8%), and lignin (2.7-13.9%) in the undigested materials from animal waste [280], efforts have been dedicated to its utilisation as a feedstock for cellulose extraction. This new route is presented as a good fit into the circular economy due to its abundance, low cost, and great potential to address waste management challenges associated with animal husbandry.

In this work, the upcycling of waste materials is achieved by extracting nanocellulose from two sources: the insoluble residue of sugar kelp after Alg extraction and cow manure from a local dairy farm waste. This is accomplished through a combination of chemical treatments and mechanical homogenisation. The extracted cellulose subsequently served as the spinning feedstock for the modified nozzle-PG integrating with a coagulation bath. These pressure-spun

cellulose products hold the potential of becoming value-added commodities due to their inherent characteristics, thereby realising the concept of “Waste to Wealth”. In addition to natural and sustainable raw materials, the entire processing procedure avoided to use/produce chemicals or byproducts that pose significant environmental hazards and was simple, efficient, and low-cost, in line with the requirements of a circular economy.

6.2 Solution Properties

Surface tension and viscoelasticity are two main factors that determine the solution spinnability in nozzle-PG. Solutions with a very low viscosity cannot provide sufficient chain entanglement to form spinning jets while an extremely viscous solution cannot overcome its surface tension, resulting in the inability to form fibres. **Table 6-1** shows the viscosity results of cellulose solutions derived from seaweed and animal waste, respectively. As discussed in Section 5.2, the measurement method significantly affects the accuracy of surface tension measurements for highly viscous solutions [281]. Consequently, surface tension data for the cellulose solutions used in this study was not analysed.

Table 6-1 Cellulose solution properties at different polymer concentrations.

Polymer	**Solvent**	**Concentration [wt%]**	**Viscosity [mPa s]**
Seaweed-Derived Cellulose	A mixture of EMIM OAc and DMSO (1: 1, w/w)	1	127.0 ± 1.0
		1.5	781.0 ± 3.1
		2	9634 ± 313
		2.5	36233 ± 2310

		3	110626 ± 3355
Animal Waste-Derived Cellulose	A mixture of EMIM OAc and DMSO (1: 1, w/w)	2	155.5 ± 0.3
		4	1421 ± 27
		6	16787 ± 106
		8	95357 ± 4427
		10	223552 ± 1997

As presented in **Table 6-1**, a slight increase in cellulose concentration led to a significant rise in solution viscosity, which was accompanied by a rapid decline in solution fluidity. This phenomenon was observed in cellulose derived from both seaweed and animal waste, from 127.0 ± 1.0 mPa s to 110626 ± 3355 mPa s and from 155.5 ± 0.3 mPa s to 223552 ± 1997 mPa s, respectively. These results exhibited the typical viscosity−concentration dependence of cellulose/EMIM OAc solutions, which is consistent with the previously reported work [64, 282-284]. It was observed that the cellulose extracted from seaweed exhibited a higher solution viscosity compared to that extracted from animal waste at the same solution concentration. This difference may be attributed to the higher impurity content in the animal waste-derived cellulose, as evidenced by the precipitation observed in its solution. Additionally, the rheological behaviour of cellulose/EMIM OAc solutions can be affected by the water impurities of the ionic liquid solvent. The water existing in the ionic liquid is considered to decrease the solubility of cellulose, which is presumably due to the competitive hydrogen bonding [285]. Therefore, cellulose extract and ionic liquid are required to be stored in a dry

environment prior to use, and the dissolution process should be conducted under moisture-free conditions to prevent interference.

6.3 Seaweed-Derived Cellulose Fibre Production

In this work, the mechanism for making cellulose fibres is essentially a combination of gyrospinning and wet spinning (dry-jet wet spinning), as discussed in Section 5.3. Nozzle-PG was used as a jet generator. The extruded cellulose fluid from nozzle-PG was stretched in the air to form continuous spinning jets, due to the pressure difference and fluid viscoelasticity. In the water coagulation bath, the solvent in polymer jets underwent diffusion exchange with water, a non-solvent to cellulose. Liquid-liquid phase separation occurred, resulting in gel-like cellulose [286]. Meanwhile, intra- and inter-molecular hydrogen bonds of cellulose were re-formed. The cellulose obtained at this stage was a highly swollen gel, which expanded more than its normal size. These cellulose products were much reduced in size after being thoroughly washed and completely dried. The swollen gel-like cellulose had a weight ratio of 1500%-1800% to the dried cellulose samples, indicating their excellent water retention capacity. The morphology and properties of cellulose products were affected by polymer solution properties, system parameters of nozzle-PG, as well as the coagulation process.

Figure 6-1 exhibits SEM images of cellulose products obtained from 2 wt%, 2.5 wt%, and 3 wt% cellulose/EMIM OAc solutions.

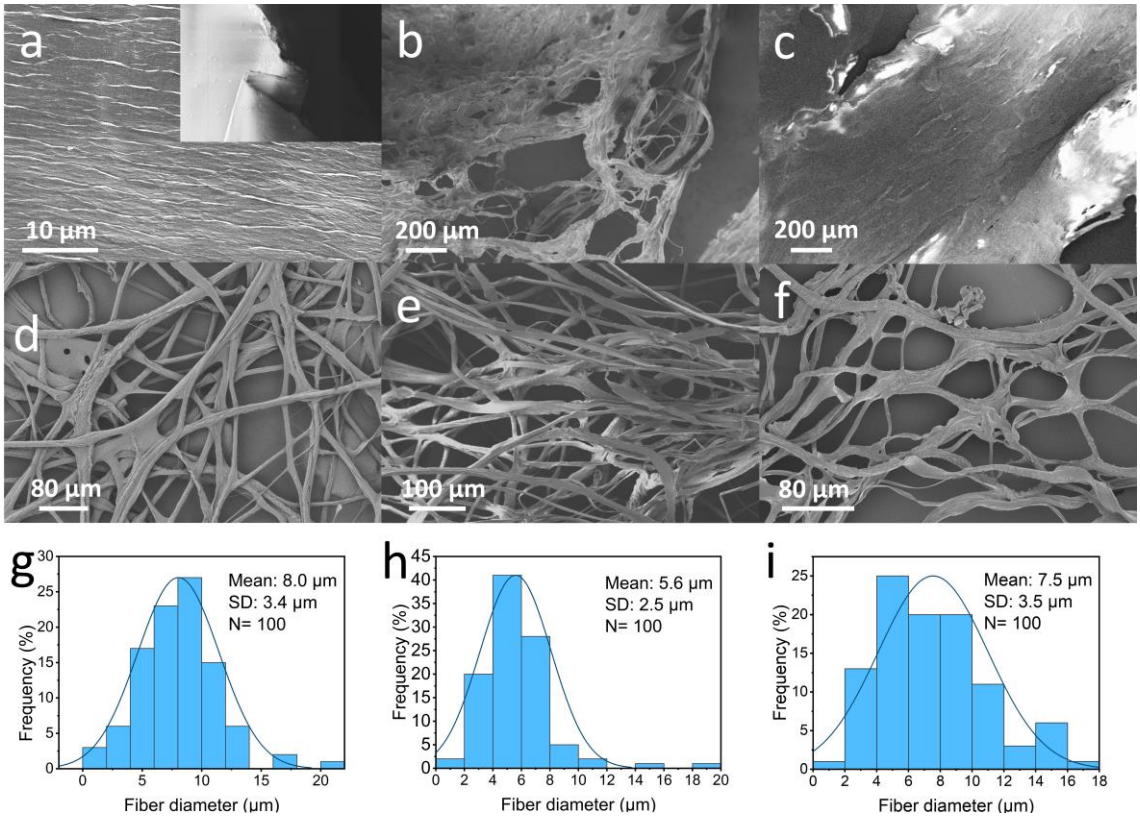

Figure 6-1 SEM images of seaweed-derived cellulose produced through nozzle-pressurised gyration at 1 × 10^5 Pa working pressure: (a) 2 wt% cellulose, 6 mm air gap length; (b, c) 2.5 wt% cellulose, 6 mm and 13 mm air gap length, respectively; (d-f) 3 wt% cellulose, 6 mm, 13 mm, and 20 mm air gap length, respectively. (g-h) diameter distributions of seaweed-derived cellulose fibres collected at 6 mm, 13 mm, and 20 mm in nozzle-pressurised gyration, respectively.

The structure and morphology of the regenerated cellulose products are highly dependent on the solution concentration. Thin films with smooth surfaces were obtained from 2 wt% cellulose solutions. An increase in solution concentration to 2.5 wt% resulted in some large pores presenting on the cellulose products, which simultaneously had fibrous structures and membrane structures with wrinkled

surfaces. Continuous interlaced cellulose fibres were spun from the 3 wt% solution.

The effect of polymer concentration on the structure and morphology of the regenerated cellulose is mainly through the fluid viscosity during the coagulation process. The low concentration of cellulose substantially reduced the viscosity of cellulose solutions. The local mobility around cellulose chains increased due to the low viscosity ratio of the cellulose solution to the coagulant, resulting in a more adequate and faster diffusion of the solvent and the coagulant, which is beneficial to the uniform distribution of cellulose molecules [287]. In addition, the less viscous solutions generally have shorter relaxation times, suggesting that the polymer jets may have relaxed somewhat before coagulation occurs [58]. Thus, the 2 wt% cellulose solution was likely to produce homogeneous cellulose films. However, the high viscosity of cellulose solutions hindered the exchange of solvent and coagulant. The coagulant was difficult to diffuse to the central region of the forming fibres, which may result in incomplete phase separation [288]. Cellulose tended to retain the filamentous structures it adopted after ejecting from nozzle-PG. In this work, 3 wt% was regarded as the optimal concentration for the formation of continuous cellulose fibres. As a result, selecting the appropriate solution concentration is critical for producing the desired morphology of the cellulose products. This relationship is illustrated in **Figure 6-2**.

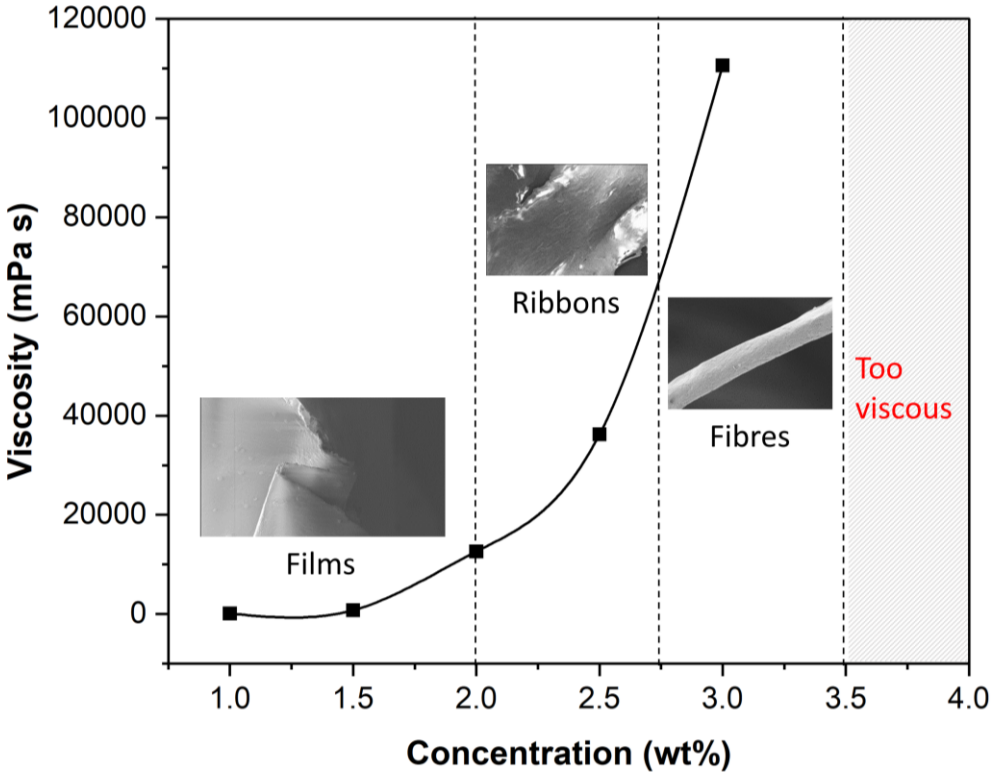

Figure 6-2 The viscosity profile of seaweed-derived cellulose solutions and the structures of corresponding products spun through nozzle-pressurised gyration. (solutions with a concentration of higher than 3 wt% are excessively viscous to be processed.)

Besides, solution concentration influences the optical properties of cellulose products obtained. The low concentration (2 wt%) of cellulose solution led to the cellulose films with good optical transmittance (**Figure 3-5**f), whereas conventional cellulose fibres with inferior transmittance were produced by the 3 wt% solutions (**Figure 3-5**e). The optical transmittance is mainly affected by the homogeneous structure of the cellulose samples rather than the thickness [289]. Previous studies have reported that, due to different phase separation processes, cellulose films with homogeneous structures were generally formed by lower

cellulose concentrations, while higher concentrations resulted in more compact but in-homogeneous structures in cellulose products [289, 290].

The effects of air gap length (collection distance) are illustrated in **Figure 6-1**d-i. According to previous work in Chapter 4, increasing collection distance facilitates the stretching and thinning of the polymer jets in the air to form finer fibres. In this study, the cellulose fibre diameter decreased from 8.0 ± 3.4 μm to 5.6 ± 2.5 μm with the increase of air gap length from 6 mm to 13 mm. While the fibre diameter increased to 7.5 ± 3.5 μm when the air gap length was further increased to 20 mm. This can be explained by the longer relaxation time at a longer air gap. The polymer jets underwent a longer relaxation time and expanded more at the 20 mm distance than those at a shorter distance, resulting in thicker fibres. A similar phenomenon can be seen from the spinning of the 2.5 wt% cellulose solution. Some filamentous structures were presented on the cellulose products that were collected at the 6 mm distance (**Figure 6-1**b), while only wide ribbon-like cellulose was obtained from the 13 mm collection distance (**Figure 6-1**c). Therefore, the influence of air gap length on the morphology of cellulose products is a synergistic result of jet stretching and relaxation. A trade-off between the two is conducive to obtaining fine fibres. In addition, the air gap conditions (temperature, humidity) were reported to affect the cellulose fibre formation, which needs to be investigated in future work [58].

The magnitude of the working pressure applied in nozzle-PG also affected the fibre morphology. When the pressure was increased from 1×10^5 Pa (**Figure 6-1**d-f) to 2×10^5 Pa, the obtained cellulose product had fibrous textures but there was significant aggregation (**Figure 6-3**a).

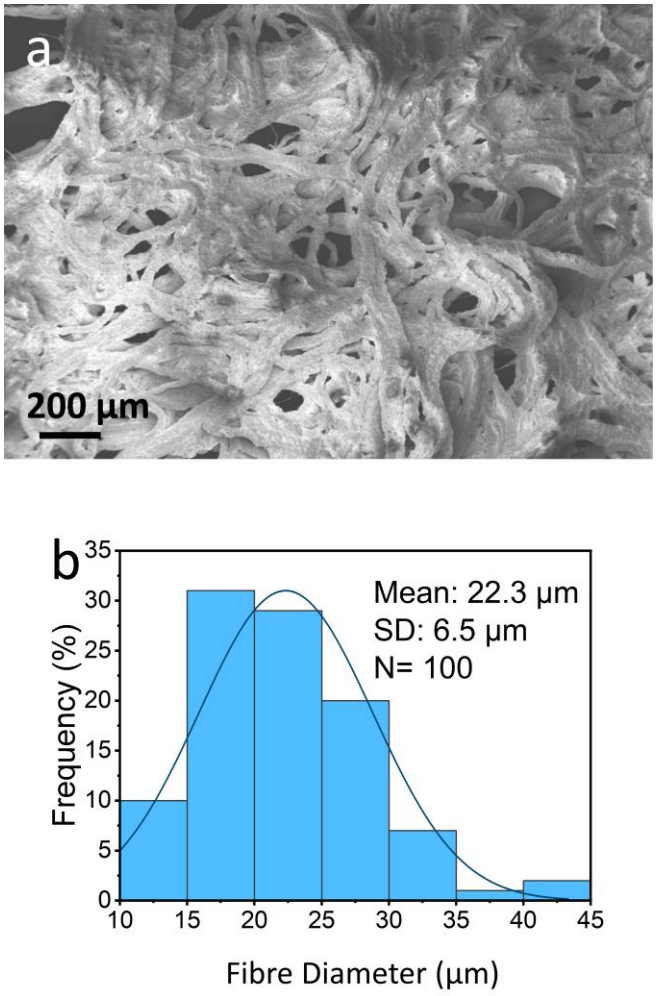

Figure 6-3 (a) SEM image and (b) diameter distribution of 3 wt% seaweed-derived cellulose solution processed by nozzle-pressurised gyration at 1 × 10^5 Pa working pressure and 13 mm air gap length.

This can be attributed to the kinetic instability and insufficient stretching time of the polymer jets caused by the high-velocity gas flow. Moreover, the fibre diameter increased to 22.3 ± 6.5 µm, which is much larger than those fibres obtained from the spinning at 1 × 10^5 Pa. The large diameter value acquired in this case can be the result of insufficient stretching or/and an artefact of fibre aggregation. However, the effect of increasing pressure is not always negative. The production rate of cellulose fibres increased from 17.6 g/h to 21.6 g/h,

indicating that the higher pressure played a role in promoting fibre formation in this work.

Figure 6-4 shows that the cellulose films have flat and relatively smooth surfaces while the cellulose fibres have distinctly wrinkled surfaces.

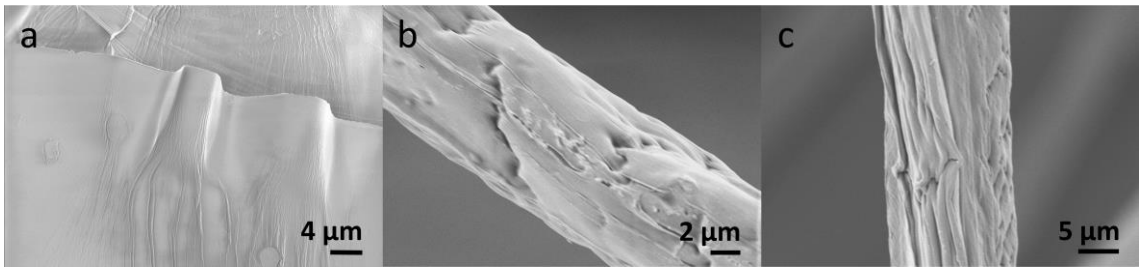

Figure 6-4 The surface topography of (a) cellulose film and (b-c) cellulose fibres.

The smooth surface of the cellulose films can be attributed to the better fluidity and the fast liquid fusion of low-viscous solutions as discussed previously. The collapsed and wrinkled surfaces of the cellulose fibres are attributed to the coagulation and drying processes. It has been discussed that the high viscoelasticity of the cellulose solution hindered the non-solvent (coagulant) from entering the central region of fibres while the surface of fibres coagulated when they entered the coagulation bath. The volume of dried fibres was significantly reduced compared to swollen fibres. The different contraction rates of the fibre surface and the fibre core during the drying process can cause wrinkles and collapse of the fibres.

6.4 Animal Waste-Derived Cellulose Fibre Production

Figure 6-5 exhibits the morphology of animal waste-derived cellulose before and after processing with modified nozzle-PG.

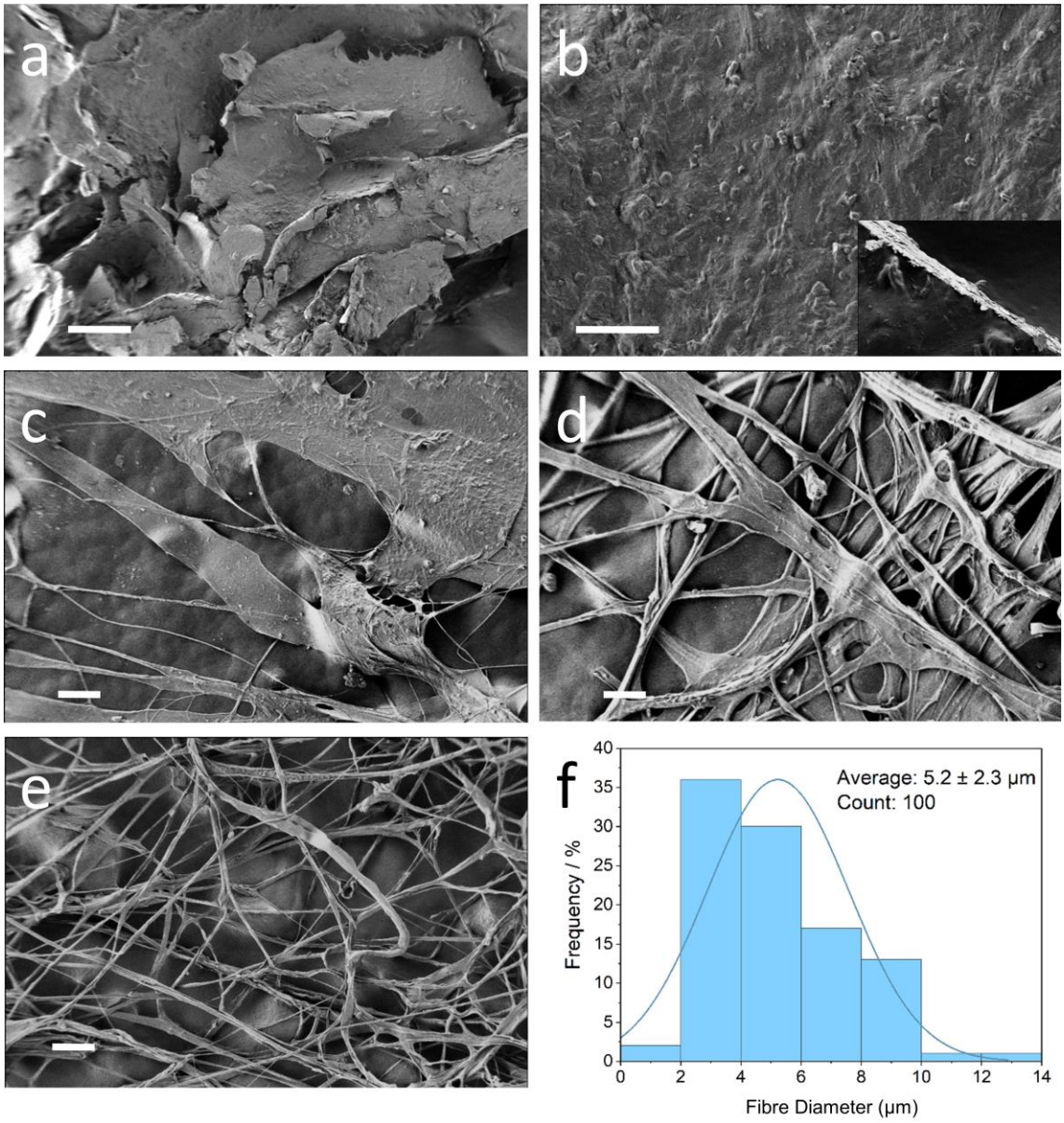

Figure 6-5 SEM images of (a) dried animal waste-derived cellulose flakes and (b-e) cellulose samples produced through nozzle-pressurised gyration from animal waste-derived cellulose solutions with concentrations of (b) 2 wt%, (c) 4 wt%, (d) 8 wt%, (e) 10 wt%, and (f) the diameter distribution of cellulose fibres produced from the 10 wt% solution. (Scale bar = 100 µm)

The freeze-dried cellulose is observed to aggregate into flakes (**Figure 6-5**a), which are much larger in size than the cellulose fibrils, losing the natural nano-structure of nanofibrils. **Figure 6-5**b-e shows the progressive transformation in

cellulose morphology following nozzle-PG processing as the cellulose concentration increases from 2 wt% to 10 wt%. Initially, the cellulose formed a thin film at the lowest concentration, which then split into broad ribbons, and finally refined further to form thin filaments with the increase in cellulose concentration. In **Figure 6-5**b, the surface roughness of the cellulose film may be attributed to the uneven viscosity of the solution resulting from impurities present in the extracted cellulose. The inset shows the cross-section of the film with a thickness of approximately 5 μm. **Figure 6-5**f suggests that the diameter distribution of the cellulose fibres obtained from the 10 wt% solution follows a Gaussian distribution, with an average diameter of 5.2 ± 2.3 μm. Similarly, this relatively large variance in fibre diameter can be caused by viscosity unevenness resulting from solution impurities.

As the processing parameters associated with nozzle-PG remained consistent, the variations observed in cellulose morphology can be attributed to the difference in solution viscosity caused by the concentration difference, which is consistent with the previous observations. The relationship between these two variables is depicted in **Figure 6-6**. For concentrations below 4 wt%, the cellulose solutions have very low viscosity, indicating their high fluidity. Consequently, despite being extruded from nozzle-PG in the form of a jet, the cellulose solutions rapidly flowed and dispersed into a uniform film after entering the water bath. Coagulation has not yet occurred at this stage. With further increases in concentration, the cellulose solution experienced a notable rise in viscosity, signifying a decrease in its fluidity. The flow and interdiffusion of the cellulose jets in the water bath became restricted. Coagulation occurred before they fully spread out, thereby resulting in the formation of broad ribbon-like cellulose

samples. The solution fluidity further deteriorated after the concentration reached 8 wt% due to the exceptionally high viscosity ratio to the water bath. Therefore, coagulation occurred while the jets maintained the filamentous morphology they adopted upon extruding from the nozzle tip, resulting in the formation of cellulose fibres. Therefore, choosing the appropriate solution concentration is crucial for achieving the desired morphology of cellulose products. This information can be obtained from **Figure 6-6**.

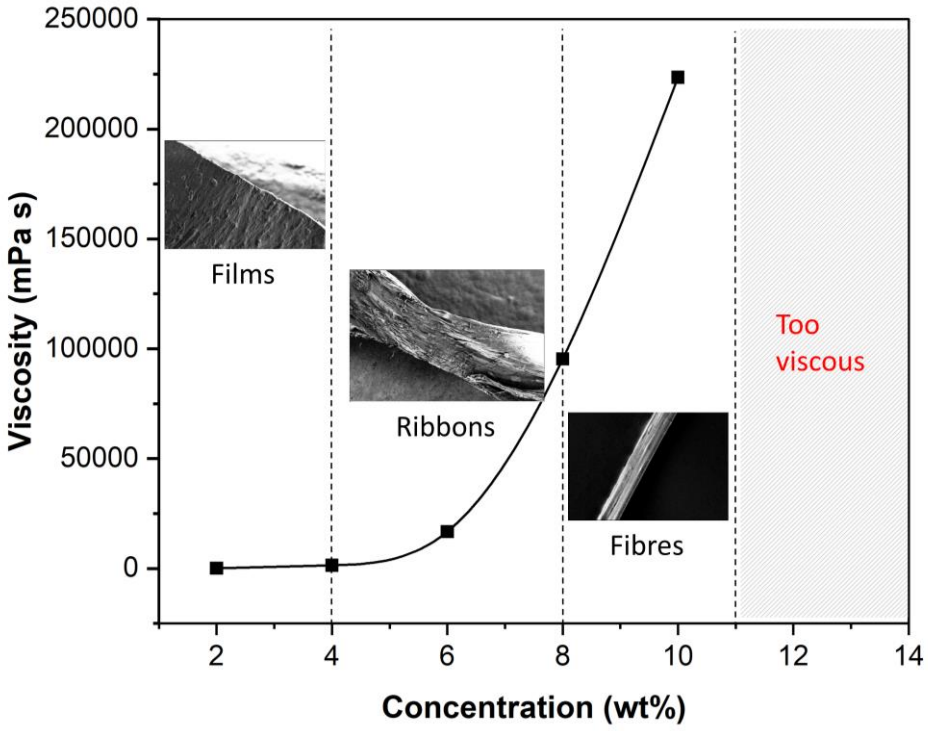

Figure 6-6 The viscosity profile of animal waste-derived cellulose solutions and the structures of corresponding products spun through nozzle-pressurised gyration. (solutions with a concentration of higher than 11 wt% are excessively viscous to be processed.)

6.5 Fourier Transform Infrared Spectroscopy

The FTIR spectrum was used to verify the chemical composition of cellulose molecules. In **Figure 6-7**, the FTIR spectrums of cellulose samples with different structures produced through nozzle-PG all show the typical bands assigned to the functional groups present in cellulose.

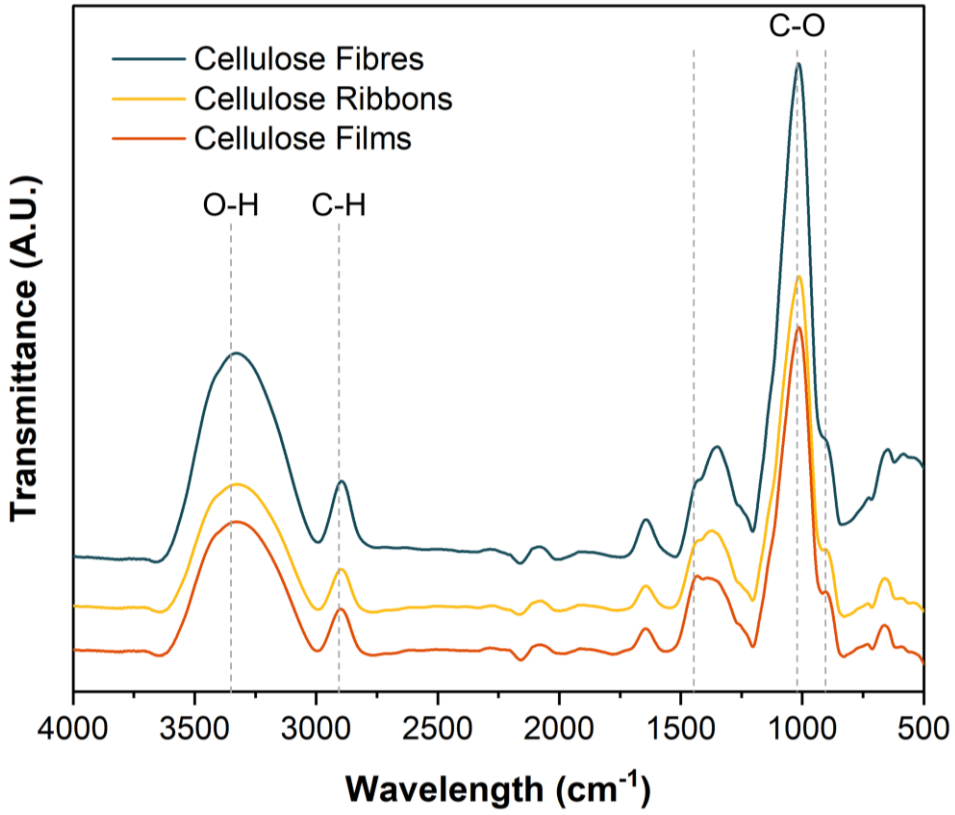

Figure 6-7 FTIR spectra of cellulose samples obtained through nozzle-pressurised gyration.

The broad absorption peak at 3346 cm^{-1} is attributed to the stretching vibration of O-H. This peak also includes inter- and intra-molecular hydrogen bond vibrations in cellulose [291]. The absorption peaks of 2900 cm^{-1} and 1080 cm^{-1} are characteristics of C-H and C-O bonds stretching vibrations in cellulose, respectively. The presence of a characteristic peak around 1640 cm^{-1} confirms

the obtained cellulose remains in their original, unmodified form. If surface modifications, such as esterification or amidation (which typically occur during chemical pre-treatment in the cellulose derivation process), had taken place, a peak shift to approximately 1740 cm^{-1} or 1590 cm^{-1},, respectively, would be observed [292]. In our study, no significant surface modifications were observed in the obtained cellulose. The band around 1420-1430 cm^{-1} can be used to analyse the crystallinity of cellulose, while the band of 898 cm^{-1} is assigned to amorphous regions in cellulose [293]. According to O'Conner et al [294], the spectral ratio of 1429/893 cm^{-1} can be defined as the crystallinity index of cellulose samples.

6.6 X-Ray Diffraction

The XRD diffractogram (**Figure 6-8**) clearly shows distinct differences in the crystallisation behaviour between the extracted cellulose and regenerated cellulose samples through nozzle-PG. In the case of extracted cellulose, the diffraction pattern exhibited characteristic peaks at 2θ = 14.4°, 16.7°, 22.7°, and 34.6°, which have been identified as corresponding to the (100), (010), (110), and (11-4) crystallographic planes for cellulose I [295]. Based on Bragg's law, the d-spacing data acquired through X-ray diffractometry were utilised in the discriminant analysis function proposed by Wada et al. [296]. The analysis revealed that the extracted cellulose predominantly belongs to the I_{α}-rich type. These results are consistent with the previous study, using the *Laminaria hyperborea* source material identified as Cellulose I_{α} [219].

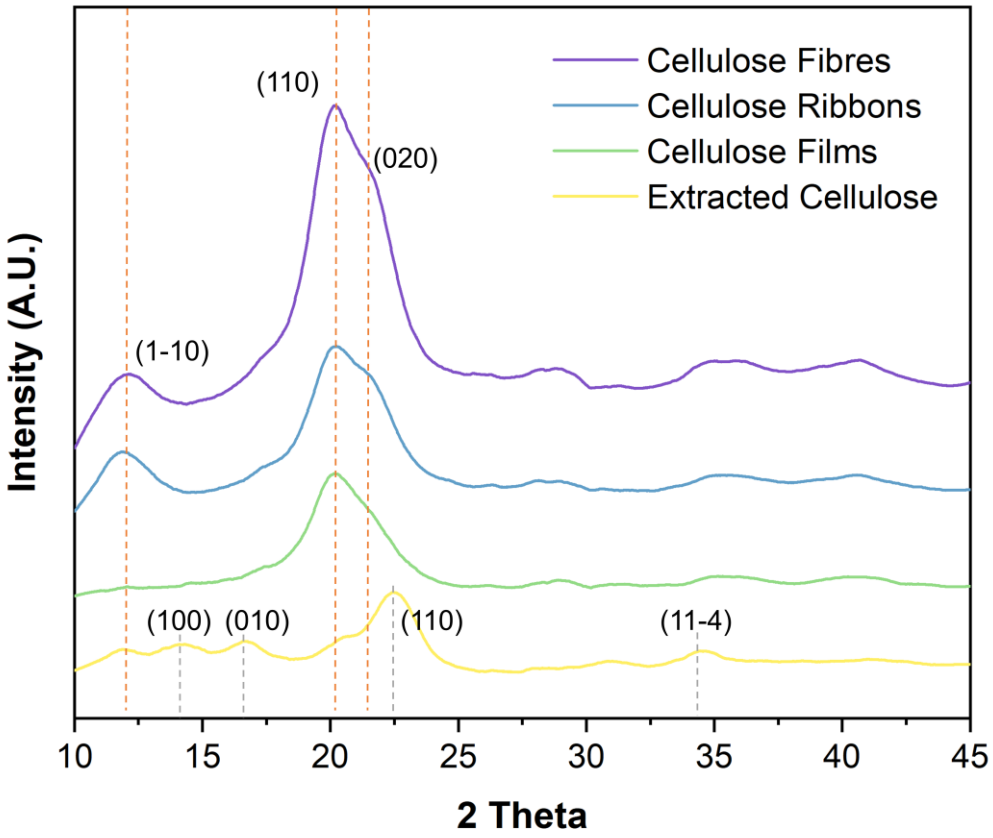

Figure 6-8 X-ray diffractograms of extracted cellulose and regenerated cellulose (films, ribbons, and fibres).

Whereas the peaks at 2θ = 12.0°, 20.2°, and 21.1° observed in the diffraction patterns of regenerated cellulose through nozzle-PG in this work were indicative of the (1-10), (110), and (020) crystallographic planes of cellulose II [295]. The change in crystallography suggests that cellulose I converted into cellulose II after the regeneration process, due to the breaking and rebuilding of hydrogen bonds of cellulose molecules in ionic liquids [297]. The hydrogen bonds in cellulose I are organised in a sheet array in (020) planes [298] while there is a three-dimensional network of hydrogen bonds in cellulose II [299]. The conversion from cellulose I to cellulose II is an irreversible process. Cellulose II is commonly acknowledged as a stable crystalline form of cellulose [300].

To evaluate the changes in cellulose molecular orientation after the regeneration process, orientation index (OI) was employed to quantify this material characteristic. OI was defined as **Equation 6-1** [301]:

$$\mathbf{OI} = \mathbf{1} - \frac{\boldsymbol{I_{am}}}{\boldsymbol{I_{tot}}}$$

Equation 6-1

where, I_{am} is the maximum intensity of the peak corresponding to the dominating amorphous fractions, and I_{tot} is the maximum intensity of the diffraction pattern. OI ranges from 0 to 1. A higher value suggests a more aligned molecular chain orientation, whereas OI = 0 signifies a completely random orientation.

The calculation results show that the extracted cellulose has an OI of 0.91, aligning with the anticipated preferred orientation seen in natural cellulose I_α [219]. However, the regenerated cellulose, processed under different parameters, displays an average OI of 0.39 ± 0.09. As previously highlighted, dissolution in ionic liquids leads to the breakage and reconstruction of hydrogen bonds in cellulose chains, resulting in the conversion of cellulose from type I to type II, which is marked by a reduced orientation. Variations in orientation among different regenerated cellulose might be attributed to disparate processing conditions during the spinning process.

6.7 Absorption Properties

Figure 6-9 exhibits the liquid absorption capacity of cellulose samples with different morphologies in PBS solutions. Within the initial 10 h, the three cellulose samples all showed a high liquid absorption rate. At the 8.5th hour after soaking,

the cellulose films prepared from the 2 wt% solution had an absorption percentage of 183 ± 23%, while the absorption percentage of fibrous cellulose obtained from the higher concentration solutions reached 210%. In the end, cellulose films, cellulose ribbons, and cellulose fibres reached the saturation level having a maximum absorption capacity of 192 ± 21%, 212 ± 6%, and 248 ± 29%, respectively.

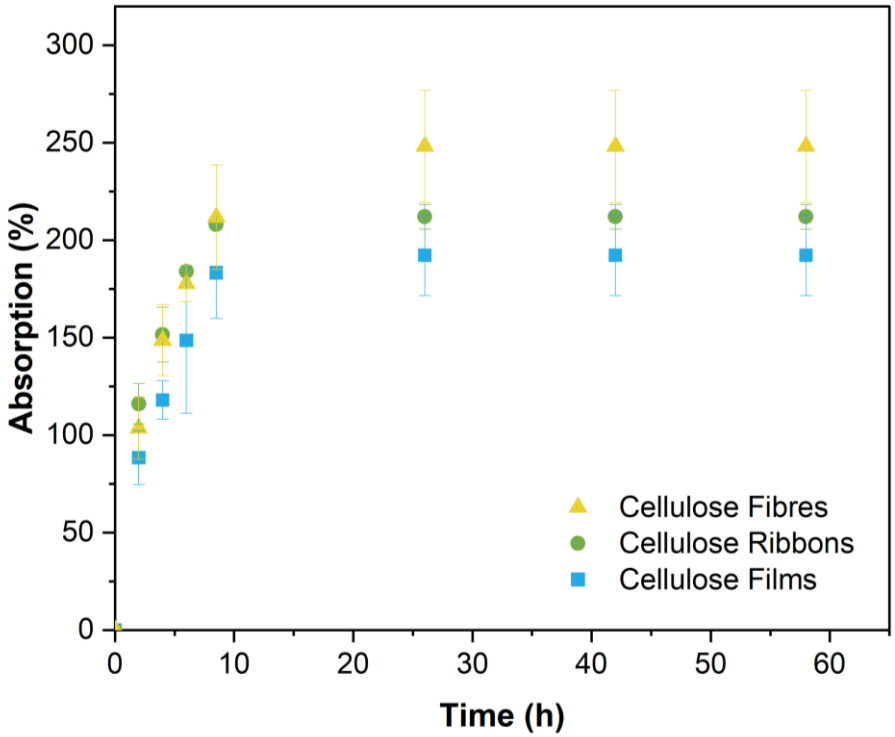

Figure 6-9 Absorption capacity of the obtained cellulose samples (films, ribbons, and fibres).

The cellulose fibres showed a higher liquid absorption capacity compared to the cellulose films, which may be attributed to the higher surface area-to-volume ratio of fibrous samples. The hydrophilic properties of cellulose materials are due to the formation of hydrogen bonds between their hydroxyl groups and water molecules [302]. This unique hydration ability of cellulose provides a moist

environment desired for wound healing, making it an attractive material for wound bandages [303, 304].

6.8 Conclusions

This work provides compelling evidence that high-value cellulose can contribute to a circular economy by deriving raw cellulose from recycled waste materials, specifically seaweed residuals left after Alg extraction and dairy farm waste. The extracted cellulose exhibited a natural cellulose nanofibril structure and characteristics.

The extracted cellulose was subsequently used as spinning feedstock in a modified nozzle-PG process, incorporating a coagulation bath. By adjusting the solution concentration and the system parameters associated with nozzle-PG, cellulose products with diverse morphologies, including thin films, broad ribbons, and long fibres, were successfully produced. Notably, thin cellulose film sheets with favourable optical properties and well-defined cellulose fibres with diameters of approximately 5 μm were fabricated using this advanced spinning technique. This method represents a straightforward, efficient, and low-consumption approach that maximises the yield of cellulose fibres, effectively addressing many of the challenges traditionally associated with the widespread use of cellulose materials.

Furthermore, the ionic liquid EMIM OAc, employed as a solvent in this study, is recognised as a green, direct solvent for cellulose fibre spinning. Unlike conventional viscose technology, which generates environmental hazards and unwanted by-products, EMIM OAc enables an environmentally friendly process

and allows for solvent recycling [305-307]. This underscores the sustainability of the innovative cellulose processing technology developed in this work.

The resulting cellulose products hold great promise for applications across various sectors. In food packaging, their transparency, strength, and excellent barrier properties against oxygen and moisture enable the development of sustainable, biodegradable alternatives to plastic [308]. In energy storage, the high surface area and network-forming capability of cellulose fibres make them ideal as a binder, separator, or component in lightweight and flexible devices such as batteries and supercapacitors [309]. Similarly, their flexibility, dielectric properties, and compatibility with functional materials position them as key materials for electronics, including substrates and dielectric layers in field-effect transistors (FETs) [310, 311]. In biomedicine, cellulose fibres stand out for their biocompatibility, high water retention, and capacity for functionalisation, supporting applications in wound dressings, drug delivery systems, and tissue engineering scaffolds [304, 312, 313]. This research highlights the potential for scalable, eco-friendly cellulose production from recycled waste materials, with significant implications for advancing sustainable materials in both industry and healthcare.

7 Summary and Outlook

PG is a scalable spinning technology that presents a promising approach for the industrial production of polymeric fibres. The process involves spinning a cylindrical vessel loaded with a polymer solution at high speeds, accompanied by a high-pressure gas flow, to rapidly generate continuous fibres. The core focus of this project was to address the current limitations of this technology, optimise its performance, and expand its application to a wider range of polymer materials. These objectives were achieved by addressing the key gaps identified in the existing literature:

1. Enhance the morphology and production consistency of polymeric fibres produced by PG through equipment design optimisation.
2. Validate the performance of the newly optimised equipment by comparing fibre morphology, properties, and production yield with those of existing spinning technologies.
3. Develop efficient and sustainable methods for manufacturing natural biopolymer fibres suitable for biomedical applications and assess their spinnability in PG.
4. Recycle and repurpose waste materials to produce high-value products via advanced spinning technique, thereby addressing environmental and public health concerns associated with waste disposal and contributing to the realisation of a circular economy.

These goals collectively advance the potential of PG for biomedical and industrial applications, while promoting sustainable material practices.

7.1 Summary of Findings

7.1.1 Development of Nozzle-Pressurised Gyration

Fibres produced by PG typically exhibit more defects and lower uniformity than those produced by electrospinning, which is likely attributed to fluid instability during spinning. External nozzles were incorporated into the spinning vessel in place of the small orifices, resulting in a modified setup termed “Nozzle-PG.” This nozzle-based approach effectively reduced fluid instability during the spinning process, resulting in notable improvements in both fibre morphology and production yield. Under identical spinning conditions, nozzle-PG reduced the diameter of PCL, PVP, and PEO fibres from **1.5 ± 1.0 µm**, **2.1 ± 1.3 µm**, and **198 ± 102 nm** in PG to **1.3 ± 0.8 µm**, **1.5 ± 0.9 µm**, and **172 ± 67 nm**, respectively, while also achieving significantly higher fibre alignment and fewer bead defects. These enhancements were particularly evident at lower working pressures, with reductions in fibre diameter and uniformity reaching up to **50%** and **60%**, respectively. Furthermore, the high-pressure airflow in the nozzle-PG setup actively clears the nozzle, effectively eliminating the risk of clogging during the spinning process.

7.1.2 Nozzle-Pressurised Gyration *versus* Electrospinning

The performance of nozzle-PG was evaluated in comparison to electrospinning, focusing on fibre production rate, mechanical properties, and drug release behaviour. The fibre production rate achieved by laboratory-scale nozzle-PG was approximately **35 times** greater than that of electrospinning, with the potential for even greater increases as nozzle-PG equipment is scaled up. Due to improved

fibre uniformity, alignment, and fewer bead defects, the tensile strength of PVP fibres produced by nozzle-PG reached **2.9 ± 0.8 MPa**, exceeding both electrospun fibres (**1.9 ± 0.6 MPa**) and conventional PG fibres (**1.2 ± 0.5 MPa**). In the transdermal release tests, nozzle-PG fibres demonstrated a release profile of CUR comparable to that of electrospun fibres. These advancements demonstrate that nozzle-PG substantially increases fibre yield while maintaining fibre quality and performance, expanding its practical application potential in industrial fields.

7.1.3 Manufacture of Antibacterial Biopolymer Fibres

Modifying the equipment with the introduction of a coagulation bath, the capability of nozzle-PG of wet spinning biopolymer fibres was developed. This modification enabled the successful fabrication of Alg fibres with an average diameter of approximately **10 µm**, effectively addressing a limitation of electrospinning in processing water-soluble biopolymers. Due to their inherent biochemical properties and exceptional biocompatibility, with cell viability rates reaching **94%**, pure Alg fibres represent a promising candidate for the new generation of biomaterial applications.

Incorporated with *Cinnamomum verum*, these Alg fibres demonstrated substantial antibacterial efficacy, achieving up to a **log 3** reduction in bacterial adhesion against *E. coli* bacteria species and a **log 5** reduction against *S. aureus* bacteria species, without inducing cytotoxic effects. This combination leverages the natural antibacterial compounds in *Cinnamomum verum* and the biocompatibility of alginate, offering a promising approach for developing advanced, biologically safe biomaterials.

7.1.4 Manufacture of Cellulose Fibres from Waste Materials

To further comply with sustainability goals within a circular economy framework, this research explored the recovery of spinning raw materials derived from waste. Cellulose was derived by repurposing waste materials (sugar kelp residual after Alg extraction and dairy farm animal waste) and used as feedstock for fibre production in nozzle-PG. The relationship between the viscoelasticity characteristics of cellulose solutions and fibre formation in nozzle-PG was plotted, providing insights into the optimal conditions for cellulose fibre production. Cellulose fibres with an average diameter of **5 µm** were successfully fabricated, which not only fills the gap in the literature on large-scale cellulose spinning but also realises the concept of ‘‘Waste to Wealth’’, demonstrating how sustainable practices can convert waste into valuable materials for industrial applications.

7.1.5 Influence of Manufacturing Parameters

The influence of experimental settings and manufacturing parameters on fibre quality, as investigated throughout this thesis, is summarised in **Table 7-1**.

Table 7-1 Effects of experimental settings and manufacturing parameters on fibre properties and performance in nozzle-pressurised gyration.

Manufacturing Parameter	**Design Justification**
Nozzle number	-Multiple nozzles enhance fibre throughput
Nozzle diameter	-Smaller nozzle diameter reduces fibre diameter -Excessive small nozzles (< 0.3 µm) hinder the ejection of spinning solution

Rotation speed	-Higher speed improves fibre throughput -Excessive high speed causes fibre aggregation
Working pressure	-Higher pressure improves fibre throughput, yet reduces fibre uniformity and causes more beads -High pressure is conducive in spinning biopolymers and highly viscous solutions -Excessive high pressure causes fibre aggregation
Collection distance	-Longer distance reduces fibre diameter -Excessive long distance leads to jet rupture and bead formation -Excessive long distance results in thicker cellulose fibres
Solution concentration	-Insufficient concentration fails to form spinning jets -Lower concentration leads to smaller fibre diameter yet results in more beads -Increasing concentration, the alginate/cellulose structure transitions from a thin film to a filamentous form -Lower concentration promotes a more homogeneous structure and higher optical transmittance in cellulose

7.2 Study Limitations

While this thesis demonstrates significant potential, it is important to acknowledge certain limitations.

Firstly, the fibre performance tests conducted in this study were primarily in-vitro experiments under controlled laboratory conditions, which differ from the complex physiological environments in which biomaterials are ultimately intended to function. As a result, these tests may not fully reflect the actual performance of the fibres in practical applications. Nonetheless, the primary objective of this research was to evaluate the feasibility and advancements of nozzle-PG as an innovative spinning technology to address the current challenges of conventional spinning methods. The comparative analysis between nozzle-PG and existing

spinning techniques provides valuable insights into the potential advantages of this approach, even if further in-vivo studies will be necessary to confirm its practical applicability.

Secondly, despite the advantages of nozzle-PG in the production of polymeric fibres, the diameter of these fibres is predominantly in the micrometre range. Research has demonstrated that nano-materials can induce unique properties—nano effects, including enhanced surface activity, improved superconductivity, and altered optical properties, which significantly expand their potential uses in high-tech applications. Therefore, to enhance the fibre performance and versatility, it is crucial to further reduce their diameter to the nanometre scale.

Thirdly, the surrounding generation of spinning jets from nozzle-PG with their reception by the coagulation bath situated on a single plane leads to a notable waste of polymer solutions. Currently, this issue is primarily mitigated by recycling the uncoagulated solution that collects on the cover plate for reuse. However, there is a need to develop more efficient coagulation bath collection systems to minimise material waste and enhance the sustainability of the production process.

7.3 Future Work

The findings of this project demonstrate that nozzle-PG is a promising scalable approach for the manufacturing of polymeric fibres, characterised by exceptional fibre productivity and excellent fibre performance. However, as highlighted in the preceding sections, these results are subjected to certain limitations that warrant further investigation. Future research should focus on the following aspects:

7.3.1 In-Vivo Study

In this thesis, the in-vitro performance of the fibres produced through nozzle-PG was studied under controlled conditions. However, this cannot fully replicate the complex physiological environment encountered in vivo, which may influence the fibres' functional properties and overall efficacy. Therefore, future work should focus on conducting in-vivo studies to evaluate the performance and biocompatibility of the fibres prepared through nozzle-PG. These studies are essential to understanding how the fibres interact with biological systems and their potential applications in biomedical applications.

Additionally, the long-term effects of these fibres within living organisms, including any immune responses or adverse reactions should be studied. These results will help to gain valuable insights into the practical applications of the produced fibres and their efficacy in real-world biological environments.

7.3.2 Production of Nanofibres

In this research, the fibres produced through nozzle-PG were primarily micrometre-sized, which limits their ability to exhibit the unique properties associated with nanomaterials—nano-effects. To address this limitation, future research should focus on several key areas: investigating the chain entanglement of polymer molecules, analysing the volatility and characteristics of the solvent, optimising the spinnability of the polymer solution, and fine-tuning the processing parameters of nozzle-PG, aiming to develop strategies for producing thinner fibres that leverage the advantages of nanoscale materials, thereby enhancing their performance and broadening their potential applications.

7.3.3 Surrounding Coagulation Bath

Biopolymers—Na-Alg and cellulose, were successfully wet spun into fibres using the modified nozzle-PG equipment in this project. However, the current single-plane coagulation bath in the modified system is unable to capture all the generated spinning jets, leading to decreased production efficiency. To address this limitation, future research should focus on the development of an enhanced coagulation bath that encompasses a surrounding design to maximise the collection of spinning jets. This innovative device would aim to capture and solidify as many jets as possible, thereby increasing the overall efficiency of the spinning process.

7.3.4 Multi-Polymer Fibres

The development of sustainable and biocompatible biopolymer fibres is a key focus of this research. However, natural biopolymers often exhibit inherent shortcomings, such as limited mechanical strength and durability, unpredictable degradation rates and chemical resistance. Future studies can be conducted to combine different polymers to integrate the properties of multiple polymers to address these challenges. This approach not only addresses the inherent limitations of individual biopolymers but also enables the development of advanced materials tailored for specific applications. The combination methods are described as follows:

Composites—The fabrication of composite fibres through the combination of two or more polymers represents an effective strategy for enhancing the overall performance of materials. For instance, integrating nanoparticles, nanofibrils or

nanocrystalline materials into biopolymer fibres can leverage the beneficial properties of each component, resulting in fibres that exhibit improved mechanical strength, durability, and functionality [314, 315].

Core-Sheath Fibres—The design of fibres with a distinct core and sheath structure can strategically combine materials with complementary properties to optimise overall performance. For example, the core could be composed of a strong, durable polymer to provide structural integrity, while the sheath could consist of a biocompatible or biodegradable material to enhance environmental sustainability and functionality [316]. This dual-component system allows for tailored responses to external stimuli and improved mechanical properties.

Supermats—The creation of supermats through the hybridisation of two or more polymeric fibres is an advanced strategy for integrating the advantageous properties of multiple materials into a single, multifunctional structure [317]. This new route offers substantial potential for developing high-performance materials tailored for specialised applications across various fields.

7.3.5 Automation and Industrialisation

Nozzle-PG was developed to address the growing demand for industrial-scale polymeric fibre production, highlighting the need for enhanced automation in the spinning process. Integrating advanced automation systems into nozzle-PG can significantly streamline fibre formation and collection, minimising material waste and enhancing fibre uniformity. Automation can further enable real-time monitoring and precise control of critical processing parameters, thereby ensuring consistent product quality across large-scale production. These

advancements will not only optimise the efficiency of fibre manufacturing but also support the scalability and reliability required for industrial applications.

7.3.6 Antibacterial Mechanism of *Cinnamomum verum*

This study has demonstrated the potential of *Cinnamomum verum* as an effective natural antimicrobial agent for biomaterial applications. However, further research is essential to fully understand and optimise its use in such applications. Future work should focus on isolating and characterising the main bioactive compounds within *Cinnamomum verum* that contribute to its antimicrobial activity, as well as their action mechanisms and synergistic effects between different active compounds, by which these components inhibit microbial growth. By advancing our knowledge of these aspects, future research can support the development of safer and more efficient biomaterials that harness natural antimicrobial agents for biomedical use.

References

[1] "Coronavirus disease (COVID-19) advice for the public: When and how to use masks." https://www.who.int/emergencies/diseases/novel-coronavirus-2019/advice-for-public/when-and-how-to-use-masks (accessed.

[2] L. Martinelli *et al.*, "Face masks during the COVID-19 pandemic: a simple protection tool with many meanings," *Frontiers in Public Health,* Original Research vol. 8, Jan 2021, doi: 10.3389/fpubh.2020.606635.

[3] N. Perra, "Non-pharmaceutical interventions during the COVID-19 pandemic: A review," *Physics Reports,* vol. 913, pp. 1-52, May 2021, doi: https://doi.org/10.1016/j.physrep.2021.02.001.

[4] C. D. Zangmeister, J. G. Radney, E. P. Vicenzi, and J. L. Weaver, "Filtration efficiencies of nanoscale aerosol by cloth mask materials used to slow the spread of SARS-CoV-2," *ACS Nano,* vol. 14, no. 7, pp. 9188-9200, Jul 2020, doi: 10.1021/acsnano.0c05025.

[5] "What is a HEPA filter?" https://www.epa.gov/indoor-air-quality-iaq/what-hepa-filter (accessed.

[6] P. Supaphol, O. Suwantong, P. Sangsanoh, S. Srinivasan, R. Jayakumar, and S. V. Nair, "Electrospinning of biocompatible polymers and their potentials in biomedical applications," in *Biomedical Applications of Polymeric Nanofibers*, R. Jayakumar and S. Nair Eds. Berlin, Heidelberg: Springer Berlin Heidelberg, 2012, pp. 213-239.

[7] D. Kai, S. S. Liow, and X. J. Loh, "Biodegradable polymers for electrospinning: Towards biomedical applications," *Materials Science and Engineering: C,* vol. 45, pp. 659-670, Dec 2014, doi: https://doi.org/10.1016/j.msec.2014.04.051.

[8] N. Reddy, R. Reddy, and Q. Jiang, "Crosslinking biopolymers for biomedical applications," *Trends in Biotechnology,* vol. 33, no. 6, pp. 362-369, Jun 2015, doi: https://doi.org/10.1016/j.tibtech.2015.03.008.

[9] Z. Chen, Z. Chen, A. Zhang, J. Hu, X. Wang, and Z. Yang, "Electrospun nanofibers for cancer diagnosis and therapy," *Biomaterials Science,* vol. 4, no. 6, pp. 922-932, 2016, doi: 10.1039/C6BM00070C.

[10] V. Thavasi, G. Singh, and S. Ramakrishna, "Electrospun nanofibers in energy and environmental applications," *Energy & Environmental Science,* vol. 1, no. 2, pp. 205-221, 2008, doi: 10.1039/B809074M.

[11] S. Chuangchote, T. Sagawa, and S. Yoshikawa, "Fabrication and optical properties of electrospun conductive polymer nanofibers from blended polymer solution," *Japanese Journal of Applied Physics,* vol. 47, no. 1S, p. 787, Jan 2008, doi: 10.1143/JJAP.47.787.

[12] S. Lotfian, C. Giraudmaillet, A. Yoosefinejad, V. K. Thakur, and H. Y. Nezhad, "Electrospun piezoelectric polymer nanofiber layers for enabling in situ measurement in high-performance composite laminates," *ACS Omega,* vol. 3, no. 8, pp. 8891-8902, Aug 2018, doi: 10.1021/acsomega.8b00940.

[13] W. Bai *et al.*, "Flame-retardant, ultralight, and superelastic electrospun fiber sponges for effective sound absorption," *The Journal of The Textile Institute,* vol. 115, no. 5, pp. 724-732, May 2024, doi: 10.1080/00405000.2023.2201553.

[14] N. Bhardwaj and S. C. Kundu, "Electrospinning: A fascinating fiber fabrication technique," *Biotechnology Advances,* vol. 28, no. 3, pp. 325-347, May 2010, doi: https://doi.org/10.1016/j.biotechadv.2010.01.004.

[15] P. L. Heseltine, J. Ahmed, and M. Edirisinghe, "Developments in pressurized gyration for the mass production of polymeric fibers," *Macromolecular Materials and Engineering,* vol. 303, no. 9, pp. 1800218, 2018, doi: https://doi.org/10.1002/mame.201800218.

[16] D. Harper, ""fiber"," in *Online Etymology Dictionary*, ed.

[17] A. L. Yarin, B. Pourdeyhimi, and S. Ramakrishna, *Fundamentals and applications of micro-and nanofibers*. Cambridge University Press, 2014.

[18] E. Weiss and D. Zohary, "The Neolithic southwest Asian founder crops: their biology and archaeobotany," *Current Anthropology,* vol. 52, no. S4, pp. S237-S254, 2011, doi: 10.1086/658367.

[19] R. M. Rowell, "1 - Natural fibres: types and properties," in *Properties and Performance of Natural-Fibre Composites*, K. L. Pickering Ed.: Woodhead Publishing, 2008, pp. 3-66.

[20] S. R. Tridico, "3 - Natural animal textile fibres: structure, characteristics and identification," in *Identification of Textile Fibers*, M. M. Houck Ed.: Woodhead Publishing, 2009, pp. 27-67.

[21] R. M. Kozłowski and M. Mackiewicz-Talarczyk, "1A - Introduction to natural textile fibres," in *Handbook of Natural Fibres (Second Edition)*, R. M. Kozłowski and M. Mackiewicz-Talarczyk Eds.: Woodhead Publishing, 2020, pp. 1-13.

[22] N. Tucker, J. J. Stanger, M. P. Staiger, H. Razzaq, and K. Hofman, "The history of the science and technology of electrospinning from 1600 to 1995," *Journal of Engineered Fibers and Fabrics,* vol. 7, no. 2, pp. 155892501200702S10, 2012, doi: 10.1177/155892501200702s10.

[23] T. Shaikh, S. Chaudhari, and A. Varma, "Viscose rayon: a legendary development in the manmade textile," *International Journal of Engineering Research and Application,* vol. 2, no. 5, pp. 675-680, 2012.

[24] J. H. Park and G. C. Rutledge, "50th anniversary perspective: advanced polymer fibers: high performance and ultrafine," *Macromolecules,* vol. 50, no. 15, pp. 5627-5642, Aug 2017, doi: 10.1021/acs.macromol.7b00864.

[25] C. J. Luo, S. D. Stoyanov, E. Stride, E. Pelan, and M. Edirisinghe, "Electrospinning versus fibre production methods: from specifics to technological convergence," *Chemical Society Reviews,* vol. 41, no. 13, pp. 4708-4735, 2012, doi: 10.1039/C2CS35083A.

[26] C. Woodings, "A brief history of regenerated cellulosic fibers," *Regenerated cellulose fibers,* pp. 1-21, 2001.

[27] A. G. Wilkes, "The viscose process," *Regenerated cellulose fibres,* pp. 37-61, 2001.

[28] J. Chen, "Chapter 4 - Synthetic textile fibers: regenerated cellulose fibers," in *Textiles and Fashion*, R. Sinclair Ed.: Woodhead Publishing, 2015, pp. 79-95.

[29] S. Sivaram, "Wallace Hume Carothers and the birth of rational polymer synthesis," *Resonance,* vol. 22, no. 4, pp. 339-353, 2017.

[30] M. Shakiba *et al.*, "Nylon—A material introduction and overview for biomedical applications," *Polymers for Advanced Technologies,* vol. 32, no. 9, pp. 3368-3383, 2021, doi: https://doi.org/10.1002/pat.5372.

[31] L. Trossarelli, "The history of nylon," *Club Alpino Italiano, Centro Studi Materiali e Tecniche, www. caimateriali. org/index,* 2010.

[32] A. Shrivastava, "1 - Introduction to plastics engineering," in *Introduction to Plastics Engineering*, A. Shrivastava Ed.: William Andrew Publishing, 2018, pp. 1-16.

[33] M. O. Christen and F. Vercesi, "Polycaprolactone: how a well-known and futuristic polymer has become an innovative collagen-stimulator in Esthetics," (in eng), *Clin Cosmet Investig Dermatol,* vol. 13, pp. 31-48, 2020, doi: 10.2147/ccid.S229054.

[34] M. A. Ntrivala *et al.*, "Polycaprolactone (PCL): the biodegradable polyester shaping the future of materials – a review on synthesis, properties, biodegradation, applications and future perspectives," *European Polymer Journal,* vol. 234, p. 114033, Jun 2025, doi: https://doi.org/10.1016/j.eurpolymj.2025.114033.

[35] X. Liu, Y. Xu, Z. Wu, and H. Chen, "Poly(N-vinylpyrrolidone)-modified surfaces for biomedical applications," *Macromolecular Bioscience,* vol. 13, no. 2, pp. 147-154, 2013, doi: https://doi.org/10.1002/mabi.201200269.

[36] M. Julinová, L. Vaňharová, and M. Jurča, "Water-soluble polymeric xenobiotics – polyvinyl alcohol and polyvinylpyrrolidon – and potential solutions to environmental issues: a brief review," *Journal of Environmental Management,* vol. 228, pp. 213-222, Dec 2018, doi: https://doi.org/10.1016/j.jenvman.2018.09.010.

[37] A. Subramaniam and S. Sethuraman, "Chapter 18 - biomedical applications of nondegradable polymers," in *Natural and Synthetic Biomedical Polymers*, S. G. Kumbar, C. T. Laurencin, and M. Deng Eds. Oxford: Elsevier, 2014, pp. 301-308.

[38] J. M. Harris, *Poly (ethylene glycol) chemistry: biotechnical and biomedical applications*. Springer Science & Business Media, 1992.

[39] A. Gandini and M. N. Belgacem, "Chapter 1 - The state of the art," in *Monomers, Polymers and Composites from Renewable Resources*, M. N. Belgacem and A. Gandini Eds. Amsterdam: Elsevier, 2008, pp. 1-16.

[40] S. Karlsson and A.-c. Albertsson, "Biodegradable polymers and environmental interaction," *Polymer Engineering & Science,* vol. 38, no. 8, pp. 1251-1253, Aug 1998, doi: https://doi.org/10.1002/pen.10294.

[41] H. P. Ramesh and R. N. Tharanathan, "Carbohydrates—the renewable raw materials of high biotechnological value," *Critical Reviews in Biotechnology,* vol. 23, no. 2, pp. 149-173, Jan 2003, doi: 10.1080/713609312.

[42] A. Aravamudhan, D. M. Ramos, A. A. Nada, and S. G. Kumbar, "Chapter 4 - Natural polymers: polysaccharides and their derivatives for biomedical applications," in *Natural and Synthetic Biomedical Polymers*, S. G. Kumbar, C. T. Laurencin, and M. Deng Eds. Oxford: Elsevier, 2014, pp. 67-89.

[43] H. Zhang, J. Cheng, and Q. Ao, "Preparation of alginate-based biomaterials and their applications in biomedicine," *Marine Drugs,* vol. 19, no. 5, p. 264, 2021. [Online]. Available: https://www.mdpi.com/1660-3397/19/5/264.

[44] J. W. Doyle, T. P. Roth, R. M. Smith, Y. Q. Li, and R. M. Dunn, "Effect of calcium alginate on cellular wound healing processes modeled in vitro," *Journal of Biomedical Materials Research,* vol. 32, no. 4, pp. 561-568, 1996, doi: https://doi.org/10.1002/(SICI)1097-4636(199612)32:4<561::AIDJBM9>3.0.CO;2-P.

[45] A. F. Stockwell, S. S. Davis, and S. E. Walker, "In vitro evaluation of alginate gel systems as sustained release drug delivery systems," *Journal of Controlled Release,* vol. 3, no. 1, pp. 167-175, Jan 1986, doi: https://doi.org/10.1016/0168-3659(86)90077-5.

[46] L. Cai *et al.*, "Engineered biomaterials for cancer immunotherapy," *MedComm,* vol. 1, no. 1, pp. 35-46, 2020, doi: https://doi.org/10.1002/mco2.8.

[47] O. Tsur-Gang *et al.*, "The effects of peptide-based modification of alginate on left ventricular remodeling and function after myocardial infarction," *Biomaterials,* vol. 30, no. 2, pp. 189-195, Jan 2009, doi: https://doi.org/10.1016/j.biomaterials.2008.09.018.

[48] D. Trache *et al.*, "Nanocellulose: from fundamentals to advanced applications," (in eng), *Front Chem,* vol. 8, p. 392, 2020, doi: 10.3389/fchem.2020.00392.

[49] S. i. Honda, N. Miyata, and K. Iwahori, "Recovery of biomass cellulose from waste sewage sludge," *Journal of Material Cycles and Waste*

Management, vol. 4, no. 1, pp. 46-50, Apr 2002, doi: 10.1007/s10163-001-0054-y.

[50] S. A. Ogundare, V. Moodley, and W. E. van Zyl, "Nanocrystalline cellulose isolated from discarded cigarette filters," *Carbohydrate Polymers,* vol. 175, pp. 273-281, Nov 2017, doi: https://doi.org/10.1016/j.carbpol.2017.08.008.

[51] A. Antony and R. thottiam Vasudevan, "A review on cellulose and its utilization from agro-industrial waste," *Drug Invention Today,* vol. 10, pp. 89-94, Mar 2018.

[52] S. Yousef *et al.*, "Sustainable industrial technology for recovery of cellulose from banknote production waste and reprocessing into cellulose nanocrystals," *Resources, Conservation and Recycling,* vol. 149, pp. 510-520, Oct 2019, doi: https://doi.org/10.1016/j.resconrec.2019.06.026.

[53] B. Liu *et al.*, "Corncob cellulose nanosphere as an eco-friendly detergent," *Nature Sustainability,* vol. 3, no. 6, pp. 448-458, Jun 2020, doi: 10.1038/s41893-020-0501-1.

[54] C. M. Chandrasekar *et al.*, "Valorization of citrus peel industrial wastes for facile extraction of extractives, pectin, and cellulose nanocrystals through ultrasonication: An in-depth investigation," *Carbohydrate Polymers,* vol. 344, p. 122539, Nov 2024, doi: https://doi.org/10.1016/j.carbpol.2024.122539.

[55] S. Padhi, A. Singh, and W. Routray, "Nanocellulose from agro-waste: a comprehensive review of extraction methods and applications," *Reviews in Environmental Science and Bio/Technology,* vol. 22, no. 1, pp. 1-27, Mar 2023, doi: 10.1007/s11157-023-09643-6.

[56] X. Yang *et al.*, "Characteristics and functional application of cellulose fibers extracted from cow dung wastes," *Materials,* vol. 16, no. 2, p. 648, 2023. [Online]. Available: https://www.mdpi.com/1996-1944/16/2/648.

[57] H. Seddiqi *et al.*, "Cellulose and its derivatives: towards biomedical applications," (in English), *Cellulose,* Review vol. 28, no. 4, pp. 1893-1931, Mar 2021, doi: 10.1007/s10570-020-03674-w.

[58] H. P. Fink, P. Weigel, H. Purz, and J. Ganster, "Structure formation of regenerated cellulose materials from NMMO-solutions," *Progress in Polymer Science,* vol. 26, no. 9, pp. 1473-1524, 2001.

[59] C. L. McCormick, P. A. Callais, and B. H. Hutchinson Jr, "Solution studies of cellulose in lithium chloride and N, N-dimethylacetamide," *Macromolecules,* vol. 18, no. 12, pp. 2394-2401, 1985.

[60] H. Wang, G. Gurau, and R. D. Rogers, "Ionic liquid processing of cellulose," *Chem. Soc. Rev.,* vol. 41, no. 4, pp. 1519-1537, 2012.

[61] A. Pinkert, K. N. Marsh, S. Pang, and M. P. Staiger, "Ionic liquids and their interaction with cellulose," *Chemical Reviews,* vol. 109, no. 12, pp. 6712-6728, Dec 2009, doi: 10.1021/cr9001947.

[62] A. Salama and P. Hesemann, "Recent trends in elaboration, processing, and derivatization of cellulosic materials using ionic liquids," *ACS Sustainable Chemistry & Engineering,* vol. 8, no. 49, pp. 17893-17907, Dec 2020, doi: 10.1021/acssuschemeng.0c06913.

[63] S. Zhu *et al.*, "Dissolution of cellulose with ionic liquids and its application: a mini-review," *Green Chemistry,* vol. 8, no. 4, pp. 325-327, 2006.

[64] R. Sescousse, K. A. Le, M. E. Ries, and T. Budtova, "Viscosity of cellulose−imidazolium-based ionic liquid solutions," *The Journal of Physical Chemistry B,* vol. 114, no. 21, pp. 7222-7228, Jun 2010, doi: 10.1021/jp1024203.

[65] J. D. Holbrey and K. R. Seddon, "Ionic liquids," *Clean Products and Processes,* vol. 1, no. 4, pp. 223-236, Dec 1999, doi: 10.1007/s100980050036.

[66] S. T. Handy and X. Zhang, "Organic synthesis in ionic liquids: the Stille coupling," (in eng), *Org Lett,* vol. 3, no. 2, pp. 233-6, Jan 2001, doi: 10.1021/ol0068849.

[67] B. Wu, W. Liu, Y. Zhang, and H. Wang, "Do we understand the recyclability of ionic liquids?," *Chemistry – A European Journal,* vol. 15, no. 8, pp. 1804-1810, 2009, doi: https://doi.org/10.1002/chem.200801509.

[68] K. Haerens, S. Van Deuren, E. Matthijs, and B. Van der Bruggen, "Challenges for recycling ionic liquids by using pressure driven membrane processes," *Green Chemistry,* vol. 12, no. 12, pp. 2182-2188, 2010, doi: 10.1039/C0GC00406E.

[69] T. Elschner, M. Kötteritzsch, and T. Heinze, "Synthesis of cellulose tricarbonates in 1-butyl-3-methylimidazolium chloride/pyridine,"

Macromolecular Bioscience, vol. 14, no. 2, pp. 161-165, 2014, doi: https://doi.org/10.1002/mabi.201300345.

[70] W. Li, A. Jin, C. Liu, R. Sun, A. Zhang, and J. Kennedy, "Homogeneous modification of cellulose with succinic anhydride in ionic liquid using 4-dimethylaminopyridine as a catalyst," *Carbohydr. Polym.,* vol. 78, no. 3, pp. 389-395, 2009.

[71] X. Liu, J. Pang, X. Zhang, Y. Wu, and R. Sun, "Regenerated cellulose film with enhanced tensile strength prepared with ionic liquid 1-ethyl-3-methylimidazolium acetate (EMIMAc)," *Cellulose,* vol. 20, pp. 1391-1399, 2013.

[72] X. Wang, H. Li, Y. Cao, and Q. Tang, "Cellulose extraction from wood chip in an ionic liquid 1-allyl-3-methylimidazolium chloride (AmimCl)," *Bioresource Technology,* vol. 102, no. 17, pp. 7959-7965, Sep 2011, doi: https://doi.org/10.1016/j.biortech.2011.05.064.

[73] A. Michud *et al.*, "Ioncell-F: ionic liquid-based cellulosic textile fibers as an alternative to viscose and Lyocell," *Textile Research Journal,* vol. 86, no. 5, pp. 543-552, 2016, doi: 10.1177/0040517515591774.

[74] G. I. Taylor, "Disintegration of water drops in an electric field," *Proceedings of the Royal Society of London. Series A. Mathematical and Physical Sciences,* vol. 280, no. 1382, pp. 383-397, 1964, doi: doi:10.1098/rspa.1964.0151.

[75] G. I. Taylor and M. D. Van Dyke, "Electrically driven jets," *Proceedings of the Royal Society of London. A. Mathematical and Physical Sciences,* vol. 313, no. 1515, pp. 453-475, 1969, doi: doi:10.1098/rspa.1969.0205.

[76] J. Doshi and D. H. Reneker, "Electrospinning process and applications of electrospun fibers," *Journal of Electrostatics,* vol. 35, no. 2, pp. 151-160, Aug 1995, doi: https://doi.org/10.1016/0304-3886(95)00041-8.

[77] J. Doshi and D. H. Reneker, "Electrospinning process and applications of electrospun fibers," *Journal of Electrostatics,* vol. 35, no. 2-3, pp. 151-160, Aug 1995, doi: 10.1016/0304-3886(95)00041-8.

[78] C. K. S. Pillai, W. Paul, and C. P. Sharma, "Chitin and chitosan polymers: chemistry, solubility and fiber formation," *Progress in Polymer Science,* vol. 34, no. 7, pp. 641-678, Jul 2009, doi: 10.1016/j.progpolymsci.2009.04.001.

[79] Z. X. Cai *et al.*, "Fabrication of chitosan/silk fibroin composite nanofibers for wound-dressing applications," *International Journal of Molecular Sciences,* vol. 11, no. 9, pp. 3529-3539, Sep 2010, doi: 10.3390/ijms11093529.

[80] A. R. Unnithan, G. Gnanasekaran, Y. Sathishkumar, Y. S. Lee, and C. S. Kim, "Electrospun antibacterial polyurethane-cellulose acetate-zein composite mats for wound dressing," *Carbohydrate Polymers,* vol. 102, pp. 884-892, Feb 2014, doi: 10.1016/j.carbpol.2013.10.070.

[81] D. H. Reneker and I. Chun, "Nanometre diameter fibres of polymer, produced by electrospinning," *Nanotechnology,* vol. 7, no. 3, p. 216, 1996.

[82] D. H. Reneker, A. L. Yarin, H. Fong, and S. Koombhongse, "Bending instability of electrically charged liquid jets of polymer solutions in electrospinning," *Journal of Applied Physics,* vol. 87, no. 9, pp. 4531-4547, 2000, doi: 10.1063/1.373532.

[83] R. Asmatulu and W. S. Khan, "Chapter 2 - Historical background of the electrospinning process," in *Synthesis and Applications of Electrospun Nanofibers*, R. Asmatulu and W. S. Khan Eds.: Elsevier, 2019, pp. 17-39.

[84] H. Xu, S. Yagi, S. Ashour, L. Du, M. E. Hoque, and L. Tan, "A review on current nanofiber technologies: electrospinning, centrifugal spinning, and electro-centrifugal spinning," *Macromolecular Materials and Engineering,* vol. 308, no. 3, p. 2200502, 2023, doi: https://doi.org/10.1002/mame.202200502.

[85] A. Keirouz *et al.*, "The history of electrospinning: past, present, and future developments," *Advanced Materials Technologies,* vol. 8, no. 11, p. 2201723, 2023, doi: https://doi.org/10.1002/admt.202201723.

[86] O. Ero-Phillips, M. Jenkins, and A. Stamboulis, "Tailoring crystallinity of electrospun plla fibres by control of electrospinning parameters," *Polymers,* vol. 4, no. 3, pp. 1331-1348, Sep 2012, doi: 10.3390/polym4031331.

[87] H. Chen, H. Xu, J. Sun, C. Liu, and B. Yang, "Effective method for high-throughput manufacturing of ultrafine fibres via needleless centrifugal spinning," *Micro & Nano Letters,* vol. 10, no. 2, pp. 81-84, 2015.

[88] W. E. Teo and S. Ramakrishna, "A review on electrospinning design and nanofibre assemblies," *Nanotechnology,* vol. 17, no. 14, p. R89, Jun 2006, doi: 10.1088/0957-4484/17/14/R01.

[89] D. Li and Y. Xia, "Electrospinning of nanofibers: reinventing the wheel?," *Advanced Materials,* vol. 16, no. 14, pp. 1151-1170, 2004, doi: https://doi.org/10.1002/adma.200400719.

[90] H. Zannini Luz and L. A. Loureiro dos Santos, "Centrifugal spinning for biomedical use: A review," *Critical Reviews in Solid State and Materials Sciences,* vol. 48, no. 4, pp. 519-534, 2023.

[91] F. R. Jones and N. T. Huff, "9 - The structure and properties of glass fibres," in *Handbook of Textile Fibre Structure*, vol. 2, S. J. Eichhorn, J. W. S. Hearle, M. Jaffe, and T. Kikutani Eds.: Woodhead Publishing, 2009, pp. 307-352.

[92] X. Zhang and Y. Lu, "Centrifugal spinning: an alternative approach to fabricate nanofibers at high speed and low cost," *Polymer Reviews,* vol. 54, no. 4, pp. 677-701, 2014.

[93] N. E. Zander, "Formation of melt and solution spun polycaprolactone fibers by centrifugal spinning," *Journal of Applied Polymer Science,* vol. 132, no. 2, Jan 2015, doi: https://doi.org/10.1002/app.41269.

[94] T. Hou, X. Li, Y. Lu, and B. Yang, "Highly porous fibers prepared by centrifugal spinning," *Materials & Design,* vol. 114, pp. 303-311, Jan 2017, doi: https://doi.org/10.1016/j.matdes.2016.11.019.

[95] S. Mahalingam and M. Edirisinghe, "Forming of polymer nanofibers by a pressurised gyration process," *Macromolecular rapid communications,* vol. 34, no. 14, pp. 1134-1139, 2013.

[96] P. Mellado, H. A. McIlwee, M. R. Badrossamay, J. A. Goss, L. Mahadevan, and K. K. Parker, "A simple model for nanofiber formation by rotary jet-spinning," *Applied Physics Letters,* vol. 99, no. 20, p. 203107, 2011, doi: 10.1063/1.3662015.

[97] H. Alenezi, M. E. Cam, and M. Edirisinghe, "Experimental and theoretical investigation of the fluid behavior during polymeric fiber formation with and without pressure," *Applied Physics Reviews,* vol. 6, no. 4, p. 041401, 2019, doi: 10.1063/1.5110965.

[98] R. T. Weitz, L. Harnau, S. Rauschenbach, M. Burghard, and K. Kern, "Polymer nanofibers via nozzle-free centrifugal spinning," *Nano Letters,* vol. 8, no. 4, pp. 1187-1191, Apr 2008, doi: 10.1021/nl080124q.

[99] H. Xu, H. Chen, X. Li, C. Liu, and B. Yang, "A comparative study of jet formation in nozzle- and nozzle-less centrifugal spinning systems," *Journal of Polymer Science Part B: Polymer Physics,* vol. 52, no. 23, pp. 1547-1559, 2014, doi: https://doi.org/10.1002/polb.23596.

[100] A. Gañán-Calvo, "Generation of steady liquid microthreads and micron-sized monodisperse sprays in gas streams," *Physical Review Letters,* vol. 80, p. 285, Jan 1998, doi: 10.1103/PhysRevLett.80.285.

[101] Y. Dai, J. Ahmed, A. Delbusso, and M. Edirisinghe, "Nozzle-pressurized gyration: a novel fiber manufacturing process," *Macromolecular Materials and Engineering,* vol. 307, no. 9, p. 2200268, doi: https://doi.org/10.1002/mame.202200268.

[102] R. Matharu, Z. Charani, L. Ciric, E. Illangakoon, and M. Edirisinghe, "Antimicrobial activity of tellurium-loaded polymeric fiber meshes," *Journal of Applied Polymer Science,* vol. 135, p. 46368, Mar 2018, doi: 10.1002/app.46368.

[103] B. T. Raimi-Abraham, S. Mahalingam, M. Edirisinghe, and D. Q. M. Craig, "Generation of poly(N-vinylpyrrolidone) nanofibres using pressurised gyration," *Materials Science and Engineering: C,* vol. 39, pp. 168-176, Jun 2014, doi: https://doi.org/10.1016/j.msec.2014.02.016.

[104] M. Gultekinoglu, Ş. Öztürk, B. Chen, M. Edirisinghe, and K. Ulubayram, "Preparation of poly(glycerol sebacate) fibers for tissue engineering applications," *European Polymer Journal,* vol. 121, p. 109297, Dec 2019, doi: https://doi.org/10.1016/j.eurpolymj.2019.109297.

[105] S. Mahalingam, S. Homer-Vanniasinkam, and M. Edirisinghe, "Novel pressurised gyration device for making core-sheath polymer fibres," *Materials & Design,* vol. 178, p. 107846, Sep 2019, doi: https://doi.org/10.1016/j.matdes.2019.107846.

[106] S. Mahalingam, S. Huo, S. Homer-Vanniasinkam, and M. Edirisinghe, "Generation of core–sheath polymer nanofibers by pressurised gyration," *Polymers,* vol. 12, no. 8, p. 1709, 2020. [Online]. Available: https://www.mdpi.com/2073-4360/12/8/1709.

[107] P. Mehta *et al.*, "Recent applications of electrical, centrifugal, and pressurised emerging technologies for fibrous structure engineering in drug delivery, regenerative medicine and theranostics," *Advanced Drug*

Delivery Reviews, vol. 175, p. 113823, Aug 2021, doi: https://doi.org/10.1016/j.addr.2021.05.033.

[108] Y. Ide and J. L. White, "The spinnability of polymer fluid filaments," *Journal of Applied Polymer Science,* vol. 20, no. 9, pp. 2511-2531, 1976, doi: https://doi.org/10.1002/app.1976.070200919.

[109] X. Hong, M. Edirisinghe, and S. Mahalingam, "Beads, beaded-fibres and fibres: Tailoring the morphology of poly(caprolactone) using pressurised gyration," *Materials Science and Engineering: C,* vol. 69, pp. 1373-1382, Dec 2016, doi: https://doi.org/10.1016/j.msec.2016.07.071.

[110] X. Hong, S. Mahalingam, and M. Edirisinghe, "Simultaneous application of pressure-infusion-gyration to generate polymeric nanofibers," *Macromolecular Materials and Engineering,* vol. 302, no. 6, p. 1600564, 2017, doi: https://doi.org/10.1002/mame.201600564.

[111] X. Hong, A. Harker, and M. Edirisinghe, "Process modeling for the fiber diameter of polymer, spun by pressure-coupled infusion gyration," *ACS Omega,* vol. 3, no. 5, pp. 5470-5479, May 2018, doi: 10.1021/acsomega.8b00452.

[112] X. Hong, A. Harker, and M. Edirisinghe, "Empirical modelling and optimization of pressure-coupled infusion gyration parameters for the nanofibre fabrication," *Proceedings of the Royal Society A: Mathematical, Physical and Engineering Sciences,* vol. 475, no. 2225, p. 20190008, 2019, doi: doi:10.1098/rspa.2019.0008.

[113] Z. Xu *et al.*, "Making nonwoven fibrous poly(ε-caprolactone) constructs for antimicrobial and tissue engineering applications by pressurized melt gyration," *Macromolecular Materials and Engineering,* vol. 301, no. 8, pp. 922-934, 2016, doi: https://doi.org/10.1002/mame.201600116.

[114] H. Majd, A. Harker, M. Edirisinghe, and M. Parhizkar, "Optimised release of tetracycline hydrochloride from core-sheath fibres produced by pressurised gyration," *Journal of Drug Delivery Science and Technology,* vol. 72, p. 103359, Jun 2022, doi: https://doi.org/10.1016/j.jddst.2022.103359.

[115] H. Alenezi, M. E. Cam, and M. Edirisinghe, "Core–sheath polymer nanofiber formation by the simultaneous application of rotation and

pressure in a novel purpose-designed vessel," *Applied Physics Reviews,* vol. 8, no. 4, p. 041412, 2021, doi: 10.1063/5.0071257.

[116] S. Mahalingam, R. Matharu, S. Homer-Vanniasinkam, and M. Edirisinghe, "Current methodologies and approaches for the formation of core–sheath polymer fibers for biomedical applications," *Applied Physics Reviews,* vol. 7, no. 4, p. 041302, 2020, doi: 10.1063/5.0008310.

[117] S. Mahalingam, C. Bayram, M. Gultekinoglu, K. Ulubayram, S. Homer-Vanniasinkam, and M. Edirisinghe, "Co-axial gyro-spinning of PCL/PVA/HA core-sheath fibrous scaffolds for bone tissue engineering," *Macromolecular Bioscience,* vol. 21, no. 10, p. 2100177, 2021, doi: https://doi.org/10.1002/mabi.202100177.

[118] U. E. Illangakoon, S. Mahalingam, R. K. Matharu, and M. Edirisinghe, "Evolution of surface nanopores in pressurised gyrospun polymeric microfibers," *Polymers,* vol. 9, no. 10, p. 508, 2017.

[119] A. Amir *et al.*, "Microstructure of fibres pressure-spun from polyacrylonitrile–graphene oxide composite mixtures," *Composites Science and Technology,* vol. 197, p. 108214, 2020.

[120] H. Zhao *et al.*, "Processing and electrochemical properties of CNT reinforced carbon nanofibers prepared by pressurized gyration," *Journal of Materials Research,* vol. 33, no. 24, pp. 4251-4260, 2018, doi: 10.1557/jmr.2018.400.

[121] M. E. Cam *et al.*, "A novel treatment strategy for preterm birth: Intra-vaginal progesterone-loaded fibrous patches," *International Journal of Pharmaceutics,* vol. 588, p. 119782, 2020.

[122] P. L. Heseltine, J. Hosken, C. Agboh, D. Farrar, S. Homer-Vanniasinkam, and M. Edirisinghe, "Fiber formation from silk fibroin using pressurized gyration," *Macromolecular Materials and Engineering,* vol. 304, no. 1, p. 1800577, 2019.

[123] P. L. Heseltine, C. Bayram, M. Gultekinoglu, S. Homer-Vanniasinkam, K. Ulubayram, and M. Edirisinghe, "Facile one-pot method for all aqueous green formation of biocompatible silk fibroin-poly(ethylene oxide) fibers for use in tissue engineering," *ACS Biomaterials Science & Engineering,* vol. 8, no. 3, pp. 1290-1300, Mar 2022, doi: 10.1021/acsbiomaterials.1c01555.

[124] P. Basnett *et al.*, "Harnessing polyhydroxyalkanoates and pressurized gyration for hard and soft tissue engineering," *ACS Applied Materials & Interfaces,* vol. 13, no. 28, pp. 32624-32639, 2021.

[125] S. Mahalingam, G. Ren, and M. Edirisinghe, "Rheology and pressurised gyration of starch and starch-loaded poly (ethylene oxide)," *Carbohydrate polymers,* vol. 114, pp. 279-287, 2014.

[126] S. Mahalingam, G. Pierin, P. Colombo, and M. Edirisinghe, "Facile one-pot formation of ceramic fibres from preceramic polymers by pressurised gyration," *Ceramics International,* vol. 41, no. 4, pp. 6067-6073, 2015.

[127] S. Mahalingam, Z. Xu, and M. Edirisinghe, "Antibacterial activity and biosensing of PVA-lysozyme microbubbles formed by pressurized gyration," *Langmuir,* vol. 31, no. 36, pp. 9771-9780, 2015.

[128] S. Mahalingam, B. T. Raimi-Abraham, D. Q. Craig, and M. Edirisinghe, "Formation of protein and protein–gold nanoparticle stabilized microbubbles by pressurized gyration," *Langmuir,* vol. 31, no. 2, pp. 659-666, 2015.

[129] J. R. Lindner, "Microbubbles in medical imaging: current applications and future directions," *Nature reviews Drug discovery,* vol. 3, no. 6, pp. 527-533, 2004.

[130] S. Cesur *et al.*, "Metformin-Loaded Polymer-Based Microbubbles/Nanoparticles Generated for the Treatment of Type 2 Diabetes Mellitus," *Langmuir,* vol. 38, no. 17, pp. 5040-5051, May 2022, doi: 10.1021/acs.langmuir.1c00587.

[131] P. Dijkmans *et al.*, "Microbubbles and ultrasound: from diagnosis to therapy," *European Journal of Echocardiography,* vol. 5, no. 4, pp. 245-246, 2004.

[132] J. M. Tsutsui, F. Xie, and R. T. Porter, "The use of microbubbles to target drug delivery," *Cardiovascular Ultrasound,* vol. 2, no. 1, pp. 1-7, 2004.

[133] K. Kundu, A. Afshar, D. R. Katti, M. Edirisinghe, and K. S. Katti, "Composite nanoclay-hydroxyapatite-polymer fiber scaffolds for bone tissue engineering manufactured using pressurized gyration," *Composites Science and Technology,* vol. 202, p. 108598, 2021/01/20/ 2021, doi: https://doi.org/10.1016/j.compscitech.2020.108598.

[134] M. O. Aydogdu, E. Altun, J. Ahmed, O. Gunduz, and M. Edirisinghe, "Fiber Forming Capability of Binary and Ternary Compositions in the Polymer System: Bacterial Cellulose–Polycaprolactone–Polylactic Acid," *Polymers,* vol. 11, no. 7, p. 1148, 2019. [Online]. Available: https://www.mdpi.com/2073-4360/11/7/1148.

[135] J. Ahmed *et al.*, "Anti-fungal bandages containing cinnamon extract," *International Wound Journal,* vol. 16, no. 3, pp. 730-736, 2019, doi: https://doi.org/10.1111/iwj.13090.

[136] J. Ahmed, M. Gultekinoglu, C. Bayram, D. Kart, K. Ulubayram, and M. Edirisinghe, "Alleviating the toxicity concerns of antibacterial cinnamon-polycaprolactone biomaterials for healthcare-related biomedical applications," *MedComm,* vol. 2, no. 2, pp. 236-246, 2021, doi: https://doi.org/10.1002/mco2.71.

[137] S. Zhang *et al.*, "Coupling Infusion and Gyration for the Nanoscale Assembly of Functional Polymer Nanofibers Integrated with Genetically Engineered Proteins," *Macromolecular Rapid Communications,* vol. 36, no. 14, pp. 1322-1328, 2015, doi: https://doi.org/10.1002/marc.201500174.

[138] U. E. Illangakoon, S. Mahalingam, P. Colombo, and M. Edirisinghe, "Tailoring the surface of polymeric nanofibres generated by pressurised gyration," *Surface Innovations,* vol. 4, no. 3, pp. 167-178, 2016.

[139] M. Karimpoor, E. Illangakoon, A. G. Reid, S. Claudiani, M. Edirisinghe, and J. S. Khorashad, "Development of artificial bone marrow fibre scaffolds to study resistance to anti-leukaemia agents," *British journal of haematology,* 2017.

[140] R. K. Matharu *et al.*, "Microstructure and antibacterial efficacy of graphene oxide nanocomposite fibres," *Journal of colloid and interface science,* vol. 571, pp. 239-252, 2020.

[141] R. K. Matharu, L. Ciric, G. Ren, and M. Edirisinghe, "Comparative study of the antimicrobial effects of tungsten nanoparticles and tungsten nanocomposite fibres on hospital acquired bacterial and viral pathogens," *Nanomaterials,* vol. 10, no. 6, p. 1017, 2020.

[142] U. E. Illangakoon *et al.*, "Gyrospun antimicrobial nanoparticle loaded fibrous polymeric filters," *Materials Science and Engineering: C,* vol. 74, pp. 315-324, 2017.

[143] R. K. Matharu, H. Porwal, L. Ciric, and M. Edirisinghe, "The effect of graphene–poly (methyl methacrylate) fibres on microbial growth," *Interface Focus,* vol. 8, no. 3, p. 20170058, 2018.

[144] J. Ahmed, R. K. Matharu, T. Shams, U. E. Illangakoon, and M. Edirisinghe, "A comparison of electric-field-driven and pressure-driven fiber generation methods for drug delivery," *Macromolecular Materials and Engineering,* vol. 303, no. 5, p. 1700577, 2018.

[145] B. T. Raimi-Abraham, S. Mahalingam, P. J. Davies, M. Edirisinghe, and D. Q. Craig, "Development and characterization of amorphous nanofiber drug dispersions prepared using pressurized gyration," *Molecular pharmaceutics,* vol. 12, no. 11, pp. 3851-3861, 2015.

[146] M. E. Cam *et al.*, "Evaluation of burst release and sustained release of pioglitazone-loaded fibrous mats on diabetic wound healing: an in vitro and in vivo comparison study," *Journal of the Royal Society Interface,* vol. 17, no. 162, p. 20190712, 2020.

[147] S. Mahalingam, X. Wu, and M. Edirisinghe, "Evolution of self-generating porous microstructures in polyacrylonitrile-cellulose acetate blend fibres," *Materials & Design,* vol. 134, pp. 259-271, 2017.

[148] X. Wu *et al.*, "Novel preparation, microstructure, and properties of polyacrylonitrile-based carbon nanofiber–graphene nanoplatelet materials," *ACS omega,* vol. 1, no. 2, pp. 202-211, 2016.

[149] R. Huang, Y. Dai, J. Ahmed, and M. Edirisinghe, "Facile one-step synthesis of PVDF bead-on-string fibers by pressurized gyration for reusable face masks," *Polymers,* vol. 14, no. 21, p. 4498, 2022. [Online]. Available: https://www.mdpi.com/2073-4360/14/21/4498.

[150] S. Mahalingam, B. T. Raimi-Abraham, D. Q. Craig, and M. Edirisinghe, "Solubility–spinnability map and model for the preparation of fibres of polyethylene (terephthalate) using gyration and pressure," *Chem. Eng. J.,* vol. 280, pp. 344-353, 2015.

[151] Z. Xu, S. Mahalingam, J. Rohn, G. Ren, and M. Edirisinghe, "Physio-chemical and antibacterial characteristics of pressure spun nylon nanofibres embedded with functional silver nanoparticles," *Materials Science and Engineering: C,* vol. 56, pp. 195-204, 2015.

[152] A. Amir *et al.*, "Graphene nanoplatelets loaded polyurethane and phenolic resin fibres by combination of pressure and gyration," *Composites Science and Technology,* vol. 129, pp. 173-182, Jun 2016, doi: https://doi.org/10.1016/j.compscitech.2016.03.031.

[153] X. Su, S. Mahalingam, M. Edirisinghe, and B. Chen, "Highly stretchable and highly resilient polymer–clay nanocomposite hydrogels with low hysteresis," *ACS applied materials & interfaces,* vol. 9, no. 27, pp. 22223-22234, 2017.

[154] A. Kelly, J. Ahmed, and M. Edirisinghe, "Manufacturing cyclodextrin fibers using water," *Macromolecular Materials and Engineering,* p. 2100891, 2022.

[155] F. Brako, R. Thorogate, S. Mahalingam, B. Raimi-Abraham, D. Q. Craig, and M. Edirisinghe, "Mucoadhesion of progesterone-loaded drug delivery nanofiber constructs," *ACS applied materials & interfaces,* vol. 10, no. 16, pp. 13381-13389, 2018.

[156] F. Brako, B. T. Raimi-Abraham, S. Mahalingam, D. Q. Craig, and M. Edirisinghe, "The development of progesterone-loaded nanofibers using pressurized gyration: A novel approach to vaginal delivery for the prevention of pre-term birth," *International journal of pharmaceutics,* vol. 540, no. 1-2, pp. 31-39, 2018.

[157] F. Brako, B. Raimi-Abraham, S. Mahalingam, D. Q. Craig, and M. Edirisinghe, "Making nanofibres of mucoadhesive polymer blends for vaginal therapies," *Eur. Polym. J.,* vol. 70, pp. 186-196, 2015.

[158] E. Altun *et al.*, "Novel making of bacterial cellulose blended polymeric fiber bandages," *Macromolecular Materials and Engineering,* vol. 303, no. 3, p. 1700607, 2018.

[159] E. Altun *et al.*, "Co-culture of Keratinocyte-Staphylococcus aureus on Cu-Ag-Zn/CuO and Cu-Ag-W nanoparticle loaded bacterial cellulose: PMMA bandages," *Macromolecular Materials and Engineering,* vol. 304, no. 1, p. 1800537, 2019.

[160] X. Wu, S. Mahalingam, S. K. VanOosten, C. Wisdom, C. Tamerler, and M. Edirisinghe, "New generation of tunable bioactive shape memory mats integrated with genetically engineered proteins," *Macromolecular bioscience,* vol. 17, no. 2, p. 1600270, 2017.

[161] M. E. Cam *et al.*, "Accelerated diabetic wound healing by topical application of combination oral antidiabetic agents-loaded nanofibrous scaffolds: an in vitro and in vivo evaluation study," *Materials Science and Engineering: C,* vol. 119, p. 111586, 2021.

[162] K. Y. Lee and D. J. Mooney, "Alginate: properties and biomedical applications," *Progress in Polymer Science,* vol. 37, no. 1, pp. 106-126, Jan 2012, doi: https://doi.org/10.1016/j.progpolymsci.2011.06.003.

[163] F. J. Pavinatto, L. Caseli, and O. N. Oliveira, Jr., "Chitosan in nanostructured thin films," *Biomacromolecules,* vol. 11, no. 8, pp. 1897-1908, Aug 2010, doi: 10.1021/bm1004838.

[164] A. B. Bello, D. Kim, D. Kim, H. Park, and S. H. Lee, "Engineering and functionalization of gelatin biomaterials: from cell culture to medical applications," *Tissue Engineering Part B: Reviews,* vol. 26, no. 2, pp. 164-180, 2020, doi: 10.1089/ten.teb.2019.0256.

[165] T. Liebert, "Cellulose solvents – remarkable history, bright future," in *Cellulose Solvents: For Analysis, Shaping and Chemical Modification*, vol. 1033, (ACS Symposium Series, no. 1033): American Chemical Society, 2010, ch. 1, pp. 3-54.

[166] D. Puppi and F. Chiellini, "Wet-spinning of biomedical polymers: from single-fibre production to additive manufacturing of three-dimensional scaffolds," *Polymer International,* vol. 66, no. 12, pp. 1690-1696, 2017, doi: https://doi.org/10.1002/pi.5332.

[167] C. Pereira, T. V. Pinto, R. M. Santos, and N. Correia, "Sustainable and naturally derived wet spun fibers: a systematic literature review," *Fibers,* vol. 12, no. 9, p. 75, 2024. [Online]. Available: https://www.mdpi.com/2079-6439/12/9/75.

[168] A. Rohani Shirvan, A. Nouri, and A. Sutti, "A perspective on the wet spinning process and its advancements in biomedical sciences," *European Polymer Journal,* vol. 181, p. 111681, Dec 2022, doi: https://doi.org/10.1016/j.eurpolymj.2022.111681.

[169] D. R. Paul, "Diffusion during the coagulation step of wet-spinning," *Journal of Applied Polymer Science,* vol. 12, no. 3, pp. 383-402, 1968, doi: https://doi.org/10.1002/app.1968.070120301.

[170] X. Zhang, X. Wang, W. Fan, Y. Liu, Q. Wang, and L. Weng, "Fabrication, property and application of calcium alginate fiber: a review," *Polymers,* vol. 14, no. 15, p. 3227, 2022. [Online]. Available: https://www.mdpi.com/2073-4360/14/15/3227.

[171] X. Zeng, J. Hu, J. Zhao, Y. Zhang, and D. Pan, "Investigating the jet stretch in the wet spinning of PAN fiber," *Journal of Applied Polymer Science,* vol. 106, no. 4, pp. 2267-2273, 2007, doi: https://doi.org/10.1002/app.26929.

[172] R. C. Ruaan, T. Chang, and D. M. Wang, "Selection criteria for solvent and coagulation medium in view of macrovoid formation in the wet phase inversion process," *Journal of Polymer Science Part B: Polymer Physics,* vol. 37, no. 13, pp. 1495-1502, 1999.

[173] N. R. Visaveliya *et al.*, "Surface wrinkling and porosity of polymer particles toward biological and biomedical applications," *Advanced Materials Interfaces,* vol. 4, no. 24, p. 1700929, 2017, doi: https://doi.org/10.1002/admi.201700929.

[174] H. C. Kim, D. Kim, J. Y. Lee, L. Zhai, and J. Kim, "Effect of wet spinning and stretching to enhance mechanical properties of cellulose nanofiber filament," *International Journal of Precision Engineering and Manufacturing-Green Technology,* vol. 6, no. 3, pp. 567-575, Jul 2019, doi: 10.1007/s40684-019-00070-z.

[175] M. Stasiak, A. Studer, A. Greiner, and J. H. Wendorff, "Polymer fibers as carriers for homogeneous catalysts," *Chemistry – A European Journal,* vol. 13, no. 21, pp. 6150-6156, 2007, doi: https://doi.org/10.1002/chem.200601555.

[176] S. Marx, M. V. Jose, J. D. Andersen, and A. J. Russell, "Electrospun gold nanofiber electrodes for biosensors," *Biosensors and Bioelectronics,* vol. 26, no. 6, pp. 2981-2986, Feb 2011, doi: https://doi.org/10.1016/j.bios.2010.11.050.

[177] X. Zeng, L. Ye, K. Guo, R. Sun, J. Xu, and C. P. Wong, "Fibrous epoxy substrate with high thermal conductivity and low dielectric property for flexible electronics," *Advanced Electronic Materials,* vol. 2, no. 5, p. 1500485, 2016, doi: https://doi.org/10.1002/aelm.201500485.

[178] S. Ponce-Alcántara, D. Martín-Sánchez, A. Pérez-Márquez, J. Maudes, N. Murillo, and J. García-Rupérez, "Optical sensors based on polymeric

nanofibers layers created by electrospinning," *Opt. Mater. Express,* vol. 8, no. 10, pp. 3163-3175, Oct 2018, doi: 10.1364/OME.8.003163.

[179] S. Nemati, S. J. Kim, Y. M. Shin, and H. Shin, "Current progress in application of polymeric nanofibers to tissue engineering," *Nano Convergence,* vol. 6, no. 1, p. 36, Nov 2019, doi: 10.1186/s40580-019-0209-y.

[180] "Polymeric nanofibers in tissue engineering," *Tissue Engineering Part B: Reviews,* vol. 17, no. 5, pp. 349-364, 2011, doi: 10.1089/ten.teb.2011.0238.

[181] J. Fang, H. Niu, T. Lin, and X. Wang, "Applications of electrospun nanofibers," *Chinese Science Bulletin,* vol. 53, no. 15, pp. 2265-2286, Aug 2008, doi: 10.1007/s11434-008-0319-0.

[182] "Electrospinning of polymeric nanofibers for tissue engineering applications: a review," *Tissue Engineering,* vol. 12, no. 5, pp. 1197-1211, 2006, doi: 10.1089/ten.2006.12.1197.

[183] M. Ottosson, A. Jakobsson, and F. Johansson, "Accelerated wound closure-differently organized nanofibers affect cell migration and hence the closure of artificial wounds in a cell based in vitro model," *PLoS One,* vol. 12, no. 1, p. e0169419, 2017.

[184] B. M. Baker *et al.*, "The potential to improve cell infiltration in composite fiber-aligned electrospun scaffolds by the selective removal of sacrificial fibers," *Biomaterials,* vol. 29, no. 15, pp. 2348-2358, May 2008, doi: https://doi.org/10.1016/j.biomaterials.2008.01.032.

[185] S. Zhong, W. E. Teo, X. Zhu, R. W. Beuerman, S. Ramakrishna, and L. Y. L. Yung, "An aligned nanofibrous collagen scaffold by electrospinning and its effects on in vitro fibroblast culture," *Journal of Biomedical Materials Research Part A,* vol. 79A, no. 3, pp. 456-463, 2006, doi: https://doi.org/10.1002/jbm.a.30870.

[186] "Improved cellular infiltration in electrospun fiber via engineered porosity," *Tissue Engineering,* vol. 13, no. 9, pp. 2249-2257, 2007, doi: 10.1089/ten.2006.0306.

[187] S. Soliman, S. Sant, J. W. Nichol, M. Khabiry, E. Traversa, and A. Khademhosseini, "Controlling the porosity of fibrous scaffolds by modulating the fiber diameter and packing density," *Journal of Biomedical*

Materials Research Part A, vol. 96A, no. 3, pp. 566-574, 2011, doi: https://doi.org/10.1002/jbm.a.33010.

[188] X. Hu, S. Liu, G. Zhou, Y. Huang, Z. Xie, and X. Jing, "Electrospinning of polymeric nanofibers for drug delivery applications," *Journal of Controlled Release,* vol. 185, pp. 12-21, Jul 2014, doi: https://doi.org/10.1016/j.jconrel.2014.04.018.

[189] B. Wang, Y. Wang, T. Yin, and Q. Yu, "Applications of electrospinning technique in drug delivery," *Chemical Engineering Communications,* vol. 197, no. 10, pp. 1315-1338, Jun 2010, doi: 10.1080/00986441003625997.

[190] E.-R. Kenawy, F. I. Abdel-Hay, M. H. El-Newehy, and G. E. Wnek, "Processing of polymer nanofibers through electrospinning as drug delivery systems," in *Nanomaterials: Risks and Benefits*: Springer, 2009, pp. 247-263.

[191] S. Kalepu and V. Nekkanti, "Insoluble drug delivery strategies: review of recent advances and business prospects," *Acta Pharmaceutica Sinica B,* vol. 5, no. 5, pp. 442-453, 2015.

[192] F. Ignatious, L. Sun, C. P. Lee, and J. Baldoni, "Electrospun nanofibers in oral drug delivery," *Pharmaceutical Research,* vol. 27, no. 4, pp. 576-588, Apr 2010, doi: 10.1007/s11095-010-0061-6.

[193] A. Luraghi, F. Peri, and L. Moroni, "Electrospinning for drug delivery applications: a review," *Journal of Controlled Release,* vol. 334, pp. 463-484, Jun 2021, doi: https://doi.org/10.1016/j.jconrel.2021.03.033.

[194] T. J. Sill and H. A. von Recum, "Electrospinning: applications in drug delivery and tissue engineering," *Biomaterials,* vol. 29, no. 13, pp. 1989-2006, May 2008, doi: https://doi.org/10.1016/j.biomaterials.2008.01.011.

[195] R. Romero, L. Yeo, P. Chaemsaithong, T. Chaiworapongsa, and S. S. Hassan, "Progesterone to prevent spontaneous preterm birth," *Seminars in Fetal and Neonatal Medicine,* vol. 19, no. 1, pp. 15-26, Feb 2014, doi: https://doi.org/10.1016/j.siny.2013.10.004.

[196] H. C. Zierden, R. L. Shapiro, K. DeLong, D. M. Carter, and L. M. Ensign, "Next generation strategies for preventing preterm birth," *Advanced Drug Delivery Reviews,* vol. 174, pp. 190-209, Jul 2021, doi: https://doi.org/10.1016/j.addr.2021.04.021.

[197] G. Broughton, II, J. E. Janis, and C. E. Attinger, "Wound healing: an overview," *Plastic and Reconstructive Surgery,* vol. 117, no. 7S, 2006. [Onli. Available: https://journals.lww.com/plasreconsurg/Fulltext/2006/06001/Wound_Healing__An_Overview.29.aspx.

[198] S. Dhivya, V. V. Padma, and E. Santhini, "Wound dressings – a review," *BioMedicine,* vol. 5, no. 4, p. 22, Nov 2015, doi: 10.7603/s40681-015-0022-9.

[199] F. Wang, S. Hu, Q. Jia, and L. Zhang, "Advances in electrospinning of natural biomaterials for wound dressing," *Journal of Nanomaterials,* vol. 2020, p. 8719859, Mar 2020, doi: 10.1155/2020/8719859.

[200] Y. F. Goh, I. Shakir, and R. Hussain, "Electrospun fibers for tissue engineering, drug delivery, and wound dressing," *Journal of Materials Science,* vol. 48, no. 8, pp. 3027-3054, Apr 2013, doi: 10.1007/s10853-013-7145-8.

[201] S. Schreml, R. M. Szeimies, L. Prantl, M. Landthaler, and P. Babilas, "Wound healing in the 21st century," *Journal of the American Academy of Dermatology,* vol. 63, no. 5, pp. 866-881, Nov 2010, doi: https://doi.org/10.1016/j.jaad.2009.10.048.

[202] Y. Liu, T. Li, Y. Han, F. Li, and Y. Liu, "Recent development of electrospun wound dressing," *Current Opinion in Biomedical Engineering,* vol. 17, p. 100247, Mar 2021, doi: https://doi.org/10.1016/j.cobme.2020.100247.

[203] V. V. Kadam, L. Wang, and R. Padhye, "Electrospun nanofibre materials to filter air pollutants – a review," *Journal of Industrial Textiles,* vol. 47, no. 8, pp. 2253-2280, 2018, doi: 10.1177/1528083716676812.

[204] T. Lu *et al.*, "Multistructured electrospun nanofibers for air filtration: a review," *ACS Applied Materials & Interfaces,* vol. 13, no. 20, pp. 23293-23313, May 2021, doi: 10.1021/acsami.1c06520.

[205] K. Azuma, U. Yanagi, N. Kagi, H. Kim, M. Ogata, and M. Hayashi, "Environmental factors involved in SARS-CoV-2 transmission: effect and role of indoor environmental quality in the strategy for COVID-19 infection control," *Environmental Health and Preventive Medicine,* vol. 25, no. 1, p. 66, Nov 2020, doi: 10.1186/s12199-020-00904-2.

[206] R. S. Barhate and S. Ramakrishna, "Nanofibrous filtering media: filtration problems and solutions from tiny materials," *J. Membr. Sci.,* vol. 296, no. 1, pp. 1-8, Jun 2007, doi: https://doi.org/10.1016/j.memsci.2007.03.038.

[207] A. Podgorski, A. Balazy, and L. Gradon, "Application of nanofibers to improve the filtration efficiency of the most penetrating aerosol particles in fibrous filters," (in English), *Chem. Eng. Sci.,* Article vol. 61, no. 20, pp. 6804-6815, Oct 2006, doi: 10.1016/j.ces.2006.07.022.

[208] X. Qin and S. Subianto, "17 - Electrospun nanofibers for filtration applications," in *Electrospun Nanofibers*, M. Afshari Ed.: Woodhead Publishing, 2017, pp. 449-466.

[209] J. Wang, S. C. Kim, and D. Y. H. Pui, "Investigation of the figure of merit for filters with a single nanofiber layer on a substrate," *Journal of Aerosol Science,* vol. 39, no. 4, pp. 323-334, Apr 2008, doi: https://doi.org/10.1016/j.jaerosci.2007.12.003.

[210] Q. Zhang, J. Welch, H. Park, C. Y. Wu, W. Sigmund, and J. C. M. Marijnissen, "Improvement in nanofiber filtration by multiple thin layers of nanofiber mats," *Journal of Aerosol Science,* vol. 41, no. 2, pp. 230-236, Feb 2010, doi: https://doi.org/10.1016/j.jaerosci.2009.10.001.

[211] L. Ji, Z. Lin, A. J. Medford, and X. Zhang, "Porous carbon nanofibers from electrospun polyacrylonitrile/SiO_2 composites as an energy storage material," *Carbon,* vol. 47, no. 14, pp. 3346-3354, Nov 2009, doi: https://doi.org/10.1016/j.carbon.2009.08.002.

[212] B. Zhang, F. Kang, J. M. Tarascon, and J. K. Kim, "Recent advances in electrospun carbon nanofibers and their application in electrochemical energy storage," *Progress in Materials Science,* vol. 76, pp. 319-380, Mar 2016, doi: https://doi.org/10.1016/j.pmatsci.2015.08.002.

[213] Q. Liu, J. Zhu, L. Zhang, and Y. Qiu, "Recent advances in energy materials by electrospinning," *Renewable and Sustainable Energy Reviews,* vol. 81, pp. 1825-1858, Jan 2018, doi: https://doi.org/10.1016/j.rser.2017.05.281.

[214] X. Li, Y. Chen, H. Huang, Y. W. Mai, and L. Zhou, "Electrospun carbon-based nanostructured electrodes for advanced energy storage – a review," *Energy Storage Materials,* vol. 5, pp. 58-92, Oct 2016, doi: https://doi.org/10.1016/j.ensm.2016.06.002.

[215] L. Sun, X. Wang, Y. Wang, and Q. Zhang, "Roles of carbon nanotubes in novel energy storage devices," *Carbon,* vol. 122, pp. 462-474, Oct 2017, doi: https://doi.org/10.1016/j.carbon.2017.07.006.

[216] L. Wen, F. Li, and H. M. Cheng, "Carbon nanotubes and graphene for flexible electrochemical energy storage: from materials to devices," *Advanced Materials,* vol. 28, no. 22, pp. 4306-4337, 2016, doi: https://doi.org/10.1002/adma.201504225.

[217] D. Jang, M. E. Lee, J. Choi, S. Y. Cho, and S. Lee, "Strategies for the production of PAN-based carbon fibers with high tensile strength," *Carbon,* vol. 186, pp. 644-677, Jan 2022, doi: https://doi.org/10.1016/j.carbon.2021.10.061.

[218] E. N. Durmaz and P. Zeynep Çulfaz-Emecen, "Cellulose-based membranes via phase inversion using [EMIM]OAc-DMSO mixtures as solvent," *Chemical Engineering Science,* vol. 178, pp. 93-103, Mar 2018, doi: https://doi.org/10.1016/j.ces.2017.12.020.

[219] A. J. Onyianta, D. O'Rourke, D. Sun, C. M. Popescu, and M. Dorris, "High aspect ratio cellulose nanofibrils from macroalgae Laminaria hyperborea cellulose extract via a zero-waste low energy process," *Cellulose,* vol. 27, no. 14, pp. 7997-8010, Sep 2020, doi: 10.1007/s10570-020-03223-5.

[220] H. Nie, A. He, J. Zheng, S. Xu, J. Li, and C. C. Han, "Effects of chain conformation and entanglement on the electrospinning of pure alginate," *Biomacromolecules,* vol. 9, no. 5, pp. 1362-1365, May 2008, doi: 10.1021/bm701349j.

[221] A. S. Giz *et al.*, "A detailed investigation of the effect of calcium crosslinking and glycerol plasticizing on the physical properties of alginate films," *International Journal of Biological Macromolecules,* vol. 148, pp. 49-55, Apr 2020, doi: https://doi.org/10.1016/j.ijbiomac.2020.01.103.

[222] E. Fonck *et al.*, "Effect of aging on elastin functionality in human cerebral arteries," *Stroke,* vol. 40, no. 7, pp. 2552-2556, 2009, doi: 10.1161/STROKEAHA.108.528091.

[223] E. A. Aksoy, G. Taskor, M. Gultekinoglu, F. Kara, and K. Ulubayram, "Synthesis of biodegradable polyurethanes chain-extended with (2S)-bis(2-hydroxypropyl) 2-aminopentane dioate," *Journal of Applied Polymer*

Science, vol. 135, no. 5, p. 45764, 2018, doi: https://doi.org/10.1002/app.45764.

[224] M. Gultekinoglu *et al.*, "Designing of dynamic polyethyleneimine (PEI) brushes on polyurethane (PU) ureteral stents to prevent infections," *Acta Biomaterialia,* vol. 21, pp. 44-54, Jul 2015, doi: https://doi.org/10.1016/j.actbio.2015.03.037.

[225] X. Hong, M. Edirisinghe, and S. Mahalingam, "Beads, beaded-fibres and fibres: Tailoring the morphology of poly (caprolactone) using pressurised gyration," *Materials Science and Engineering: C,* vol. 69, pp. 1373-1382, 2016.

[226] R. Casasola, N. L. Thomas, A. Trybala, and S. Georgiadou, "Electrospun poly lactic acid (PLA) fibres: effect of different solvent systems on fibre morphology and diameter," *Polymer,* vol. 55, no. 18, pp. 4728-4737, 2014.

[227] J. Yoon, H. S. Yang, B. S. Lee, and W. R. Yu, "Recent progress in coaxial electrospinning: new parameters, various structures, and wide applications," *Advanced Materials,* vol. 30, no. 42, p. 1704765, 2018.

[228] M. Pakravan, M. C. Heuzey, and A. Ajji, "Core–shell structured PEO-chitosan nanofibers by coaxial electrospinning," *Biomacromolecules,* vol. 13, no. 2, pp. 412-421, 2012.

[229] Y. Zhang, Y. Feng, Z. Huang, S. Ramakrishna, and C. Lim, "Fabrication of porous electrospun nanofibres," *Nanotechnology,* vol. 17, no. 3, p. 901, 2006.

[230] K. Joy, C. W. Smith, E. Hequet, S. Ed Hughs, and S. Hague, "Extra long staple upland cotton for the production of superior yarns," *Crop science,* vol. 52, no. 5, pp. 2089-2096, 2012.

[231] H. Hajiali, S. Shahgasempour, M. R. Naimi-Jamal, and H. Peirovi, "Electrospun PGA/gelatin nanofibrous scaffolds and their potential application in vascular tissue engineering," *International journal of nanomedicine,* vol. 6, p. 2133, 2011.

[232] C. J. Tan, J. J. L. Lee, B. C. Ang, A. Andriyana, G. Chagnon, and M. S. Sukiman, "Design of polyurethane fibers: relation between the spinning technique and the resulting fiber topology," *Journal of Applied Polymer Science,* vol. 136, no. 26, p. 47706, 2019.

[233] Z. M. Huang, Y. Zhang, S. Ramakrishna, and C. Lim, "Electrospinning and mechnical characterization of gelatin nanofibers," *Polymer,* vol. 45, no. 15, pp. 5361-5368, 2004.

[234] Y. Liu, Y. Ji, K. Ghosh, R. A. Clark, L. Huang, and M. H. Rafailovich, "Effects of fiber orientation and diameter on the behavior of human dermal fibroblasts on electrospun PMMA scaffolds," *Journal of Biomedical Materials Research Part A: An Official Journal of The Society for Biomaterials, The Japanese Society for Biomaterials, and The Australian Society for Biomaterials and the Korean Society for Biomaterials,* vol. 90, no. 4, pp. 1092-1106, 2009.

[235] R. Murugan and S. Ramakrishna, "Design strategies of tissue engineering scaffolds with controlled fiber orientation," *Tissue engineering,* vol. 13, no. 8, pp. 1845-1866, 2007.

[236] S. Zhong, W. E. Teo, X. Zhu, R. W. Beuerman, S. Ramakrishna, and L. Y. L. Yung, "An aligned nanofibrous collagen scaffold by electrospinning and its effects on in vitro fibroblast culture," *Journal of Biomedical Materials Research Part A: An Official Journal of The Society for Biomaterials, The Japanese Society for Biomaterials, and The Australian Society for Biomaterials and the Korean Society for Biomaterials,* vol. 79, no. 3, pp. 456-463, 2006.

[237] N. A. Norzain and W. C. Lin, "Orientated and diameter-controlled fibrous scaffolds fabricated using the centrifugal electrospinning technique for stimulating the behaviours of fibroblast cells," *Journal of Industrial Textiles,* p. 1528083720988127, 2021.

[238] Z. Li, S. Mei, Y. Dong, F. She, and L. Kong, "High efficiency fabrication of chitosan composite nanofibers with uniform morphology via centrifugal spinning," *Polymers,* vol. 11, no. 10, p. 1550, 2019.

[239] P. Basnett *et al.*, "Harnessing polyhydroxyalkanoates and pressurized gyration for hard and soft tissue engineering," *ACS Applied Materials & Interfaces,* vol. 13, no. 28, pp. 32624-32639, Jul 2021, doi: 10.1021/acsami.0c19689.

[240] Y. Duan, Z. Zhang, B. Lu, B. Chen, and Z. Lai, "The movement and forces of spinning solution in the nozzle during high-speed centrifugal spinning,"

Journal of Engineered Fibers and Fabrics, vol. 14, p. 1558925019828207, 2019, doi: 10.1177/1558925019828207.

[241] B. L. Smith and A. Glezer, "Jet vectoring using synthetic jets," *Journal of Fluid Mechanics,* vol. 458, pp. 1-34, 2002.

[242] R. E. Benavides, S. C. Jana, and D. H. Reneker, "Role of liquid jet stretching and bending instability in nanofiber formation by gas jet method," *Macromolecules,* vol. 46, no. 15, pp. 6081-6090, Aug 2013, doi: 10.1021/ma400900s.

[243] M. J. Divvela, A.-C. Ruo, Y. Zhmayev, and Y. L. Joo, "Discretized modeling for centrifugal spinning of viscoelastic liquids," *Journal of Non-Newtonian Fluid Mechanics,* vol. 247, pp. 62-77, Sep 2017, doi: https://doi.org/10.1016/j.jnnfm.2017.06.005.

[244] Z. Zhiming, C. Boya, L. Zilong, W. Jiawei, and D. Yaoshuai, "Spinning solution flow model in the nozzle and experimental study of nanofibers fabrication via high speed centrifugal spinning," *Polymer,* vol. 205, p. 122794, Sep 2020, doi: https://doi.org/10.1016/j.polymer.2020.122794.

[245] S. Noroozi, W. Arne, R. G. Larson, and S. M. Taghavi, "A comprehensive mathematical model for nanofibre formation in centrifugal spinning methods," *Journal of Fluid Mechanics,* vol. 892, p. A26, 2020, Art no. A26, doi: 10.1017/jfm.2020.196.

[246] X. Li *et al.*, "Jet evolution and fiber formation mechanism of amylopectin rich starches in centrifugal spinning system," *Journal of Applied Polymer Science,* vol. 138, no. 17, p. 50275, 2021, doi: https://doi.org/10.1002/app.50275.

[247] J. Merchiers, C. D. Martínez Narváez, C. Slykas, N. K. Reddy, and V. Sharma, "Evaporation and rheology chart the processability map for centrifugal force spinning," *Macromolecules,* vol. 54, no. 23, pp. 11061-11073, 2021.

[248] H. M. Golecki *et al.*, "Effect of solvent evaporation on fiber morphology in rotary jet spinning," *Langmuir,* vol. 30, no. 44, pp. 13369-13374, Nov 2014, doi: 10.1021/la5023104.

[249] M. Amarakoon, H. Alenezi, S. Homer-Vanniasinkam, and M. Edirisinghe, "Environmental impact of polymer fiber manufacture," *Macromolecular*

Materials and Engineering, vol. 307, no. 11, p. 2200356, 2022, doi: https://doi.org/10.1002/mame.202200356.

[250] S. Huang, L. Zhou, M. C. Li, Q. Wu, Y. Kojima, and D. Zhou, "Preparation and properties of electrospun poly (vinyl pyrrolidone)/cellulose nanocrystal/silver nanoparticle composite fibers," *Materials,* vol. 9, no. 7, p. 523, 2016. [Online]. Available: https://www.mdpi.com/1996-1944/9/7/523.

[251] D. Edikresnha, T. Suciati, M. M. Munir, and K. Khairurrijal, "Polyvinylpyrrolidone/cellulose acetate electrospun composite nanofibres loaded by glycerine and garlic extract with in vitro antibacterial activity and release behaviour test," *RSC advances,* vol. 9, no. 45, pp. 26351-26363, 2019.

[252] A. S. Álvarez-Suárez *et al.*, "Electrospun fibers and sorbents as a possible basis for effective composite wound dressings," *Micromachines,* vol. 11, no. 4, p. 441, 2020.

[253] S. Adanur and T. Liao, "Fiber arrangement characteristics and their effects on nonwoven tensile behavior," *Textile Research Journal,* vol. 69, no. 11, pp. 816-824, 1999, doi: 10.1177/004051759906901104.

[254] B. Isaac, R. M. Taylor, and K. Reifsnider, "Mechanical and dielectric properties of aligned electrospun fibers," *Fibers,* vol. 9, no. 1, p. 4, 2021. [Online]. Available: https://www.mdpi.com/2079-6439/9/1/4.

[255] T. U. Rashid, R. E. Gorga, and W. E. Krause, "Mechanical properties of electrospun fibers—a critical review," *Advanced Engineering Materials,* vol. 23, no. 9, p. 2100153, 2021, doi: https://doi.org/10.1002/adem.202100153.

[256] D. C. Manatunga, J. A. B. Jayasinghe, C. Sandaruwan, R. M. De Silva, and K. M. N. De Silva, "Enhancement of release and solubility of curcumin from electrospun PEO-EC-PVP tripolymer-based nanofibers: a study on the effect of hydrogenated castor oil," (in eng), *ACS Omega,* vol. 7, no. 42, pp. 37264-37278, Oct 2022, doi: 10.1021/acsomega.2c03495.

[257] L. Modica de Mohac, A. V. Keating, M. de Fátima Pina, and B. T. Raimi-Abraham, "Engineering of nanofibrous amorphous and crystalline solid dispersions for oral drug delivery," (in eng), *Pharmaceutics,* vol. 11, no. 1, Dec 2018, doi: 10.3390/pharmaceutics11010007.

[258] "Annual production of plastics worldwide from 1950 to 2021 (in million metric tons)." PlasticsEurope (PEMRG). https://www.statista.com/statistics/282732/global-production-of-plastics-since-1950/ (accessed Dec, 2022.

[259] R. Geyer, J. R. Jambeck, and K. L. Law, "Production, use, and fate of all plastics ever made," *Science Advances,* vol. 3, no. 7, p. e1700782, doi: 10.1126/sciadv.1700782.

[260] R. S. Lampitt *et al.*, "Stakeholder alliances are essential to reduce the scourge of plastic pollution," *Nature Communications,* vol. 14, no. 1, p. 2849, May 2023, doi: 10.1038/s41467-023-38613-3.

[261] A. Corma, S. Iborra, and A. Velty, "Chemical routes for the transformation of biomass into chemicals," *Chemical Reviews,* vol. 107, no. 6, pp. 2411-2502, Jun 2007, doi: 10.1021/cr050989d.

[262] L. Suriyagoda *et al.*, "“Ceylon cinnamon”: much more than just a spice," *PLANTS, PEOPLE, PLANET,* vol. 3, no. 4, pp. 319-336, Jul 2021, doi: https://doi.org/10.1002/ppp3.10192.

[263] J. Ahmed, M. Gultekinoglu, C. Bayram, D. Kart, K. Ulubayram, and M. Edirisinghe, "Alleviating the toxicity concerns of antibacterial cinnamon-polycaprolactone biomaterials for healthcare-related biomedical applications," (in eng), *MedComm (2020),* vol. 2, no. 2, pp. 236-246, Jun 2021, doi: 10.1002/mco2.71.

[264] P. Ranasinghe and P. Galappaththy, "Health benefits of Ceylon cinnamon (Cinnamomum zeylanicum): a summary of the current evidence," 2016.

[265] W. Wang *et al.*, "Dietary patterns and cardiometabolic health: clinical evidence and mechanism," *MedComm,* vol. 4, no. 1, p. e212, 2023, doi: https://doi.org/10.1002/mco2.212.

[266] M. A. LeRoux, F. Guilak, and L. A. Setton, "Compressive and shear properties of alginate gel: effects of sodium ions and alginate concentration," *Journal of Biomedical Materials Research,* vol. 47, no. 1, pp. 46-53, Oct 1999, doi: https://doi.org/10.1002/(SICI)1097-4636(199910)47:1<46::AID-JBM6>3.0.CO;2-N.

[267] B. B. Lee, E. Chan, P. Ravindra, and T. Khan, "Surface tension of viscous biopolymer solutions measured using the du Nouy ring method and the

drop weight methods," *Polymer bulletin,* vol. 69, pp. 1-19, Aug 2012, doi: 10.1007/s00289-012-0782-2.

[268] Y. Dai, J. Ahmed, A. Delbusso, and M. Edirisinghe, "Nozzle-pressurized gyration: a novel fiber manufacturing process," *Macromolecular Materials and Engineering,* vol. 307, no. 9, p. 2200268, 2022, doi: https://doi.org/10.1002/mame.202200268.

[269] K. Y. Lee and D. J. Mooney, "Alginate: properties and biomedical applications," (in eng), *Prog Polym Sci,* vol. 37, no. 1, pp. 106-126, Jan 2012, doi: 10.1016/j.progpolymsci.2011.06.003.

[270] Y. Qin, "Alginate fibres: an overview of the production processes and applications in wound management," *Polymer International,* vol. 57, no. 2, pp. 171-180, Feb 2008, doi: https://doi.org/10.1002/pi.2296.

[271] M. Brzezińska and G. Szparaga, "The effect of sodium alginate concentration on the rheological parameters of spinning solutions," vol. 15, no. 2, pp. 123-126, 2015, doi: doi:10.2478/aut-2014-0044.

[272] X. Zhang, L. Weng, Q. Liu, D. Li, and B. Deng, "Facile fabrication and characterization on alginate microfibres with grooved structure via microfluidic spinning," *Royal Society Open Science,* vol. 6, no. 5, p. 181928, May 2019, doi: 10.1098/rsos.181928.

[273] M. Yan *et al.*, "Preparation of high-strength and high-toughness sodium alginate fibers based on the study of multi-ion diffusion kinetics in a low temperature dissolution system," *New Journal of Chemistry,* vol. 45, no. 13, pp. 5981-5991, 2021, doi: 10.1039/D1NJ00747E.

[274] G. Orive, A. M. Carcaboso, R. M. Hernández, A. R. Gascón, and J. L. Pedraz, "Biocompatibility evaluation of different alginates and alginate-based microcapsules," *Biomacromolecules,* vol. 6, no. 2, pp. 927-931, Mar 2005, doi: 10.1021/bm049380x.

[275] E. Altun *et al.*, "Pressure-spun fibrous surgical sutures for localized antibacterial delivery: development, characterization, and in vitro evaluation," *ACS Applied Materials & Interfaces,* vol. 15, no. 39, pp. 45561-45573, Oct 2023, doi: 10.1021/acsami.3c07956.

[276] Y. Zhang, X. Liu, Y. Wang, P. Jiang, and S. Quek, "Antibacterial activity and mechanism of cinnamon essential oil against Escherichia coli and

Staphylococcus aureus," *Food Control,* vol. 59, pp. 282-289, Jan 2016, doi: https://doi.org/10.1016/j.foodcont.2015.05.032.

[277] N. G. Vasconcelos, J. Croda, and S. Simionatto, "Antibacterial mechanisms of cinnamon and its constituents: A review," *Microbial Pathogenesis,* vol. 120, pp. 198-203, July 2018, doi: https://doi.org/10.1016/j.micpath.2018.04.036.

[278] D. M. Berendes, P. J. Yang, A. Lai, D. Hu, and J. Brown, "Estimation of global recoverable human and animal faecal biomass," *Nature Sustainability,* vol. 1, no. 11, pp. 679-685, Nov 2018, doi: 10.1038/s41893-018-0167-0.

[279] K. K. Gupta, K. R. Aneja, and D. Rana, "Current status of cow dung as a bioresource for sustainable development," *Bioresources and Bioprocessing,* vol. 3, no. 1, p. 28, Jun 2016, doi: 10.1186/s40643-016-0105-9.

[280] S. Chen *et al.*, "Value-added chemicals from animal manure," Pacific Northwest National Lab., Richland, WA (US), Environmental Molecular …, 2003.

[281] B. B. Lee, E. S. Chan, P. Ravindra, and T. A. Khan, "Surface tension of viscous biopolymer solutions measured using the du Nouy ring method and the drop weight methods," *Polymer Bulletin,* vol. 69, no. 4, pp. 471-489, Aug 2012, doi: 10.1007/s00289-012-0782-2.

[282] M. Gericke, K. Schlufter, T. Liebert, T. Heinze, and T. Budtova, "Rheological properties of cellulose/ionic liquid solutions: from dilute to concentrated states," *Biomacromolecules,* vol. 10, no. 5, pp. 1188-1194, May 2009, doi: 10.1021/bm801430x.

[283] X. Tan, X. Li, L. Chen, and F. Xie, "Solubility of starch and microcrystalline cellulose in 1-ethyl-3-methylimidazolium acetate ionic liquid and solution rheological properties," *Physical Chemistry Chemical Physics,* vol. 18, no. 39, pp. 27584-27593, 2016.

[284] S.-L. Quan, S. G. Kang, and I. J. Chin, "Characterization of cellulose fibers electrospun using ionic liquid," *Cellulose,* vol. 17, no. 2, pp. 223-230, Apr 2010, doi: 10.1007/s10570-009-9386-x.

[285] R. P. Swatloski, S. K. Spear, J. D. Holbrey, and R. D. Rogers, "Dissolution of cellose with ionic liquids," *Journal of the American Chemical Society,* vol. 124, no. 18, pp. 4974-4975, May 2002, doi: 10.1021/ja025790m.

[286] L. Zhang, Y. Mao, J. P. Zhou, and J. Cai, "Effects of coagulation conditions on the properties of regenerated cellulose films prepared in NaOH/urea aqueous solution," (in English), *Ind. Eng. Chem. Res.,* Article vol. 44, no. 3, pp. 522-529, Feb 2005, doi: 10.1021/ie0491802.

[287] A. Hedlund, T. Kohnke, J. Hagman, U. Olsson, and H. Theliander, "Microstructures of cellulose coagulated in water and alcohols from 1-ethyl-3-methylimidazolium acetate: contrasting coagulation mechanisms," (in English), *Cellulose,* Article vol. 26, no. 3, pp. 1545-1563, Feb 2019, doi: 10.1007/s10570-018-2168-6.

[288] I. S. Makarov *et al.*, "Morphological transformations in the process of coagulation of cellulose solution in N-methylmorpholine N-oxide with isobutanol," (in English), *Polym. Sci. Ser. C,* Review vol. 63, no. 2, pp. 161-169, Sep 2021, doi: 10.1134/s181123822102003x.

[289] S. L. Liu and L. N. Zhang, "Effects of polymer concentration and coagulation temperature on the properties of regenerated cellulose films prepared from LiOH/urea solution," (in English), *Cellulose,* Article vol. 16, no. 2, pp. 189-198, Apr 2009, doi: 10.1007/s10570-008-9268-7.

[290] J. Cai, L. X. Wang, and L. N. Zhang, "Influence of coagulation temperature on pore size and properties of cellulose membranes prepared from NaOH-urea aqueous solution," (in English), *Cellulose,* Article vol. 14, no. 3, pp. 205-215, Jun 2007, doi: 10.1007/s10570-007-9106-3.

[291] M. C. Popescu, C. M. Popescu, G. Lisa, and Y. Sakata, "Evaluation of morphological and chemical aspects of different wood species by spectroscopy and thermal methods," *Journal of Molecular Structure,* vol. 988, no. 1, pp. 65-72, Mar 2011, doi: https://doi.org/10.1016/j.molstruc.2010.12.004.

[292] A. Onyianta, M. Dorris, and R. Williams, "Aqueous morpholine pre-treatment in cellulose nanofibril (CNF) production: comparison with carboxymethylation and TEMPO oxidisation pre-treatment methods," *Cellulose,* vol. 25, pp. 1-18, Feb 2018, doi: 10.1007/s10570-017-1631-0.

[293] M. Poletto, H. L. Ornaghi, and A. J. Zattera, "Native cellulose: structure, characterization and thermal properties," (in English), *Materials,* Article vol. 7, no. 9, pp. 6105-6119, Sep 2014, doi: 10.3390/ma7096105.

[294] M. L. Nelson and R. T. O'Connor, "Relation of certain infrared bands to cellulose crystallinity and crystal lattice type. Part II. A new infrared ratio for estimation of crystallinity in celluloses I and II," *Journal of Applied Polymer Science,* vol. 8, no. 3, pp. 1325-1341, 1964, doi: https://doi.org/10.1002/app.1964.070080323.

[295] A. D. French, "Idealized powder diffraction patterns for cellulose polymorphs," *Cellulose,* vol. 21, no. 2, pp. 885-896, Apr 2014, doi: 10.1007/s10570-013-0030-4.

[296] M. Wada, T. Okano, and J. Sugiyama, "Allomorphs of native crystalline cellulose I evaluated by two equatoriald-spacings," *Journal of Wood Science,* vol. 47, no. 2, pp. 124-128, Apr 2001, doi: 10.1007/BF00780560.

[297] Y. Liu, S. Jing, D. Carvalho, J. Fu, M. Martins, and A. Cavaco-Paulo, "Cellulose dissolved in ionic liquids for modification of the shape of keratin fibers," *ACS Sustainable Chemistry & Engineering,* vol. 9, no. 11, pp. 4102-4110, Mar 2021, doi: 10.1021/acssuschemeng.0c08945.

[298] K. H. Gardner and J. Blackwell, "The structure of native cellulose," *Biopolymers,* vol. 13, no. 10, pp. 1975-2001, 1974, doi: https://doi.org/10.1002/bip.1974.360131005.

[299] P. Langan, Y. Nishiyama, and H. Chanzy, "A revised structure and hydrogen-bonding system in cellulose II from a neutron fiber diffraction analysis," *Journal of the American Chemical Society,* vol. 121, no. 43, pp. 9940-9946, Nov 1999, doi: 10.1021/ja9916254.

[300] Y. Habibi, L. A. Lucia, and O. J. Rojas, "Cellulose nanocrystals: chemistry, self-assembly, and applications," *Chemical Reviews,* vol. 110, no. 6, pp. 3479-3500, Jun 2010, doi: 10.1021/cr900339w.

[301] C. Croitoru and S. Patachia, "Biocomposites obtained from wood saw dust using ionic liquids," *Acta Chemica Iasi,* vol. 22, no. 2, pp. 113-134, 2014.

[302] H. Alamri and I. M. Low, "Mechanical properties and water absorption behaviour of recycled cellulose fibre reinforced epoxy composites," *Polymer Testing,* vol. 31, no. 5, pp. 620-628, Aug 2012, doi: https://doi.org/10.1016/j.polymertesting.2012.04.002.

[303] W. C. Lin, C. C. Lien, H. J. Yeh, C. M. Yu, and S. H. Hsu, "Bacterial cellulose and bacterial cellulose–chitosan membranes for wound dressing applications," *Carbohydr. Polym.,* vol. 94, no. 1, pp. 603-611, Apr 2013, doi: https://doi.org/10.1016/j.carbpol.2013.01.076.

[304] J. Miao *et al.*, "Lysostaphin-functionalized cellulose fibers with antistaphylococcal activity for wound healing applications," *Biomaterials,* vol. 32, no. 36, pp. 9557-9567, Dec 2011, doi: https://doi.org/10.1016/j.biomaterials.2011.08.080.

[305] D. Klemm, B. Heublein, H. P. Fink, and A. Bohn, "Cellulose: fascinating biopolymer and sustainable raw material," *Angewandte Chemie International Edition,* vol. 44, no. 22, pp. 3358-3393, 2005, doi: https://doi.org/10.1002/anie.200460587.

[306] K. Dhali, M. Ghasemlou, F. Daver, P. Cass, and B. Adhikari, "A review of nanocellulose as a new material towards environmental sustainability," *Science of The Total Environment,* vol. 775, p. 145871, Jun 2021, doi: https://doi.org/10.1016/j.scitotenv.2021.145871.

[307] J. M. Rieland and B. J. Love, "Ionic liquids: a milestone on the pathway to greener recycling of cellulose from biomass," *Resources, Conservation and Recycling,* vol. 155, p. 104678, Apr 2020, doi: https://doi.org/10.1016/j.resconrec.2019.104678.

[308] B. Bideau, J. Bras, N. Adoui, E. Loranger, and C. Daneault, "Polypyrrole/nanocellulose composite for food preservation: Barrier and antioxidant characterization," *Food Packaging and Shelf Life,* vol. 12, pp. 1-8, Jun 2017, doi: https://doi.org/10.1016/j.fpsl.2017.01.007.

[309] J.-H. Kim *et al.*, "Functionalized nanocellulose-integrated heterolayered nanomats toward smart battery separators," *Nano Letters,* vol. 16, no. 9, pp. 5533-5541, Sep 2016, doi: 10.1021/acs.nanolett.6b02069.

[310] J. Huang *et al.*, "Highly transparent and flexible nanopaper transistors," *ACS Nano,* vol. 7, no. 3, pp. 2106-2113, Mar 2013, doi: 10.1021/nn304407r.

[311] I. Cunha *et al.*, "Reusable cellulose-based hydrogel sticker film applied as gate dielectric in paper electrolyte-gated transistors," *Advanced Functional Materials,* vol. 27, no. 16, p. 1606755, 2017, doi: https://doi.org/10.1002/adfm.201606755.

[312] M. Yusefi *et al.*, "Fabrication of cellulose nanocrystals as potential anticancer drug delivery systems for colorectal cancer treatment," *International Journal of Biological Macromolecules,* vol. 199, pp. 372-385, 2022.

[313] C. Ao, Y. Niu, X. Zhang, X. He, W. Zhang, and C. Lu, "Fabrication and characterization of electrospun cellulose/nano-hydroxyapatite nanofibers for bone tissue engineering," *International journal of biological macromolecules,* vol. 97, pp. 568-573, 2017.

[314] X. Ma *et al.*, "Biopolymer composite fibres composed of calcium alginate reinforced with nanocrystalline cellulose," *Composites Part A: Applied Science and Manufacturing,* vol. 96, pp. 155-163, May 2017, doi: https://doi.org/10.1016/j.compositesa.2017.02.021.

[315] Y. Wang, H. Chen, L. Cui, C. Tu, C. Yan, and Y. Guo, "Toughen and strengthen alginate fiber by incorporation of polyethylene glycol grafted cellulose nanocrystals," *Cellulose,* vol. 29, no. 9, pp. 5021-5035, Jun 2022, doi: 10.1007/s10570-022-04601-x.

[316] M. M. Kareem, T. Hodgkinson, M. S. Sanchez, M. J. Dalby, and K. E. Tanner, "Hybrid core–shell scaffolds for bone tissue engineering," *Biomedical Materials,* vol. 14, no. 2, p. 025008, Jan 2019, doi: 10.1088/1748-605X/aafbf1.

[317] A. Kelly, J. Ahmed, and M. Edirisinghe, "Manufacturing cyclodextrin fibers using water," *Macromolecular Materials and Engineering,* vol. 307, no. 6, p. 2100891, 2022, doi: https://doi.org/10.1002/mame.202100891.